Radiometric analysis of LEDs and the use of rapidly pulsed infrared LEDs for portable sensing of gases

By

Ansara Noori

A thesis submitted in fulfilment of the requirements for the degree of

Doctor of Philosophy

School of Physical Science – Chemistry

University of Tasmania

June 2017

DECLARATION

This thesis contains no material which has been accepted for a degree or diploma by the University or any other institution except the way of background information and duly acknowledge in the thesis. To the best of my knowledge and belief, no material which has been previously published or written by another person, except where due reference is made in the text of the thesis nor does this thesis contains any material that infringes copyright.

The publishers of the papers in this thesis (comprising Chapter 2 to 4) will hold the copyright for that content, and access to the material should be sought from the respective journals. The remaining non-published content of the thesis may be made available for loan and limited copying and communication in accordance with the Copyright Act 1968.

Ansara Noori

June 2017

ACKNOWLEDGEMENTS

In the name of Allah, the Most Gracious and the Most Merciful, all praises to Allah for the strengths and His blessing in completing this PhD thesis. Sincere appreciation and thanks goes to my supervisor Professor Mirek Macka for giving me the opportunity to work with him and for his continuous support throughout my PhD. I would also like to thank my co-supervisors Dr. Parvez Mahbub and Dr. Arko Lucieer for their valuable supervisions, positive encouragement constructive advice. and collaboration. The long-term visitor to our group, Miloš Dvořák, for the inspiration, interesting discussions and friendly collaboration during his stays and short-term research fellow Dr. Nantana Nuchtachvorn for her supervision during the absences of my primary supervisors. I would like to extend my heartfelt gratitude to all members of Australian Centre for Research in Separation Science (ACROSS) for all the time they spent in helping me with my research as well as their kindness and friendship. Also, my sincere thanks to the friendly and very helpful staffs in Chemistry department and Morris Miller Library, and to all the friendly people elsewhere at the University of Tasmania. My special appreciation goes to the UTAS Central Science Laboratory staffs, namely Mr. John S. parry for his great IT support in constructing the computer programs for my microcontroller system, Mr. John Davis for his electrical work support, integrating my detection system, assembling in-house electronics and making me understand the programs and electronics by answering my silly questions. They have restlessly helped me, as well as giving technical and moral support whenever I need them. My acknowledgement also goes to another two Central Science Laboratory staffs Mr. Paul Waller and Mr Chris Young, who enabled my research experiments through construction of electrical and mechanical hardware. Financial support from the Australian government in the form of SET Tasmania Graduate Research Scholarship.

My last but the greatest acknowledgement to my husband Muhammad Zakarul Islam, for your utmost moral support, sacrifices, without his support it was almost impossible to peruse my PhD and to our dearest daughter Miss Juwairya Islam who gave my life a new direction. It has been a lot of joys, tears, sweat, and patience for the past four years pursuing this dream. I am really grateful to my parents, sisters, in-laws and all other family members for always being there whenever I need their encouragement.

LIST OF ABBREVIATIONS

Acronym	Representation
ADC	Analog to digital converter
A/D	Analog to digital conversion
AGGI	Annual greenhouse gases index
AlGaAs	Aluminium gallium arsenide
AlInGaP	Aluminium indium gallium phosphide
AlN	Aluminium nitride
BTEX	Benzene, toluene, ethylbenzene, xylene
CA	Chemical actinometry
CC	Cosine corrector
CCD	Charge-coupled device
CIE	Commission internationale de l'Éclairage
COV	Coefficient of variations
CPU	Central processing Unit
CRDS	cavity ring-down spectroscopy
CW	Continuous wave
(D/A)	Digital to analog
DC	Direct current
DDS	direct digital synthesiser
DIAL	Differential absorption light detection and ranging
DMM	Digital multimeter
DOAS	Differential optical absorption spectroscopy
eDAQ	Electronic data acquisition
EL	Electroluminescence
FFP	Far field pattern

FFT	Fast Fourier transformation
FID	Flame ionisation detector
FPGA	Field programmable gate array
FTIR	Fourier transform infrared
FWHM	Full width at half maximum
GaN	Gallium nitride
GC	Gas chromatography
GPIO	General purpose input output
HC	Hydrocarbon
HEP	High-energy physics
HITRAN	High-resolution transmission
I/O	Input/output
IR	Infrared
IR PD	Infrared photodiode
IR LED	Infrared light emitting diode
IS	Integrating sphere
LCU	Light curing unit
LED	Light Emitting Diode
LEL	Lower explosion limit
LOD	Limit of detection
µC	Microcontroller
MIR	Mid infra-red
MS	Mass spectrometer
NDIR	Nondispersive infra-red spectroscopy
NG	Natural gas
NIF	National ignition facility
NIR	Near infra-red

NIST	National Institute of Standards and Technology
PA	Preamplifier
PAS	Photoacoustic absorption spectroscopy
PD	Photodiode
PID	Photo-ionisation detector
PMIT	Photomultiplier tube
PNNL	Pacific Northwest National Laboratory
ppb	Parts per billion
ppm	Parts per million
PRF	Pulse repetition frequency
PTFE	Polytetrafluoroethylene
QCL	Quantum cascade leaser
QCW	quasi continuous wave
QY	Quantum yield
RAM	Random access memory
RF	Radio frequency
rms	root mean square
SD	Secure digital
S-G	Savitzky-Golay
Si-PD	Silicon photodiodes
SM	Surface mount
SMA	SubMiniature Version A
SNR	Signal-to-noise ratio
SoC	System on chip
SSH	Secure shell
SVOCs	Semi-volatile organic compounds
TDLAS	Tuneable diode laser absorption spectroscopy

UAV	Unmanned aerial vehicle
UEL	Upper explosion limit
USB	Universal Serial Bus
UV	Ultra violet
V-to-I	Voltage to current converter
VOCs	Volatile organic compounds

STATEMENT OF CO-AUTHORSHIP

The following people and institutions contributed to the publication of work undertaken as part of this thesis:

Ansara Noori, Australia Centre for Research on Separation Science (ACROSS) and School of Physical Sciences- Chemistry, University of Tasmania, Tasmania, Australia: Candidate and primary author of all Chapters

Parvez Mahbub, Australia Centre for Research on Separation Science (ACROSS) and School of Physical Sciences- Chemistry, University of Tasmania, Tasmania, Australia: Co-author of papers included in Chapters 2, 3 and 4

John Parry, Central Science laboratory, University of Tasmania, Private Bag 74, Hobart 7001, Australia: Co-author of papers included in Chapters 3 and 4

John Davis, Central Science laboratory, University of Tasmania, Private Bag 74, Hobart 7001, Australia: Co-author of papers included in Chapters 3 and 4

Arko Lucieer, School of Land and Food, University of Tasmania, Tasmania, Australia: Co-author of papers included in Chapters 2, 3 and 4

Mirek Macka, Australia Centre for Research on Separation Science (ACROSS) and School of Physical Sciences- Chemistry, University of Tasmania, Tasmania, Australia: Co-author of papers included in Chapters 2, 3 and 4

Author details and their roles:

Paper 1, < Noori, A.; Mahbub P.; Dvořák M.; Lucieer A.; Macka M.; **Radiometric analysis of UV to near infrared LEDs enabling fast, accurate and facile radiometric measurements in photochemical systems**. *Sensors and Actuators B: Chemical*, **2017** (in review)> This paper comprises Chapter 2.

Candidate was the primary author (65%) and conducted all the experiments, analysed data and wrote the manuscript. The co-authors contributed a total of 35% to the published work. Mirek Macka, Parvez Mahbub, Milos Dvorak and Arko Lucieer contributed to idea, its formalisation and development. Milos Dvorak and Parvez Mahbub offered experimental assistance. All co-authors assisted with refinement and presentation.

Paper 2, < Noori, A.; Mahbub P.; Parry, J. S.; Davis, J.; Lucieer A.; Macka M.; **Portable Device for Continuous Sensing with Rapidly Pulsed LEDs – Part 1: Rapid On-the-fly Processing of Large Data Streams using an Open Source Microcontroller with Field Programmable Gate Array.** *Analytical Chemistry*, **2017**. (Final draft for submission) >: This paper comprises Chapter 3.

Ansara Noori was the primary author (70%) and conducted all the experiments, analysed data and wrote the manuscript. The co-authors contributed a total of 30% to the work. Mirek Macka, Parvez Mahbub, John S Parry, John Davis and Arko Lucieer contributed to the concept, development, refinement and presentation.

Paper 3, < Noori, A.: Mahbub, P.: Parry, J.S.: Davis, J.: Lucieer, A., Macka, M.; **Portable Device for Continuous Sensing with Rapidly Pulsed LEDs – Part 2: Continuous Real-time**

Methane Sensing with Wireless Analytical Signal Transfer using IR LEDs for Indoor and Outdoor Monitoring of Gases. *Analytical Chemistry,* **2017**, (in preparation). >: This paper comprises Chapter 4.

Ansara Noori was the primary author (70%) and conducted all the experiments, interpreted the results and wrote the manuscript. The co-authors contributed a total of 30% to work. Mirek Macka, Parvez Mahbub, John S Parry, John Davis and Arko Lucieer contributed to the concept, development, refinement and presentation..

We the undersigned agree with the above stated "proportion of work undertaken" for each of the above submitted and ready to submit (or in preparation) manuscripts contributing to this thesis:

Signed:

Prof. Mirek Macka	Prof. John Dickey
Supervisor	Head of School
School of Physical Science	School of Physical Science
University of Tasmania	University of Tasmania
Date: 31/05/2017	Date: 1/6/17

LIST OF PUBLICATIONS

LIST OF ARTICLES

1. Noori, A.; Mahbub P.; Dvořák M.; Lucieer A.; Macka M.; Radiometric analysis of UV to near infrared LEDs enabling fast, accurate and facile radiometric measurements in photochemical systems. Sensors and Actuators B: Chemical, Volume 262, 1 June **2018**, Pages 171-179. (Chapter 2)

2. Noori, A., Mahbub, P., Parry, J. S., Davis, J., Lucieer, A., Macka, M., Portable Device for Continuous Sensing with Rapidly Pulsed LEDs – Part 1: Rapid On-the-fly Processing of Large Data Streams using an Open Source Microcontroller with Field Programmable Gate Array. **2017** (Final draft ready for submission) (Chapter 3)

3. Noori, A., Mahbub, P., Parry, J. S., Davis, J., Lucieer, A., Macka M., Portable Device for Continuous Sensing with Rapidly Pulsed LEDs – Part 2: Continuous Real-time Methane Sensing with Wireless Analytical Signal Transfer using IR LEDs for Indoor and Outdoor Monitoring of Gases. **2017** (under preparation) (Chapter 4)

LIST OF POSTER PRESENTATIONS

1. Noori, A., Lucieer, A., Mack. M., (2013) Infra-red light emitting diodes (IR-LEDs) as light sources for methane and natural gas detection for portable and remote analysis platforms. *21st Annual RACI Environmental and Analytic Division Research and Development Topic Conference*, Australian National University (ANU), NSW, Australia, 11 – 13 December **2013**

2. Noori, A., Lucieer, A., Parry, J., Macka, M., (2015) Portable IR-LED Based Atmospheric Monitoring: Automated Data Handling of Large Data Streams. *23rd Annual RACI R&D Topics Analytical and Environmental Chemistry Conference,* The University of Melbourne, Victoria, Australia, 6-9 December **2015**.

3. Noori, A., Mahbub, P., Lucieer, A., Macka M., Actinometric Validation of Radiometric Power Output of UV-Vis-NIR Light Emitting Diodes. *2nd ACROSS Symposium on Advances in Separation Science (ASASS 2),* Hobart, Tasmania,

Australia 30 November - 2 December **2016**

4. Noori, A., Mahbub, P., Parry, J. S., Davis, J., Lucieer, A., Macka M., Portable IR-LED Based Atmospheric Monitoring: Automated Data Handling of Large Data Streams. *24th Annual RACI R&D Topics Analytical and Environmental Chemistry Conference,* The University of Melbourne, Victoria, Australia, 4-7 December **2016**.

5. Noori, A., Mahbub, P., Parry, J. S., Davis, J., Lucieer, A., M. Macka, Highly Sensitive and Quantitative Measurements of Atmospheric Methane with On-the-fly Rapid Data Handling for UAV based monitoring. UAS4RS Conference 2017, Hobart, Australia, 24-25 May **2017**.

ABSTRACT

This thesis focuses on the radiometric analysis of commercial light emitting diodes (LEDs) and investigation and development of an infrared (IR) LED based optical sensing system for continuous monitoring of methane gas with wireless, on-the-fly and flexible data processing capabilities in indoor and outdoor environments. The areas of analytical use of LEDs as well as of gas monitoring with IR LEDs covered in the scientific literature are reviewed in Chapter 1.

The first experimental section of this thesis (Chapter 2) focuses on radiometric analysis of LEDs. LEDs have been established as light sources in countless areas where they offer a better alternative to traditional light sources in terms of low-cost, small size and robustness supporting portability, performance parameters such as low noise and wide applicability. Lack of rapid, facile and accurate radiometric analysis of LEDs is a major limiting factor which constrains their purposeful use in analytical chemistry. A holistic radiometric analysis of LEDs in terms of absolute emission spectra analyses, radiometric power output, irradiances, radiant efficiencies as well as uncertainties are invaluable to analytical chemists as such analysis has the capability to justify the purposes of LEDs as light sources in analytical chemistry. We demonstrate and cross-validate a rapid, facile, accurate and low-cost radiometric analysis of LEDs with directional light output using a large active area silicon photodiode in a simple optical design with the LED light source in proximity, without the need for a calibrated light source. The obtained radiometric data for a wide range of 21 commercial LEDs in UV, visible and near-infrared (NIR) spectral range (255-950 nm) agree very well with two completely independent approaches: chemical actinometric and spectrophotometric methods. At first, an excellent agreement was achieved with accuracy

within 5% for radiometric power output (mW) measured using chemical actinometric methods and further, the accuracy of irradiance (mW/cm^2) measurement was within 2% when compared with a spectrophotometric method based on a radiometrically calibrated spectrophotometer. The measurement uncertainty at 95% confidence level for the values of radiometric power output were reduced 3-folds compared to the existing techniques. It is also demonstrated that this facile, accurate and low-cost radiometric analysis can be further extended to accurately measure quantum yield of photochemical reactions and fluence values in actinometric systems.

The second experimental section of this thesis (Chapter 3) explores design of a portable platform for rapid pulsed signal generation and on-the-fly data processing using an open source micro controller (μC) with built-in field programmable gate array (FPGA). IR LEDs operated in a rapid pulsed mode are suitable for portable low-cost optical sensing of gases with the transmitted light detected by a IR sensitive photodiode. We design a μC-FPGA based flexible and portable system, programmed with custom software, for rapid current pulse generation (ca. 2 μs short pulses with a typical repetition rate of 1 kHz) to drive the sensing IR LED as well as for the optical sensing data acquisition and processing. Instrumental signal to noise ratio values (SNR) are investigated as the crucial performance characteristics of the system governing the limit of detection values. Digital data filtering is accomplished first by repetitive smoothing (averaging a number of raw data pulses usually 10 - 10,000), followed by boxcar averaging and Savitzky-Golay (2nd degree polynomial regression) based smoothing. Repetitive smoothing resulted in SNR improvement by a factor of $\sqrt{n}$ (n is the number of repetitive pulses averaged). Then to determine the detected pulsed signal attenuation (measuring the pulse height), three different statistical methods applied to the corresponding data points at the baseline and at the pulse top were compared: simple averaging, linear regression, and 2nd degree polynomial regression. Finally, each of the

digitally processed signal pulses resulted into one data point in time as a quasi-continuous data stream produced at a rate between 1000 and 0.1 Hz (1 point every 1 ms to 10 s, depending on the level of repetitive smoothing). All the in-house developed pulse generation and data processing algorithm were saved in a secure digital (SD) card and data processing was carried out on-the-fly and wirelessly transmitted via network connection. The minimum measurable absorbance corresponding to the highest SNR for n=1000 resulting in quasi-continuous data points at 1 Hz was found 10^{-4} a.u. This low cost portable system offers ultimate custom-defined software flexibility of on-the-fly data processing that can be applicable to a number of pulsed data acquisition and sensing scenarios including real-time indoor and outdoor monitoring of gases.

In the third and last experimental section (Chapter 4), we investigate the design of a nondispersive infrared (NDIR) spectroscopy based sensor for continuous monitoring of gases, considering CH_4 as a model gas, with rapidly pulsed near-infrared (NIR) LED. Continuous sensing of fugitive emission of gases in portable and remote conditions in indoor and outdoor environments are challenging due to the technical requirements for small size and low weight and the need of on-the-fly processing of large data streams. In this work, we design a facile, low-cost and weight nondispersive infrared (NDIR) spectroscopy based system for continuous sensing of atmospheric methane (CH_4) with rapidly pulsed near-infrared light emitting diode (NIR LED) at 1.65 μm. It uses a microcontroller with field programmable gate array (μC-FPGA) enabling on-the-fly and wireless streaming and processing of large data streams (~2Gbit/s). The investigated NIR LED based sensor offered favourable limit of detection (LOD) of 300 ppm (0.03%) CH_4 and precision of ±5% (RSD). All the generated raw data were processed automatically on-the-fly in the μC-FPGA and transferred wirelessly via network connection. The sensing device was then deployed in portable sensing of atmospheric CH_4 at a local landfill, resulting in quantified concentrations

within the sampling area (ca 400 m^2) in the range from 0.5% to 3.35% CH_4 and was cross-validated with GC-MS (2.1%). This NIR LED based sensor system offers a facile low-cost solution for continuous real-time, quantitative and direct measurement of CH_4 concentrations in indoor and outdoor environments, and possesses future potential for remote monitoring of gases directly from mobile platforms such as, smartphones and unmanned aerial vehicles (UAV).

TABLE OF CONTENTS

1 Chapter 1: Introduction and Literature Review

1.1 Introduction

In analytical chemistry, light emitting diodes (LEDs) coupled with sensors and detectors [a] are well established and extensively employed as light sources since last two decades.[1] The advantages of use of LEDs over traditional light sources such as, incandescent and arc lamps in analytical chemistry are numerous, but most importantly include robust performance of the solid-state emitter technology in terms of steady optical output, quasi-monochromaticity, low noise in optical detection, small size enabling portability and ability to be operated in pulsed regime in a cost-effective manner.

Although LEDs have widely been used in analytical chemistry, the diagnosis and characterisation of essential parameters (such as radiometric output power, irradiance, radiant efficiency, fluence) of the deployed LEDs remain challenging for an analytical chemist.[2] The accurate measurements of these radiometric parameters are sometimes extremely important as they directly affect the performance of numerous analytical and industrial applications of LEDs. Currently, the radiometric parameters of the deployed LEDs are either measured using spectrophotometer equipped with integrating sphere[3] requiring regularly calibrated light source or the user has to rely on reported optical output data supplied by the manufacturer. In many cases, the vendors provide radiometric power output data that mismatch with radiometrically calibrated experimental data.[2] Moreover, radiometric calibration of spectrophotometers for LED characterisation requires sophisticated calibration

[a]Devices that sense and convert physical information about the environment into a readable form such as analog voltage, current, charge, or frequency[1]

and relies on complex calculations, rigid optical design and geometry.[4] Use of integrating sphere for radiometric analysis of LED is widespread[5]. However, using integrating sphere for radiometric analysis of UV and deep-blue LEDs, the measurement uncertainty (at 95% confidence interval, i.e. expanded uncertainty, k=2) is reported 1%-6% which even increases at UV and blue region due to fluorescence from the coating material of the integrating sphere.[5] This may result over estimation of the LEDs' radiometric parameters. Hence, there is a strong need for radiometric analysis of LEDs using simple optical design and validate the data using accurate and reliable methods.

Chemical analyses of gases are most frequently associated with detection, sensing and monitoring, depending on the area of use. Greenhouse gas (GHGs) analyses in the atmospheric environment are increasingly gaining significance in Australia and overseas, particularly the detection of GHGs resulting from gas leak or other fugitive emissions in surrounding atmosphere is of growing importance in analytical chemistry.[6]

Methane (CH_4) is the most abounded hydrocarbon in the atmosphere. After carbon dioxide (CO_2), it is the second most exposed greenhouse gas, however the comparative impact of CH_4 on climate change is above 25 times greater than CO_2 over a 100-year period.[8,9] Although the atmospheric concentration of CH_4 is not that alarming (~0.0002%)[9] its global warming capability is 85 times higher than CO_2.[11]Additionally, CH_4 is extremely explosive, the lower explosion limit (LEL) is 5% and flashpoint is -45°C. Because of highly explosive nature it is necessary to know the atmospheric existence and concentration (not to exceed the LEL) of CH_4 to ensure the safety in gas facilities (gas plant, mines and residential area) and landfills as well as to maintain the air quality. In atmospheric monitoring of trace gases where sample properties can change at a fast rate, a rapid sampling and analysis technique is

required. This is well satisfied with optical detection (analysis) methods such as infra-red (IR) spectrometry. Although gas detection in IR spectral region is a well-established technique, with current developments in portable sensing instruments, designing small low-cost low power consumption analytical platforms compatible with portable and remote analysis formats present a number of challenges.[12] One of them is processing of continuous, live and rapid data streams automatically in a flexible way. In this context, small, low-cost and low power consumption IR-LED based analytical platforms pose immense possibilities for portable, rapid and remote analyses of gases. In this research study, we developed an accurate and simple method for radiometric characterisation of commercial LEDs and investigated the implications of an IR-LED based analytical platform on flexible, rapid and live analyses of GHGs in atmosphere, taking methane as a model GHG. The following discussions include in-depth literature reviews on the LEDs as a light source used in analytical chemistry and optical techniques used in atmospheric monitoring and analyses of gases, followed by the general and specific aims of this research study.

PART A: LIGHT EMITTING DIODE (LEDS)

1.2 Fundamentals of light emitting diodes (LEDs)

Light emitting diode (LED) is a semiconductor electronic device with p-n junction (semiconductor diodes), which emits photon at ultra violet (UV), infrared (IR) or visible wavelengths when required forward voltage is applied. In Figure 1.1 the junction in an LED is forward biased[b] and when electrons cross the junction from the n-type (contains an excess of electrons) to the p-type material (has "hole" or electron deficiency), the electron-hole recombination process produces some photons (a light particle) in the UV, visible or IR range in a process called electroluminescence (EL).

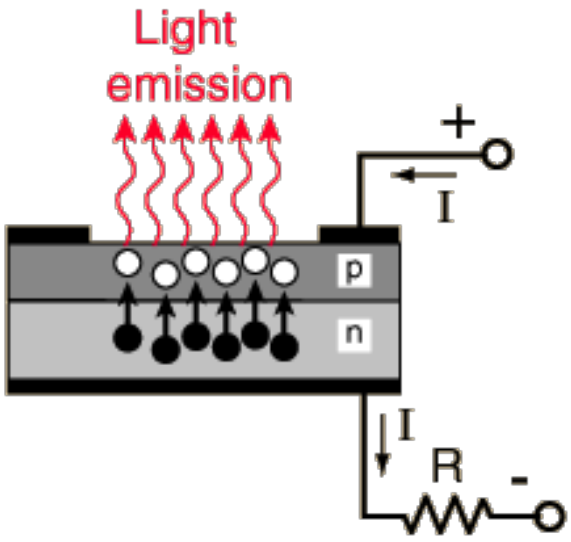

Figure 1.1 Structure of light emitting diode (LED) [13]

[b] In forward biasing the p-n junction drives holes to the junction from the p-type material and electrons to the junction from the n-type material

The energy of the generated photon corresponds to the voltage bias in the transition region which is equivalent to the "band gap" of the semiconductor material used for the LED.[14] The wavelength and colour of light depends on the energy of a light particle (photon) emitted by an LED. Band gap is an intrinsic feature of the semiconductor material and manufacturing LED with a designated wavelength is all about engineering the semiconductor materials and their band-gaps. In Figure 1.2 the bandgaps of a number of group III-V compounds are shown as a function of the lattice constant.[15]

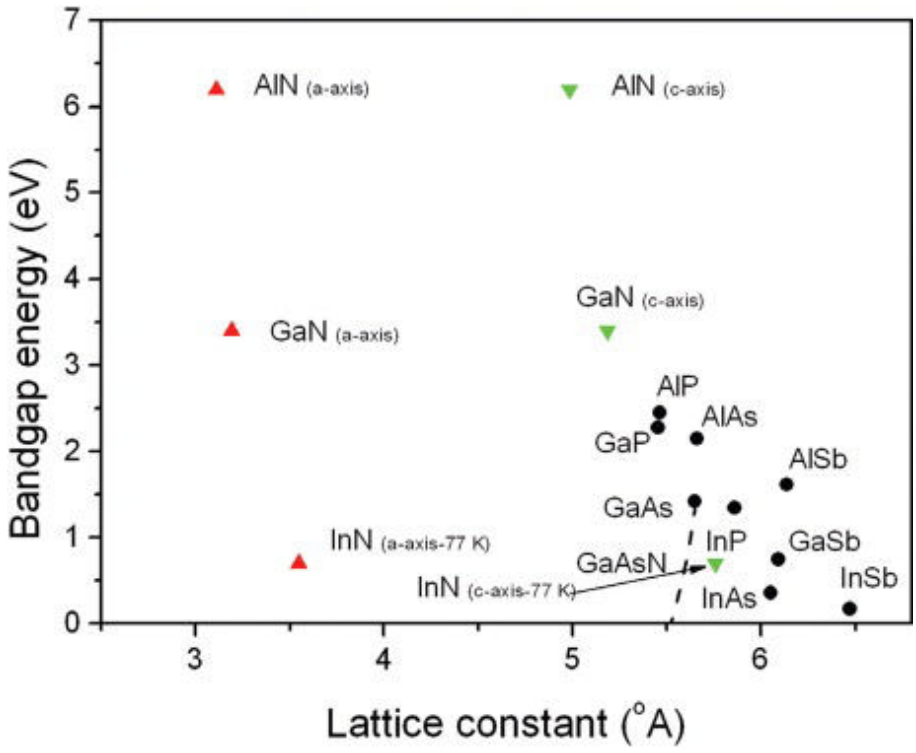

Figure 1.2 Bandgap energy (300 K) vs lattice constant[c] for III-V compound semiconductors commonly used in LEDs

[c] the physical dimension of unit cells in a crystal lattice

1.3 Brief history of the progress of light emitting diodes

After 5 decades of discovering electroluminescence (EL) effect by Henry J. Round (1907), the first light emitting diodes (LED) was developed in 1960 using Gallium Arsenide Phosphide (GaAsP) on a GaAs substrate. For this invention of red LEDs Dr. Nick Holonyak is known as the father of LEDs.[16] This first red LED was used for indicator purpose because it was not intense enough to use as a light source. Further advancements on the development of LEDs were achieved in 70's and the first large-scale production of GaAsP based LED was commenced by Monsanto Company in 1968.

In 1980's, the first super bright LEDs emitting red, green and yellow colours were introduced by synthesising quaternary semiconductor compound gallium aluminium arsenide phosphide (GaAlAsP) and in 1990's, the ultra-bright as well as blue LEDs were produced through synthesising indium gallium aluminium phosphide (InGaAlP) and silicon carbide (SiC), respectively.[15] In mid-90's, the ultra-bright blue LEDs were developed through employing gallium nitride (GaN) compounds.[17] By coating the ultra-blue LEDs chip with fluorescent phosphor, white LEDs were prepared where fluorescent phosphor absorbed the blue light and re-emitted it as white light.[11] Through this technique, other visible colours can be produced. Now-a-days, not only violet but also pure ultra-violet light is possible to develop by LED technology. Currently, traffic signals and vehicles headlights are replaced by LEDs and these light sources are bright enough to illuminate our residences, office and street as well.

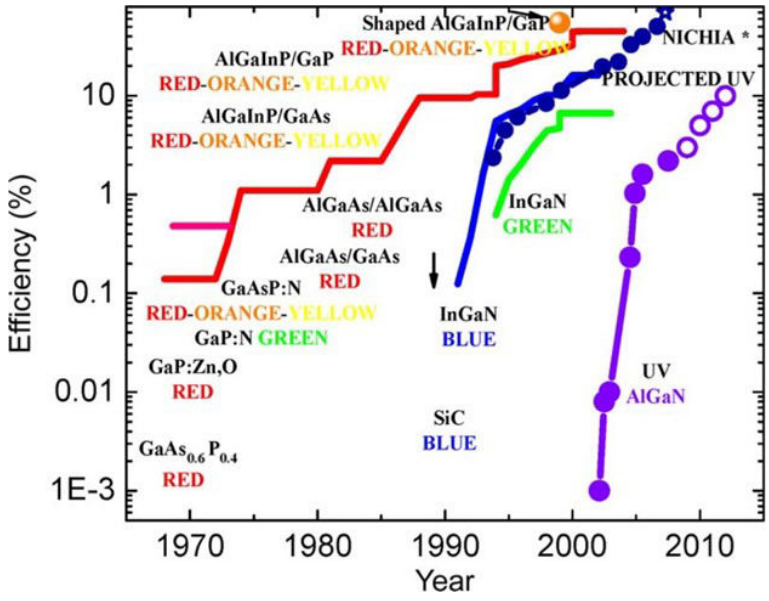

Figure 1.3 Timeline of development of construction materials of LEDs with increasing efficiency[18]

1.4 Construction materials of LEDs with different wavelength ranges and their related efficiency

LEDs are predominantly built with doped semiconductor materials. The semiconductor material of construction for the LED kept changing with time to improve their efficiency in terms of thermal stability, internal and external quantum efficiency and energy efficiency. In Figure 1.3 development of semiconductor material of construction for LEDs are shown within last five decades.

The diversity of emission spectra in terms of band width and spectral response mainly caused by specific electronic properties (piezoelectric polarization, bandgap) as well as crystal structure of the semiconductor materials used to construct the LED device.[19] However, specific electronic properties can be achieved by high quality crystal growth, controlled doping as well as multilayer integration of specific semiconductor material.[20] By

incorporating different semiconductor materials (mainly group III & V elements), energy band can be tuned and with the resulting higher bandgap, the desired efficiency (photon energy) of LEDs could be achieved.[14,20]

In Figure 1.4 currently employed semiconductor materials for different wavelength range are mentioned. The Deep UV-LED technology is mainly based on Group III (aluminium, gallium, indium) nitride semiconductor materials and this technology has been flourished within the last decade. Many of the deep UVLEDs have poor efficiency and limited lifetime (less than thousand hours). Although, aluminium nitride (AlN) has highest band energy (shown in previous section Figure 1.2), AlN based UV LEDs are less efficient than the blue LEDs (in Figure 1.3). This is due to the fact that the electron-hole recombination is much slower for AlN based semiconductors.[14] Moreover, the emission at shorter wavelength causes thermal rise within the package, which consequently downgrades the efficiency of these UV

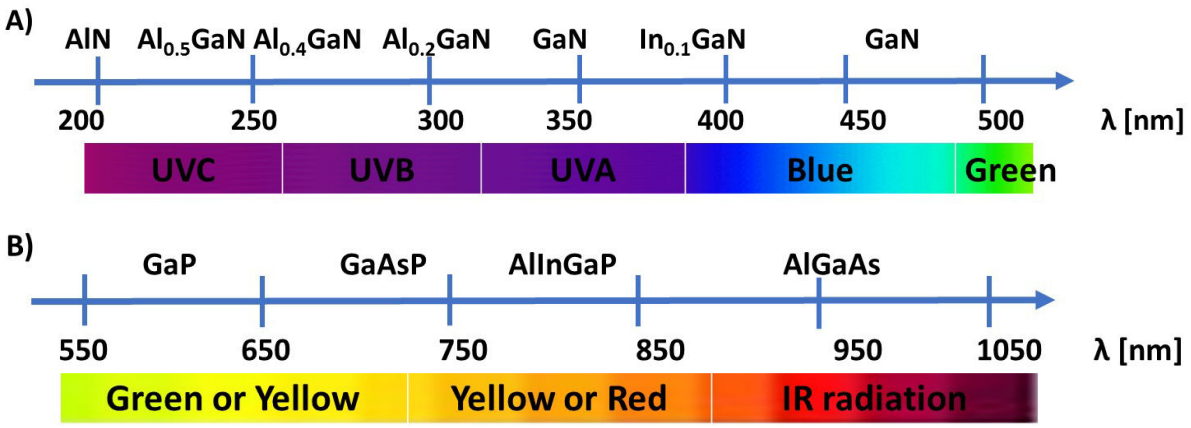

Figure 1.4 A) Group(III) -based LEDs emitting in the UVA (400-320nm), UVB (320-280nm), and UVC (280-200nm) spectral range. **B)** construction materials for Yellow, red and infrared LEDs

LEDs.[21]

Blue LEDs (400-500nm) and Green LEDs (500-570nm) are mainly based on gallium nitride (GaN) and also are combination of three binary compounds AlN, GaN and indium nitride (InN). GaN based devices exhibit minimal piezoelectric polarization[d] below 450nm wavelength which result in increase of photon emission.[14] Consequently, GaN based LEDs (below ~450nm) emitted high photon energy. However, the well-known polar c-plane of the GaN based semiconductors was reported to manifest increased piezoelectric polarisation above 450 nm wavelength that resulted gradual decrease in the quantum efficiencies of GaN based LEDs.[14] Hence the efficiency of the green LEDs are lower than the blue LEDs although both are based on GaN semiconductor materials.

Aluminium indium gallium phosphide (AlInGaP) material system allowed the creation of light in the red and amber regions of the visible spectrum and produced more intense light than green region.[22] Due to having direct bandgap (where electron can emit photon directly), gallium arsenide (GaAs) provides efficient p-n junction for infrared (IR) LEDs and are enormously intense.[19,21] Moreover, aluminium gallium arsenide (AlGaAs), which are the construction materials for NIR LEDs are reported having higher efficiency than aluminium indium gallium phosphide (AlInGaP) which are the building semiconductor materials for red LEDs.

1.5 Use of LEDs in analytical chemistry

Many gases, metal complexes, biological materials, some common anions and many other molecules whose absorption bands coincide with LEDs' emission bands, can be detected by using such LEDs as light sources and therefore, plentiful photometric detection devices based

[d] The piezoelectric effect refers to a change in electric polarization that is produced in certain materials when they are subjected to mechanical stresses

on these LEDs are developed within last five decades.[23] Many LED based portable and miniaturised instruments are commercially available for photometric analysis of environmental samples in wastewater treatment plant, chlorine and ozone detection in swimming pool water. In many handheld, robotic medical instrumentals, LEDs are the foremost choice because of its compact size. LED based oximeters are the most common example of absorbance based photometric instrument which detect blood oxygen content.[24] Other important analytical applications of LEDs are automatic titrator and optical end-point detection in titration. For complex sample analysis or more than one sample analysis with a single photometer, multi-colour LED,[25] LED arrays[26] or white LEDs with additional wavelength selective devices[27] are well established. In flow injection analysis (FIA),[28] chromatography,[23] capillary electrophoresis (CE)[29-32] and microfluidics devices (mostly fluorescence based) for analysis of trace metals (alkaline, alkaline earth metal, rare earth), anions and organic molecules, LEDs are predominantly employed. LED based FIA system are also commercially available.[32] A number of gases e.g., carbon dioxide (CO_2), methane (CH_4) and other hydrocarbons, ozone (O_3), NO_x compounds, sulphur dioxide (SO_2), hydrogen sulphide (H_2S), ammonia (NH_3), or carbon monoxide (CO) has very narrow absorption lines in the mid-IR range. Since 1992 (the first reported use of IR LED based gas detection system by Johnston, 1992[33] many other IR LED based optical gas sensors were reported.[34] Other than IR region yellow-orange LED,[35] deep UV LEDs (at 280 or 255 nm)[36,37] were also employed for O_3, SO_2 and NO_2 gas detection respectively. Currently deep UV LEDs below 240 nm (UVC) are also developed. Most of the organic molecules get absorb in UV region and excite fluorescence in most biological autofluorophores.[38] Hence, UV LEDs has potential for characterisation and identification of biological materials.[38,39]

From 2000 to 2010, a significant number of patents resulting from the analytical applications of LEDs were published as demonstrated in Figure 1.5,.[40] Also, a decreasing trend of interest in the analytical applications of fluorescent light and incandescent light technologies is observed in Figure 1.5..

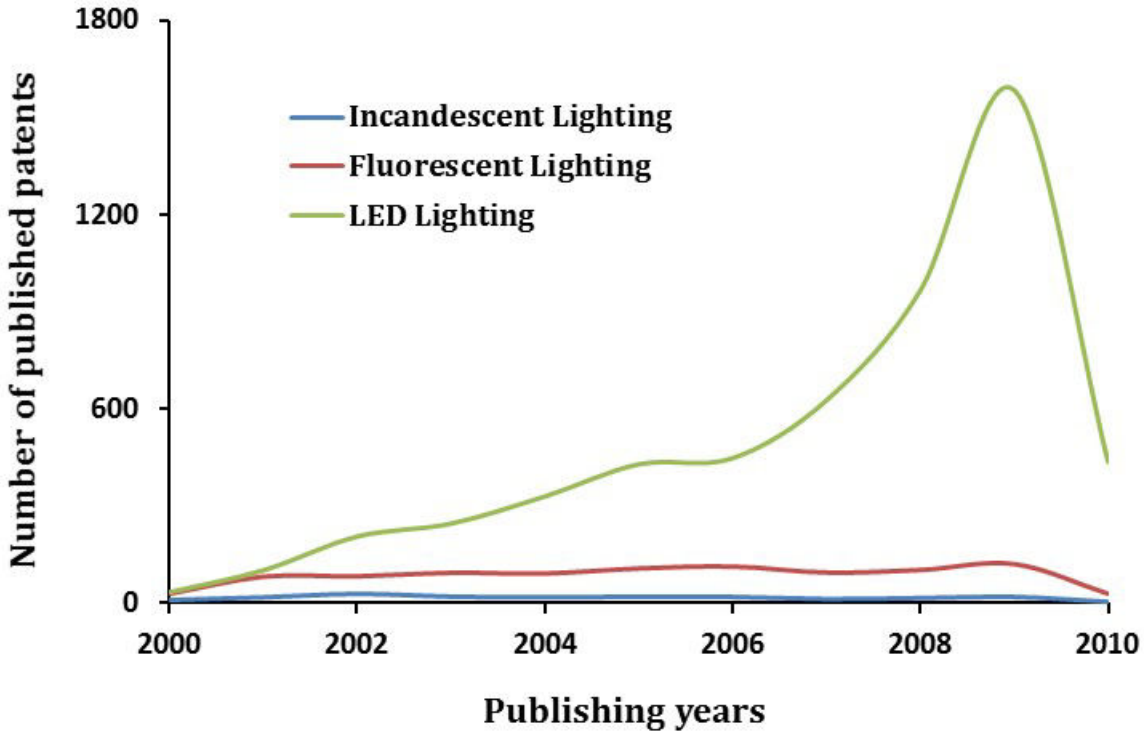

Figure 1.5. The patent trends from the last decades for comparison of the research on three lighting technologies

1.6 Advantages of LEDs over other light sources

Unlike incandescent and gas discharge lamps (a plasma of noble gases argon, neon, krypton, and xenon), LEDs have quite long lifespan and low electricity consumption. Neon lights, although having longer lifetime than incandescent lights, need higher power to operate. With LED, it is possible to obtain same luminosity as incandescent light using very low electric energy. Hence LEDs are cost effective in terms of energy, maintenance and cost saving.[41] In

addition, switching with low energy causes less CO_2 emission and hence LEDs are environmental friendly.[8]

LEDs have no risk of destruction on vibration and higher resistance to shock. In addition, small size makes them fit into any portable equipment. Their pulsing capability is tremendously good with high switching speed and some of them are meant to turn on and off with logical-level of voltage signal.[42] In short, LEDs deliver following advantages compared to the conventional light sources:

- 75% less energy needed, 25 times longer lasting than incandescent light and 3 times longer than fluorescence lamp.

- Instant lighting no warm-up time is needed in fluorescence lamp

- Less heat dissipation and unidirectional lighting is obtained

- Compact and robust due to small LED chips and no filament damage

LEDs produce nearly one colour light, but their availability is limited with blue, yellow, green, orange, red, IR and white colours, where the colour depends on the semiconductor materials as well as the epoxy lens that covers the LED chips. And for more than one colour, LEDs are built with two or more chips in it. LEDs deliver lighting in numerous electronic devices like lift, airport and rail crossing signals, mobile phone displays, televisions, computers and advertisement signage, video screen in stadium, in microscope and microscopic surgical instruments. IR LEDs from 940 nm wavelengths are usually used in TV

remote controlling, sensing and data communicating applications. Nevertheless, LEDs need defined electric current to drive them and if the current exceeds the maximum allowable limit LEDs burn out immediately.

1.7 Radiometric characterisation of LEDs

Radiometric characterisation of LED involves assessment of principal radiometric properties such as radiometric power output, radiant intensity, irradiance, radiance, radiant efficiency, fluence and spatial directivity (defined in chapter 2). Radiometric characterisation of LEDs can be undertaken using two fundamental techniques, i) physical method and ii) matrix or solution based techniques. Physical radiometric characterisation is mainly based on spectrophotometric methods whereas solution based radiometric characterisation is based on actinometric or dosimetric methods. The following actinometric and spectrophotometric methods are frequently used for radiometric characterisation of LEDs:

1.7.1 Actinometric Method

Actinometric method is based on standard photo sensitive chemical system whose rate of the photochemical reaction is known and is used to radiometrically characterise the visible light and UV radiation quantitatively (in terms of fluence, irradiance or radiometric power output) by determining the photon flux of the photochemical reaction of that standard photo sensitive chemical system. One of the advantages of actinometric method is that it is a calibration free measurement, and independent of any specific optical or geometric design, therefore, is comparatively inexpensive and easily adaptable method.[43] It is one of the oldest and most accurate and absolute method of radiometric characterisation of light sources.[44] The outcome of this method is very much dependent on the quality of reference actinometer and its

handling procedure. In Figure 1.6 schematic representation of the LED measurement with chemical actinometry is shown.

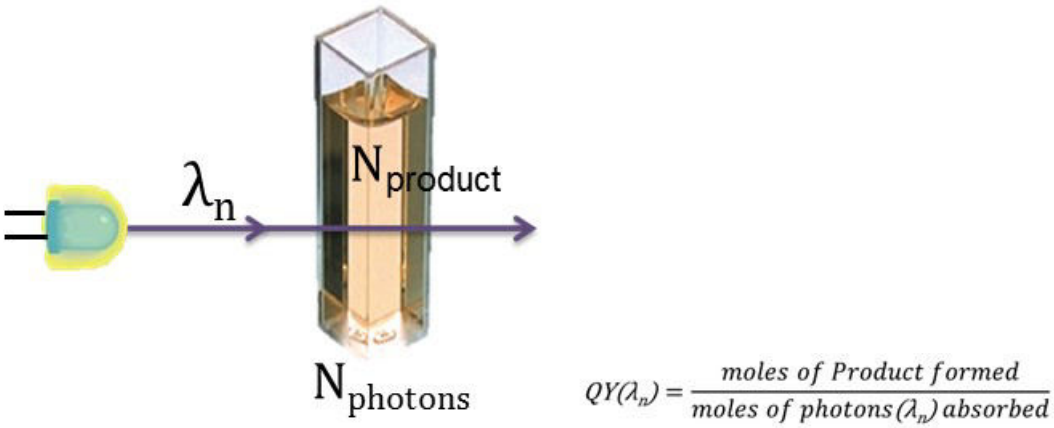

Figure 1.6 Schematic representation of characterisation of LEDs with actinometric

In Kuhn et al.,[45] 67 liquid, 22 gaseous and 9 solid state actinometers applicable from UV to red wavelength region were elucidated along with standard procedures. Solid state chemicals which were used to measure the radiation by estimating the exposure in biological organisms were termed as dosimeters instead of actinometers and most of the dosimeters were used to measure the radiation in UV region.[43,45] Among the liquid phase actinometers, potassium ferrioxalate actinometer, which was first proposed by Hatchard and Parker in 1956,[46] is the most extensively applicable in wide range of wavelengths from 250-500 nm. Another liquid state actinometer (known as iodide/iodate actinometer[47]) is suitable to radiometrically characterise LEDs in UV region (250-280 nm) where potassium ferrioxalate also works.[43] To the contrary, wide range of wavelength region between 316-750 nm (UV-Vis-NIR) are covered by Reinecke's salt actinometer (ammonium tetrathiocyanato-diamminechromate

(III)) and 208-426 nm spectral ranges are covered by uranyl oxalate.[48] However, no actinometers are currently sensitive towards wavelengths longer than 795 nm.

1.7.2 Spectrophotometric method

Spectrophotometers are widely utilised for radiometric characterisation of LEDs with sufficient spectral resolution. Any spectrophotometric method for light source characterisation require the spectrophotometer to be radiometrically calibrated using a calibration light source.[49] For small light sources from UV to infrared wavelengths that emit as intrinsic point source, bare fibre, cosine correctors[50] and integrating spheres[5,51] have been utilised along with the spectrophotometer to characterise the LEDs.

Integrating sphere

Characterisation of LEDs using integrating sphere is endorsed by International Commission on Lighting's (CIE 127:1997).[52] An integrating sphere is an optical component consisting of a hollow spherical cavity with its interior covered with a diffuse white reflective coating, with small holes for entrance and exit ports. Its relevant property is a uniform scattering or diffusing effect. Inner wall of the integrating sphere is coated with a Lambertian diffuser materials[e] like barium sulphate ($BaSO_4$), halon, opaline glass, PTFE or Spectralon® which provides >98% reflectance.[53]

CIE recommended geometry for the LED measurement are shown in Figure 1.7. For this measurement, the integrating sphere should be connected with a spectrometer through a fibre-optic cable and an auxiliary lamp may be required for further absorption correction.[52] The crucial need for this CIE 127 recommended integrating sphere based LED measurement are

[e] the materials diffusely reflecting surface's luminance is isotropic, and the luminous intensity obeys Lambert's cosine law

(i) spectral wavelength calibration and (ii) cosine correction for spatial and spectral distribution of LED. To maintain the quality of measurement, National Institute of Standards and Technology (NIST) has established calibration method for LEDs within the range 360 – 830 nm using gonio-spectroradiometer system.[46] Moreover, according to CIE 127,[4] influence of environmental circumstances and contamination in the sphere material, expiry of calibration of the spectrophotometer, LED position, ambient light, integration time, resolution also effects the measurement based on integration sphere.

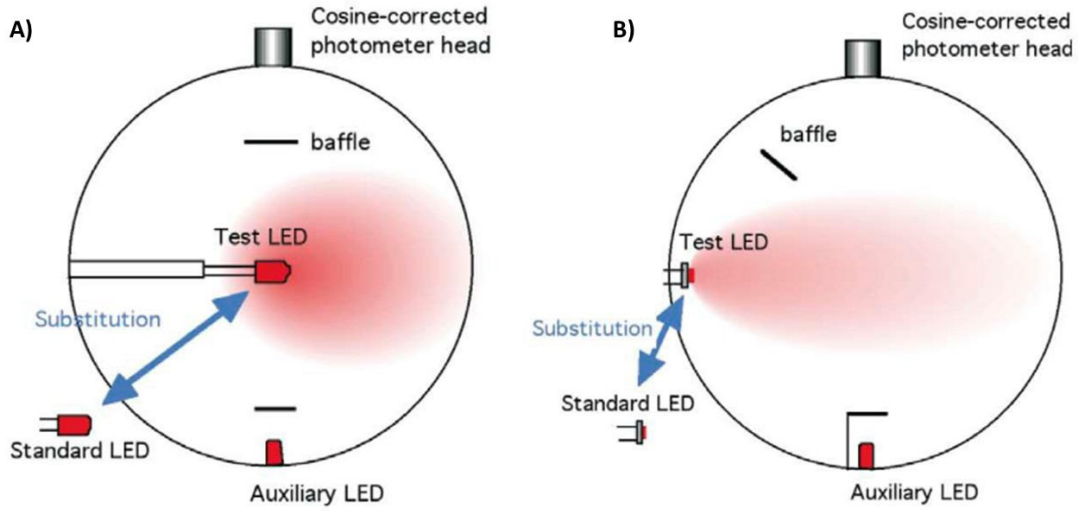

Figure 1.7 Schematic representation of CIE recommended geometry for characterisation of LEDs A) for all types of LEDs B) for LEDs with no backward emission[4]

Cosine corrector

In principle, light intensity (I) is proportional to $I_{max}cos\theta$, (Lambert's cosine law) where θ is the angle of incidence of the light beam.[54] If the angle of incidence light on the surface increases from 45° to 90°, then the light will not follow this principle which results error in radiometric measurement.[54] By using "cosine corrector" this effect can be minimized.[54] Cosine correctors are made of diffused materials same as integrating sphere ($BaSO_4$, opaline

glass, PTFE or Spectralon) and are also known as optical diffuser. For the LED characterisation the cosine corrector is usually installed to optical fibre head[56,57] which redistribute the incident light and this corrected signal is collected by the spectrophotometer or other detector. In Figure 1.8 the scheme of radiometric characterisation of LED by spectrophotometric method using a cosine corrector is illustrated.

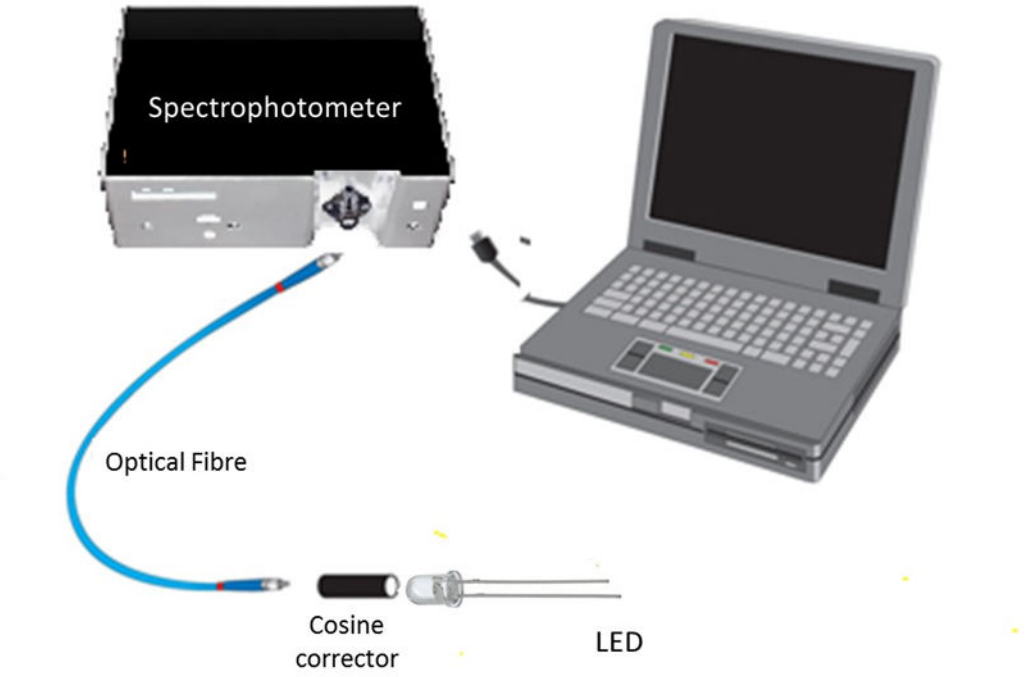

Figure 1.8 Radiometric characterisation of LED by spectrophotometric method using cosine correctors

Bare fibre

Optical fibre having a higher refractive index is the most commonly used waveguide in any optical measurement. Fibre optics consists of a core fibre where light is guided in a core region and provides maximum internal reflection. For light measurement in visible region, glass fibres are suitable, whereas in UV region, silica is required. For radiometric

characterisation of LED, bare fibre can be attached with the LED while the other end of the bare fibre is connected directly with the spectrophotometer.[58]

To maintain the quality of each of the above-mentioned spectrophotometric measurements, wavelength calibration for spectrophotometer, optical fibre, integrating sphere and cosine correctors are required. National Institute of Standards and Technology (NIST) has established calibration method for LEDs within the range 360 – 830 nm using gonio-spectroradiometer system.[5] However, the uncertainty (expanded uncertainty, k=2) for LED calibration increases at UV and blue region since significant fluorescence from the coating of integrating sphere is emitted while measuring UV LEDs and deep-blue LEDs.[58] Nonetheless, NIST has developed correction algorithms to correct the effects of fluorescence of the internal coating materials of integrating sphere and the spectral stay light for CCD based spectroradiometer.[59]

PART B GAS MONITORING AND ANALYSIS

1.8 Environmental monitoring and analysis of Gases

Gas monitoring is carried out to measure the extent of unwanted gaseous substances (air pollutants) present in air, which deteriorate the air quality and cause adverse effects on life and property. To maintain the air quality and to stipulate mitigative actions, it is also important to analyse the sources of air pollutants, the chemistry, and its concentration, effect and how to minimize it. Some of the air pollutants such as, volatile organic compounds (VOCs) which is in gaseous, vaporous, mists or dust form can cause explosion in presence of ignited sources with air when their concentration arise above a certain level. Hence, to ensure safety from explosion it is necessary to monitor these substances. In short, gas monitoring and analysis is needed for the following reasons:

- Maintain atmospheric air quality - ambient air quality and greenhouse gas (GHG) monitoring
- Ensure safety – indoor air quality monitoring in mine, factories, petrochemical and automotive industries
- Reduce cost (fugitive emission) – industrial production, other chemical facilities, etc.
- Ensure sound health – indoor as well as outdoor air quality monitoring, landfilling sites, other occupational health and safety.
- Identification of individual gases – qualitative and laboratory scale monitoring

1.8.1 Current practices in gas monitoring

There are three common practices in gas monitoring:

- Indoor gas monitoring
- Outdoor gas monitoring
- Greenhouse gas monitoring

Indoor air monitoring is needed, since most people spend their maximum time (80%) indoors and it is significant for moderate climate countries (most of the European countries). Indoor environment includes the residential buildings, non-residential buildings such as offices, schools, hospitals, stores, restaurants, and other confined working places (e.g., factory, laboratory, mine, transport facilities). The total contribution from the various activities to the indoor air affect the health and wellbeing of the occupants.[60,61] However, the tropical countries with high traffic volumes and dense population (many Asian countries) and industrialised countries, outdoor air monitoring is more significant. Additionally, ambient (outdoors) air analysis is considered extremely significant near landfills, filling stations, agricultural fields, excavation sites and probable explosive regions (e.g., volcano).

1.8.2 Important air pollutants

Air pollutants are the unwanted substances that change the natural atmospheric composition. Air pollutants can originate from both natural and anthropogenic sources. Anthropogenic sources could be stationary as well as mobile type. Big stationary anthropogenic sources are manufacturing and processing industries, power plants and landfills. To the contrary, small factories, dry cleaning, degreasing processes, household activities are small static sources. Emission from numerous vehicles such as cars, buses, trucks, trains, aircrafts even lawn mowers contribute to the air pollution as mobile sources. Air pollutants are also generated

from natural sources such as volcanic eruption, mines and air blown dusts as well as from biological sources like pollens, animal excretions and hairs. According to the Department of Environment and Energy, Australia, air pollutants are categorized into three main groups[62]:

a) Criteria Pollutants
b) Air toxins
c) Biological Pollutants

a) Criteria pollutants

Widely distributed six air pollutants that are used as ambient (outdoor) air quality indicators are collectively known as criteria pollutants.[60] The clean air act requires Environmental Protection Agency (EPA), US to set National Ambient Air Quality Standards (NAAQS) for six common air pollutants. EPA Australia has adopted the criteria pollutants that were mentioned in the clean air act of US. They are:

1. Carbon monoxide (CO)
2. Lead (Pb)
3. Nitrogen Oxide (NO_X)
4. Ozone (O_3)
5. Particulate matter (PM_2)
6. Sulphur dioxide (SO_2)

In Table 1 the main sources, health effects and the most vulnerable groups affected by these pollutants from are listed. The information in this table is collected from United States

Environmental Protection Agency, Australian Government Department of Environment and Energy and World Health Organization.

Table 1 Information about the main sources, health effects and most vulnerable groups of six internationally recognised criteria pollutants are listed [61,63-64]

Pollutants	Sources	Effect	Most vulnerable group
Carbon monoxide (CO)	Main source of CO is vehicle emission, bushfire, volcanoes, tobacco smoke and some industrial activities (e.g.: steel manufacturing)	High level of CO in air causes serious effect to human health, since it reduces the amount of oxygen carried by haemoglobin, subsequently, causes malfunction, the vital organs like brain, heart, nervous tissues, and if the concentration of CO increases more than 40% it kills human.	The newborns, children and heart patients are in serious risk for increased CO level
Lead (Pb)	**Natural:** soil erosion, volcanic eruptions, sea spray and bushfires **Anthropogenic:** Lead smelters, mining operations, waste incinerators, battery recycling, the production of lead fishing sinkers, lead-based plant, emission from lead added petrol fuel	Lead fume or dust through breathing or swelling comes to the human bodies and biomagnification causes pain in joints and muscles. Other effects are anaemia, nausea, gastric problems, sleep problems, concentration problems, headaches, and raised blood pressure. To the children: poor development of motor abilities and memory, reduced attention span, and colic and gastric problems.	New born and unborn babies (fetal) and the pregnant woman are in high risk.
Nitrogen oxides (NO_x)	Burning of fossil fuels (coal, oil and gas) from motor vehicle exhaust (about 80%), coal-fired power stations, petrol and metal refining, other manufacturing industries and food processing, gas heaters and cookers	It helps in the formation of photochemical smog, which can have significant effects on human health. When NO_x is in high level it increases the probability of respiratory problems and decrease the lungs infection immunity and causes wheezing, coughing, colds, flu and bronchitis.	People with Asthma, especially children, older people with heart diseases

Ground-level ozone (O_3)	O_3 forms in presence of sunlight from NO_X and some reactive organic chemicals by photoreaction and these chemicals comes from the emission of vehicle, petrochemicals industries, printing inks, lawn mowing, aircrafts, bushfires and burning off	If exposed to high level of ground-level O_3 people may feel chest, ears, eyes, nose, throat pain and coughing	People with asthma
Particulate matters (PM)	**Natura**l: wood smoke from bushfires, dust from storms, pollens and sea squirt. **Anthropogenic**: motor vehicle exhaust, industrial processes (e.g. electricity generation, incinerators and stone crushing), unlined roads and wood heaters.	Respiratory illness (like Asthma and bronchitis) [63] and cardiovascular diseases [64], some (from combustion) may cause cancer In addition, it reduces the luminosity and cause accident in roads and highways	Newborns and older people
Sulphur dioxide (SO_2)	From Sulphur contained fossil fuel combustion (vehicles exhaust, electricity generation, etc.), Sulphur contained mineral processing and other industrial material processing, material that contains sulphur like fertilized industries	On inhalation causes irritation of respiratory system, coughing and breath problem	People with asthma and respiratory problem

b) Air toxins

Air toxins are sometimes known as hazardous air pollutants (HAPs) which include the heavy metals, volatile and semi-volatile organic compounds (VOC and SVOC).[67] Although they are present in the air at small concentrations but persist for long time and have serious health effects. The organic pollutants that persist longer than any other pollutants are known as persistence organic pollutants (POPs). Some of these air toxics are reactive organic compounds and they contribute in the formation of ground level ozone in presence of sunlight and as mentioned in Table 1, they cause potential health risk in terms of cancer, genetic disorder, immunodeficiency, nervous system and respiratory system defects. VOCs are significant GHGs since they contribute in creating ozone hole and global warming.[68] They play significant role both as indoor and outdoor air pollutant.[69-72] In some cases indoor VOCs' levels are higher than the ambient atmospheric air,[67] and hence, indoor air pollution (IAP) sometimes impulses greater concern. Exposure to high concentrations of VOCs causes numerous health problems, which are both acute as well as chronic (due to long term exposure) respiratory problems, central nervous system disorder, mucous, dermal, eye, nose irritation and cancer.[71,73]

Generally, VOCs are alkanes (n-alkanes, cycloalkane), aromatics, such as benzene, toluene, ethylbenzene, xylene (BTEX) and chlorinated hydrocarbons (e.g. chloro fluoro carbon (CFC), vinyl chloride), terpenes, etc.[74] Petrochemical industries are considered as the main sources of these pollutants.[75]

c) Biological pollutants

Common biological pollutants are air borne bacteria, virus, cockroaches, rodents, cat saliva, moulds, mildew,[76] animal dander (dry skin), carpet dust mites, infectious agents as well as pollen.[65] Typical biological pollutants such as mould, mildew and other infectious agents come from water damaged surfaces and materials. The microorganisms need water to propagate and rainwater on the building wall, humidifiers, stagnant water and even water vapor produced from daily domestic works such as cooking and showering contributes moisture in air and thus create suitable environment for biological pollutants to propagate.[76]

The health effects of this type of pollutants are of three types:

- *Infection* - influenza, measles, chicken pox, etc.,
- *Allergic reaction* – Asthma, allergic rhinitis, hypersensitive pneumonitis, allergic reaction causes with long exposure of these pollutants
- *Toxic effect* - may cause by direct inhalation of micro toxins

Coughing, watery eyes, breathing problem, headache, and indigestion problems are also some common health effects from biological pollutants. The elderly people, kids and people with lung problems are vulnerable to biological pollutant borne diseases. By controlling the moisture level in the indoor environment and proper ventilation, it is possible to control the growth of the moisture-building microorganisms (mould, mildew, bacteria, virus and fungus) and reduce dust. Likewise, by keeping the house clean and by cleaning or replacing the carpets, growth of biological pollutants such as dust building mites can be controlled.

1.8.3 Significance of alkanes and methane in air analysis

Although VOCs present in the ambient air in low concentration, due to high level of potential hazardous risk, VOCs are considered as significant air pollutant.[77] Alkanes (n-alkanes, cycloalkanes) are the most dominant VOCs in the atmosphere.[70,74] They are identified to play parallel role both in indoors and outdoors air quality. Indoor VOCs originate from many domestic products such as construction materials (paints, adhesives, waxes, particle board and plywood flooring, vinyl flooring, including carpet), household cleaning materials (solvent, detergents, fabric softeners, dry cleaning fluids, spray propellants), ink from printer and photocopier, newspapers, pen, marker, cosmetics (hair spray, perfumes) and also from the outdoor sources' incursions.[67,78,79]

In the ambient air (outdoor) 50-60% of these alkanes are unburned gasoline and originate from vehicle exhaust.[80] Additionally, landfill facilities i.e. the common solid waste management (SWM) practices in urban communities are one of the major sources of hazardous air pollutants (HAPs). Landfills emit various VOCs which are mainly methane (50%), carbon dioxide (40%) and numerous non-methane VOCs (such as BETX, vinyl chloride, dioxins and polycyclic aromatic hydrocarbons).[81] The workers in landfill sites and the population living nearby are at the maximum direct exposure risk to HAPs and direct inhaling of HAPs may pose significant threat to their health. Workers in mining industries (e.g., oil, gas, coal), petrochemical industries and filling stations are also at direct exposure risk of VOCs (methane and other alkanes) in the same manner as landfills. Moreover, VOCs that are flammable, pose elevated risk of explosion when concentrations present between lower explosion limit (LEL) and upper explosion limit (UEL). Additionally, health and wellbeing of occupants of residences, laboratories and

factories become compromised under the exposure of methane and other alkanes from gas heater, burner, natural gas (NG) pipe leaks and gas cylinder leaks.[82-84] Hence, alkane gas analyses in terms of rapid sensing and profiling through continuous monitoring, particularly the analyses of methane as a model alkane gas, is extremely important to safeguard human health and wellbeing.

1.9 Gas sensing techniques

Gas sensing is noteworthy in the areas where there is a potential risk associated with toxic gases. Monitoring of hazardous gases that are flammable is necessary in residential areas and often obligatory in filling stations, petrochemical industries as well as in oil and gas mines. Additionally, gas sensing is necessary in automotive industries to monitor unburned hydrocarbons such as VOCs in vehicles exhaust (as well as during indoor air quality supervision and environmental studies such as GHG monitoring. Consequently, gas-sensing techniques differ depending on originating source, types and circumstances.

1.9.1 Brief history of gas sensing

At first, gas sensing came into concern in 1956 after publishing the Clean Air Act by United Kingdom[58] and now-a-days, it has become obligatory in most countries of the world. Earlier, flame safety lamps were used as a combustible gas detector[85] that usually acted as a light source in mines and sewer, but these are completely obsolete in modern days due to lack of accuracy (25%-50%) compared to real values. Afterwards the low cost and gas specific catalytic bead sensors superseded the combustible gas sensors.[86] The oxidation reaction of combustible gases occurs in the sensor head and the exothermic heat of reaction changes the head temperature, subsequently changes in electrical resistance

and by measuring this thermal change, concentrations of gases are measured.[87] This type of sensor works on thermal sensitivity, and burns out in exposure to higher gas concentration, results false alarm as well as shortened lifetime (1-2 years).[88] Additionally, both of the aforementioned sensors (combustible gas detector and catalytic bead sensors) suffer from background gas interferences (e.g. water vapour) and ambient temperature change.[34] Since late 1980 (when Japanese legislators imposed the requirement of gas sensors in the residential area where gas cylinders were used) semiconductor gas sensors found widespread use due to low cost, robustness and high sensitivity. Semiconductor gas sensors typically endure 10 years or even more in clean application and are also suitable to use in analytical purpose.[86] However, semiconductor gas sensors are not gas specific and hence are not suitable for industrial gas detection.[86,88] Furthermore, semiconductor sensors may die down (lose sensitivity) if they remain unused for long periods.

Electrochemical gas sensors having 2-3 years of lifespan are gas specific and applicable to a number of toxic gases.[89] Besides, they have outstanding reproducibility, linearity and minimal energy consumptions. However, these sensors have limitations since a little oxygen concentration is needed to work properly and an additional filter is needed to absorb the interfering gases. Like catalytic and combustible gas sensors electrochemical gas sensors are sensitive to temperature and humidity. Therefore, gas sensors with advanced gas detection mechanisms are needed in order to improve of these to overcome the existing capability gaps of above mentioned gas sensors.

1.9.2 Commonly used gas detection technologies

Gas sensing techniques are highly selective towards its application.[90] Sensitivity, stability, selectivity, robustness are key indicators regarding the performance of any gas detection techniques.[91,92] To develop economic and fast responsive gas sensors with minimal energy consumption, shorter period of signal generation is desired.[90] To meet these various requisites, different gas sensors were developed progressively based on various detection techniques. Some of these commonly used gas detection techniques are briefly described below.

a) Flame ionisation detector (FID)

Flame ionisation detectors (FID) are the most familiar to detect the concentration of hydrocarbon in gaseous stream and are extensively used in gas chromatographic (GC) based detection system. FID system relies on the proper functioning of a number of individual elements.

Basic Principle:

In a typical FID, the carbon containing compounds are ionized by using hydrogen-air flame. The ion is collected towards an electrode and is driven by electric potential, which results an electric current signal. The current produced is proportional to the amount of sample being burned. The resulting current is converted into voltage signal in an electrometer, which is filtered, and amplified as required and measured to determine the concentration of the compound. In Figure 1.9[93] the typical diagram of a flame ionization detector is shown. The fuel gas (H_2) enters through the bottom of the column, mixes with

carrier gas (air) in the flame chamber and blows the flame jet. A negative electric field is produced between the jet tip and the collector electrode. Whenever the ion is formed it impels toward the jet tip by the applied electric field and the resulting current is measured by an electrometer.

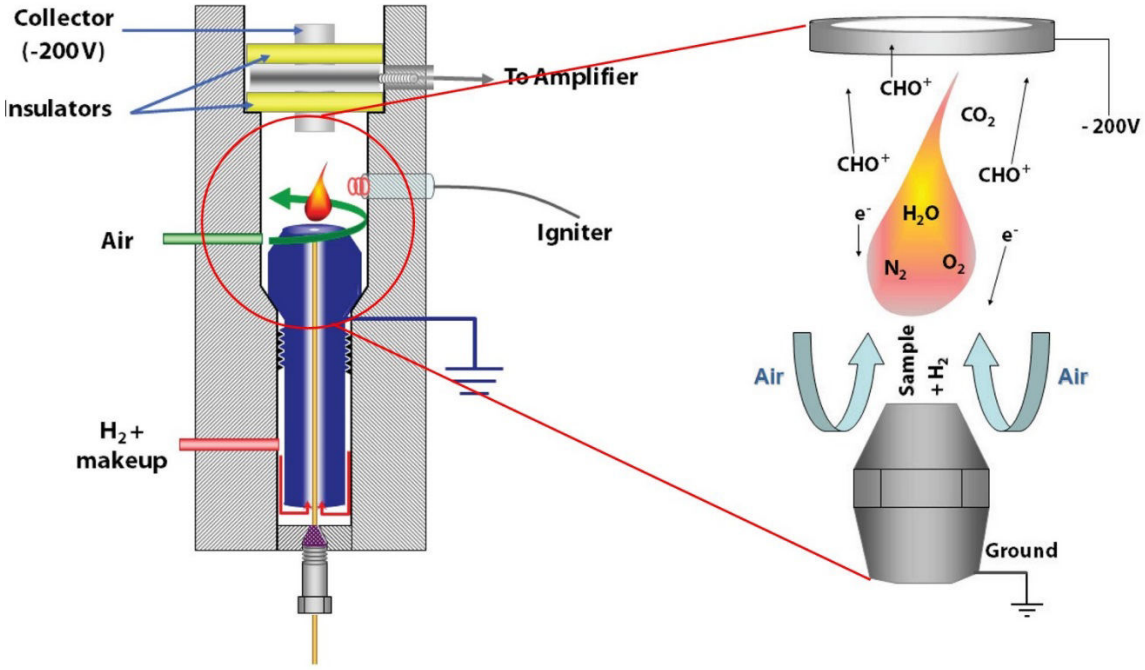

Figure 1.9 Scheme of a typical FID detector

During combustion, all organic gases produce CO_2 and H_2O in presence of air and hydrogen burning in the detector. Again, chlorinated hydrocarbons and CS_2 are not completely combustible which produces large amount of unburned hydrocarbons (HCs), carbon soots (C) as well as HCl or CCl_4. Unburned HCs, carbon soots aggregate between the jet and the collector electrode, which causes electric leaking and lower signal-to-noise ratio (SNR). Additionally, long-time exposure to HCl in presence of H_2O forms corrosive HCL acid, which corrode the detector wall. The flow rate of the sample gas, carrier gas,

the diameter of the exit, location of the collector and temperature affect the sensitivity of FID.[94] To avoid explosion, care must be taken during the handling H_2 gas, which is extremely flammable. Moreover, hydrogen fuel is very expensive which needs to be refilled frequently and large size of the detector makes them difficult to use as a portable gas monitoring system.

b) Photo-ionization detector (PID):

The photoionization detector is an efficient and inexpensive detector for many gases and vapour analyses. A PID can produce instantaneous readings and operate continuously. It is a precise method for the detection of lower level (ppm) organic gases.

Basic Principle:

UV light that has higher frequency and therefore, more energy, alit on the gas sample, which temporarily displaces electrons from the gas molecule, creating an ion. The free electrons thus produced are collected at the electrodes resulting in a current flow whose magnitude is directly proportional to the gas concentration. In Figure 1.10 the configuration of a typical PID detector is shown. UV light source is the main component in this detector and the choice of lamp depends on target gases, selectivity requirements and lamp lifetime considerations. Previously, expensive vacuum tube electrodes were used as a photon source (lamp) in PID. Now a day, UV lights with different wavelengths are produced by using different inert gases using high voltage. Generally used inert gases are krypton (photon energy =10.6 eV), xenon (photon energy =9.6 eV), and argon (photon energy = 11.7eV).

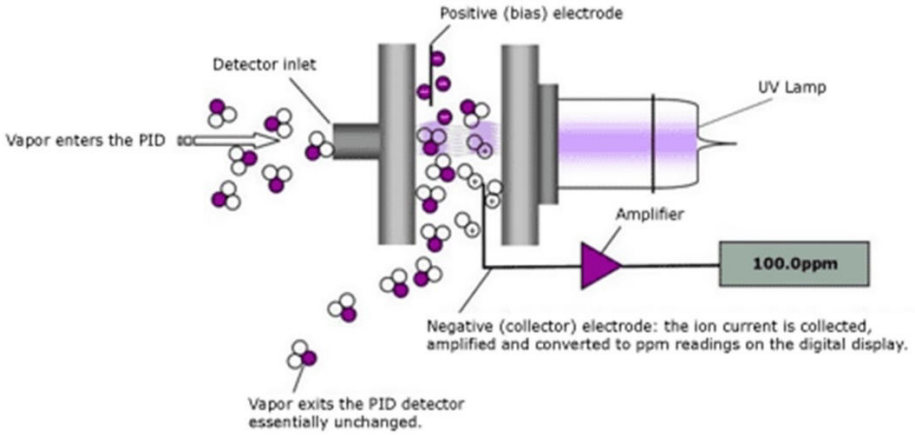

Figure 1.10 Typical configuration of a photoionization detector [95]

This technique is best suited with organic gases that have lower ionization potential and particularly the choice for VOCs' detection. Gases with higher ionisation potential like methane are not possible to be detected by PID. Although PID is suitable for low concentration determination, they were not reported to detect the lower explosive limits (LEL) of many explosive gases.[96]

c) Gas chromatography and mass spectrometry (GC-MS)

GC-MS is the combination of two techniques gas chromatography (GC) and mass spectrometry (MS), where GC is used to separate the chemical mixture according to their volatility and MS identifies the chemical based on their structure. By combining these two techniques one can qualitatively and quantitatively evaluate mixture of sample containing a number of chemicals.

Basic Principle

A sample, mixture of hydrocarbons or any other complex structure and composition, which are injected to the GC column with a syringe, are heated in the oven. In the GC column, the samples are separated according to their volatility, chemical properties and composition. The lighter fractions of the sample separate out from the heavier fractions in the GC column and travel through the chromatographic column (a part of GC/MS instrument) to the MS (Mass Spectrometry) section, where it acts as the detector. In the MS section, the separated fragments get ionized and form a fragmentation pattern. Every sample has a different composition and hence the fragmentation pattern for a given sample is unique and these fragment patterns are specific enough that they are often referred to as the molecular fingerprint. In short, the GC component acts as a separator that separates the chemical mixtures, and the MS section identifies the component at a molecular level.

Figure 1.11 illustrates the basic components of a modern capillary GC-MS system, where GC has an injection port; column in an oven and the MS needs an ion source, filter and detector. And these two coupling instruments are connected to an output device to process the data and make the graph.

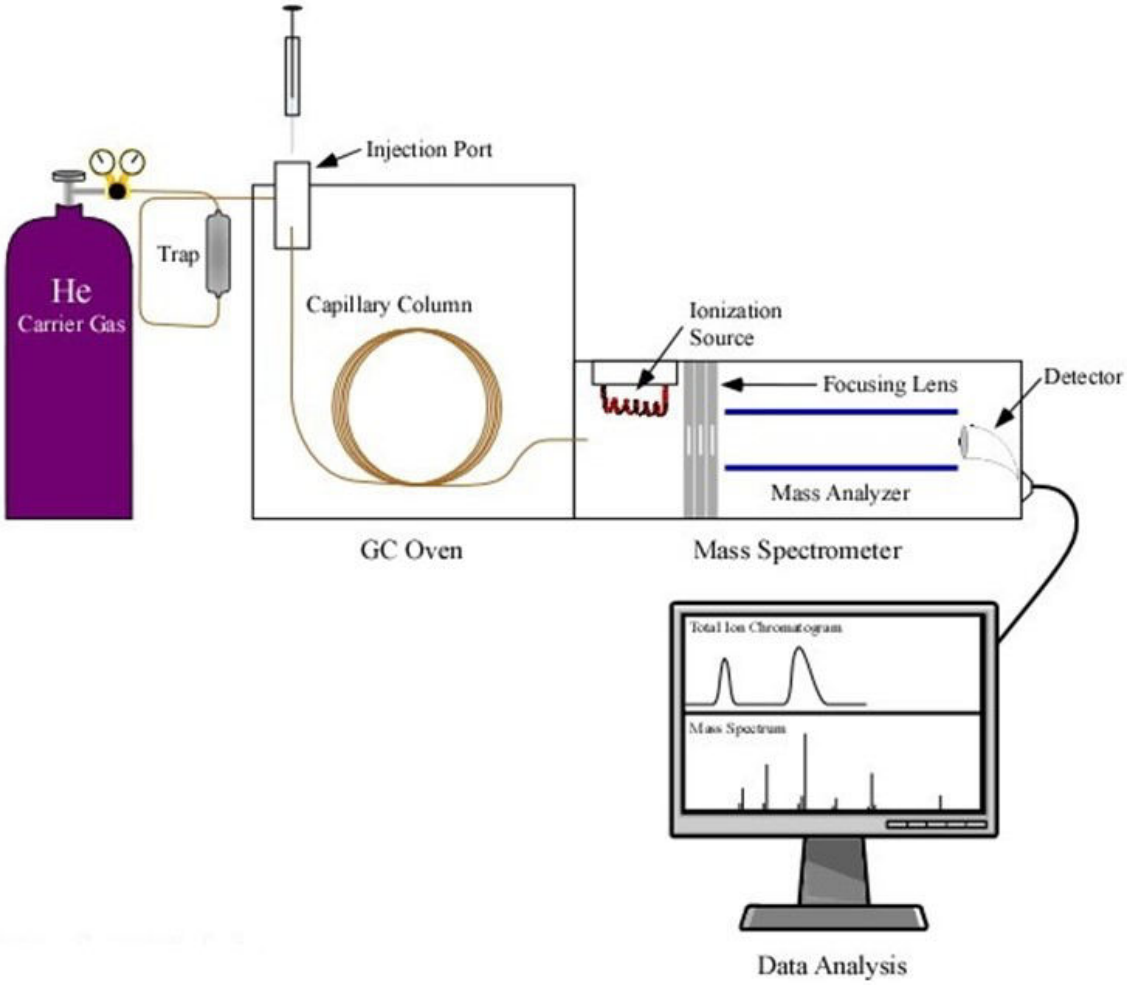

Figure 1.11 The major components of a modern capillary column gas chromatograph – mass spectrometry (GC-MS) system [90]

There are versatile uses of GC-MS and it is abundantly used in medical, pharmacological, environmental, and law enforcement fields. From existing research, it is found that in air pollutant analysis GC-MS best suits for VOCs and SVOCs analysis. Kataoka et al.[78] established it as a reliable technique for VOCs analysis and investigated the indoor VOCs level as well as characterized them, while Massolo et al.[74] investigated both the indoor (school and houses) as well as outdoor (traffic exhaust) VOC and identified them, and measured the concentration of the detected gases. On the other hand, Zhou et al.[73] used GC-MS for detecting the vehicle exposure by performing the analysis on 12 particular

VOCs. Each of these detection and quantification went through air sampling, which is an extremely laborious job. After sampling, the sample needs preparation before injecting in the GC column, and eventually the sampled air never represents the real condition of the polluted air. Hence, this technique limits the scope of in situ monitoring and emphasis on laboratory experiment only.

d) Optical methods

Optical methods of gas sensing are based on optical absorption, fluorescence, emission, scattering or ionisation of a gaseous species in presence of specific wavelength of light. Optical methods of gas sensing are highly sensitive and selective method for quantitative and qualitative analysis and sensing of gaseous species.[97] There are a number of advantages of gas sensors based on optical method over the classic gas sensors. In contrast to other gas sensors the optical gas sensors has longer life expectancy. Since there is no chemical reaction involvement in optical method of gas sensing (physical process of sensing is involved only), these type of sensors have higher sensitivity, selectivity, stability and rapidness. Most of them remain unaffected with change in atmosphere and is free from cross-response with background gases.[34] Moreover, they are inherently secure and can operate without oxygen.[98] The most commonly used optical gas sensing techniques are Fourier transform infra-red (FTIR), photoacoustic absorption spectroscopy (PAS), tuneable diode laser absorption spectroscopy (TDLAS), non-dispersive infra-red (NDIR), cavity ring-down spectroscopy (CRDS), differential absorption light detection and ranging (DIAL), UV absorption, UV fluorescence, UV differential optical absorption spectroscopy (DOAS), Chemiluminescence and photo-ionisation.[90] Among these optical techniques FTIR, TDLAS, NDIR, gas filter correlation

spectroscopy, UV absorption, UV DOAS, PAS, CRDS, are developed employing optical absorption principle. Many industrially and environmentally important gases, which absorb infra-red (IR) light, are possible to sense using IR absorption spectroscopy.

Principles of optical absorption based gas sensing

Since many of the explosive and toxic gases have strong absorption bands in different wavelength region[99] they are possible to sense using absorption spectroscopic method. Optical absorption techniques are based on application of the Bouguer's or Beer–Lambert Law[100] and according to this law the intensity of light passing through a sample relates to the concentration and initial light intensity

$$\tau_v = I_v/I_0 = \exp(-\alpha_v c\ell) \quad (1)$$

where τ_v is the gas transmittance which is the ratio of received to incident light, I_v is the light transmitted through the sample cell, $I_0$is the light incident on the sample cell, α_v is the absorption coefficient of the sample at wavenumber v (typically with units of cm^{-1}) and ℓ is the optical path length of the sample cell (typically with units of cm) and c the sample concentration (in units of molecules per cm^3). In Figure 1.12 a simple illustration of Beer-Lambert law is shown.

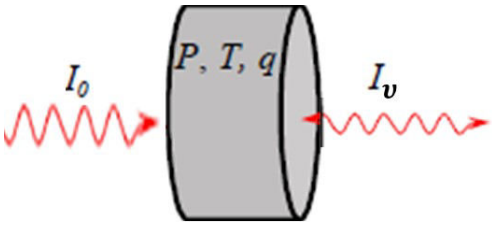

Figure 1.12 Absorption of light by a sample

For an ideal gas at pressure P, temperature T and volume mixing ratio q, the absorption coefficient α_ν can be written as equation (2)

$$\alpha_\nu = \frac{qP}{kT}\sigma_\nu \tag{2}$$

where k is Boltzmann's constant and σ_ν (cm^2/molecule) the absorption cross section and all spectral dependence is contained in the cross section. Then Beer-Lambert law can be written as

$$\tau_\nu = \exp\left(-\frac{qP}{kT} lc\sigma_\nu\right) = \exp(-uc\sigma_\nu) \tag{3}$$

where $u = \frac{qP}{kT} l$ is the mass path and gives the number of molecules per cross sectional area in the path (molecules/cm^2). To further isolate the spectral dependence the cross section is expressed as the product of a spectrally independent line intensity, S, and a spectral line shape g_ν,:

$$\sigma_\nu = Sg_\nu \tag{4}$$

S has units of cm^{-1}/(molecule/cm^2), and g_ν has units of 1/cm^{-1}. It is preferable to keep the units for wavenumber and area separated, rather than writing the result as cm/molecule. Therefore, the final expression for the spectral transmittance:

$$\tau_\nu = \exp\left(-\frac{qP}{kT} lcSg_\nu\right) \tag{5}$$

Optical method based on infrared absorption spectrometry:

The gases that have absorbance in infrared (IR) region are suitable to detect by IR spectroscopy based on optical absorptivity.[92] Typically, IR absorption spectrometry is based on interaction (causes change in dipole moment) of IR radiation of specific wavelength with IR active molecules (e.g. molecules in gas sample) resulting the attenuation of the incident radiation and by measuring the transmitted light after absorption, the molecule is identified. Both one point and open path detection is possible with IR gas sensing technology. Single point gas detectors are sensitive to low ppm level within a fixed absorption path length which is determined by the instrument design and suitable for monitoring flammable level of hydrocarbon (HC) gases whereas open path is suitable to cover a wide range of distance within the beam to measure the total gas quantity using a reflector and are suitable where gas dispersion occurs by wind or natural diffusion. Based on instrumental design IR spectroscopy could be multiplex, dispersive and non-dispersive. Among these three categories non-dispersive IR spectrometry is most commonly used because of straightforwardness.

Fourier transform infrared (FTIR) spectroscopy

FTIR is an extensively used, conventional interference based technique in optical spectroscopy by which all the gases that have absorbance in IR region are detectable. Hence, it is a very useful technique in environmental monitoring.

Basic principle:

Like other optical detection technique FTIR needs an IR light source, which guides through an interferometer, where the beam splitter splits the light beam, next the split

light beam reflected in the mirror and finally detected by the IR detector. It can be open–path as well as closed-cell type. In figure 1.13 a simple configuration of an open-path FTIR spectrophotometer is shown.

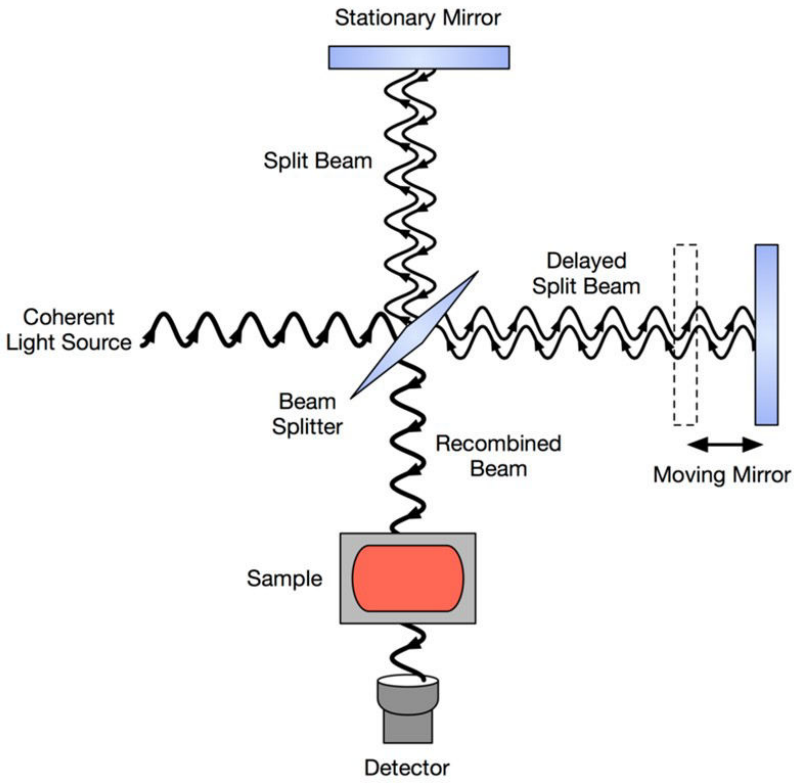

Figure 1.13 The schematic diagram of the major components of a FTIR [101]

The detector detects the interference pattern and transform into IR spectrum by Fourier transform, which could be recalculated into transmittance spectrum. FTIR detection technique is fast responsive, sensitive and has better SNR, which increases the performance, and hence limit of detection (LOD) is improved.

Griffith and Jamie[102] developed a high precision, economic FTIR spectrometry for CO_2, CO, CH_4, N_2O and $^{13}CO_2/^{12}CO_2$ in clean air. Li et al.[103] investigated the use FTIR for

a number of alkanes (n-alkanes and iso-alkanes), sulphur hexafluoride (SF_6), CO and CO_2 in mine environment gas analysis, whereas, Adler et al.[104] proposed advanced FC-FTS (frequency comb-Fourier Transform Spectroscopy) and obtained fast response in ppb level of sensitivity for CH_4, C_2H_6 , C_5H_8 (isoprene) and N_2O. All these investigations were done in the laboratory after sampling the gases by experienced personnel because of the sophisticated nature of the analyses. However, Collins et al.[105] deployed portable FTIR spectrometer in assessing the emission from modern low emitting vehicles. But the FTIR technology based on Michelson interferometer itself suffers from interference fringes and mirror tilting, as well as suffers from water vapor, CO and CO_2 interference, longer setup period, and are highly expensive.[101] Recently, Tanahashi et al.[106] invented a miniaturized FTIR based on Wishbone interferometer instead of using Michelson interferometer which is free from mirror tilting. Although many of the previously designed miniaturized FTIR has the limitation of working in the near infrared (NIR) region only, this recently invented one is in mid infrared region (MIR), but this spectrometer achieved poor resolution with unsatisfactory SNR values.[106]

Tuneable diode laser absorption spectroscopy (TDLAS)

TDLAS is widely used technique for environmental trace gases analysis, continuous emission monitoring, process control, medical, industrial and security applications with over 1,000 field instruments worldwide.[107,108] It is one of the matured and established gas sensing techniques and about 5-10% of commercial IR gas sensors are based on TDLAS.[107].

Basic principle

In TDLS, the diode laser is tuned over a small range to match exactly at the specific wavelength where the target gas has strong spectral absorbance line by adjusting the temperature and bias current.[109] In order to achieve the utmost selectivity, TDLS analysis is assembled at low-pressure condition, where absorption lines are not substantially pressure broadened.[110] Like other optical method, laser is illuminated on the gas sample and the concentration of the sample is calculated by measuring the absorbed light by the sample using Beer-Lambert law. In Figure 1.14 the basic components of TDLS are illustrated. According to the rotational and vibrational motion of the gas molecules it will absorb the light energy from the laser beam at specific wavelength. Unlike FTIR and other spectrometry, TDLS need no monochromators or filter, since laser itself adjusted exactly in one wavelength (or small range), which matches with a gas of interest, thus, less or no possibility of interference from the other gases take place. High power from laser helps the measurement at longer distance and open-path measurement up to 1000 meters as well as useful for remote gas leak detection,[111] photo acoustic (PA)[112] and cavity ring-down spectroscopy (CRDS).[113]

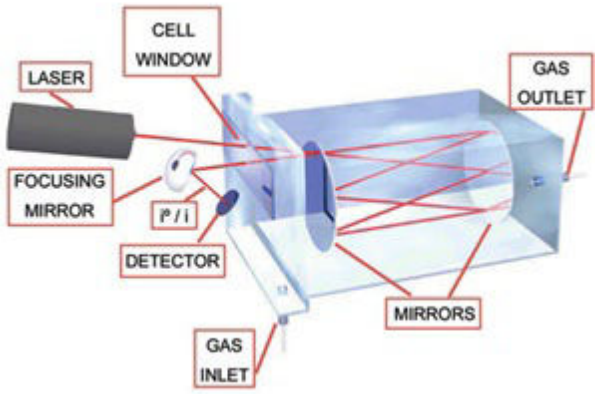

Figure 1.14 Diagram for Tuneable Diode Laser Absorption Spectroscopy[114]

The electrical current driven semiconductor TLDAS are limited by wavelength range and the compounds which has absorbance in NIR from 1.4 to 1.8 micrometre (μm) range is possible to measure using these lasers, whereas, the availability of MIR laser sources are constrained and not suitable for open path measurement. This limitation is met with the Quantum Cascade Laser (QCL), which offers a broader range of wavelength that match with the absorbance of many gases of interest. Laser itself as a light source is noisy which decreases the sensitivity of the detection[110] and are very costly (from $2000 to $3000), which makes the total TDLAS setup cost around $100,000.[101] Lasers also suffer from Fabry-Perot interference fringes that reduces the sensitivity of laser based techniques.[34] However, this problem may be adjusted by improving the design of the detector[115] that increases the cost. Besides the lasers available in limited region of wavelength, need cryogenic cooling in operation that makes the instrument complicated and increases the operating cost as well.[34]

Non-dispersive IR (NDIR) spectroscopy

NDIR spectroscopy is one of the most extensively used straightforward optical gas sensing techniques, first developed by Luft in 1943.[116] NDIR spectroscopy based gas sensors don't require gratings medium (which is needed in dispersive instrument) or interferometer (needed in multiplex IR spectroscopy), therefore, are simpler in design and lower in cost. In Figure 1.15 three main components for NDIR spectrometry: light sources, gas cell and a detector are shown.

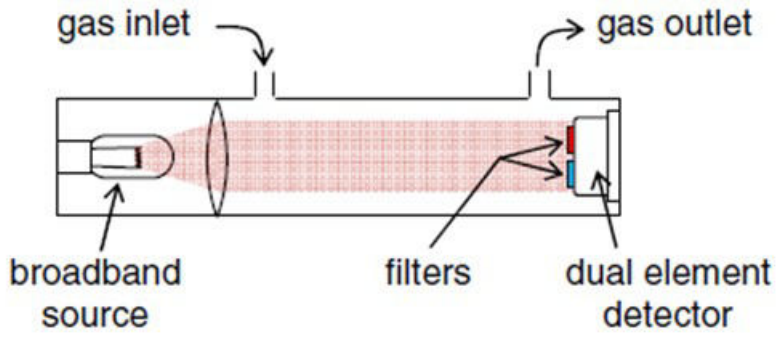

Figure 1.15 Schematic representation of a typical non-dispersive gas sensor [34]

NDIR gas sensing relies on the strength of optical absorption (i.e. absorption cross-section) in the near and mid IR (MIR). Here, the IR radiation is absorbed by the target gas in between the IR source and the detector and by measuring the intensity of the absorbed light the concentration of the gas is measured. In this technique, fixed narrow-band filters may be utilized to separate different wavelength range of IR radiation to detect few gas absorption lines across a restricted wavelength range. Configuration of NDIR gas sensors varies depending on various arrangement styles of the detectors, light sources and filters. In Figure 1.16 Massie et al.[98] have proposed four such configurations.

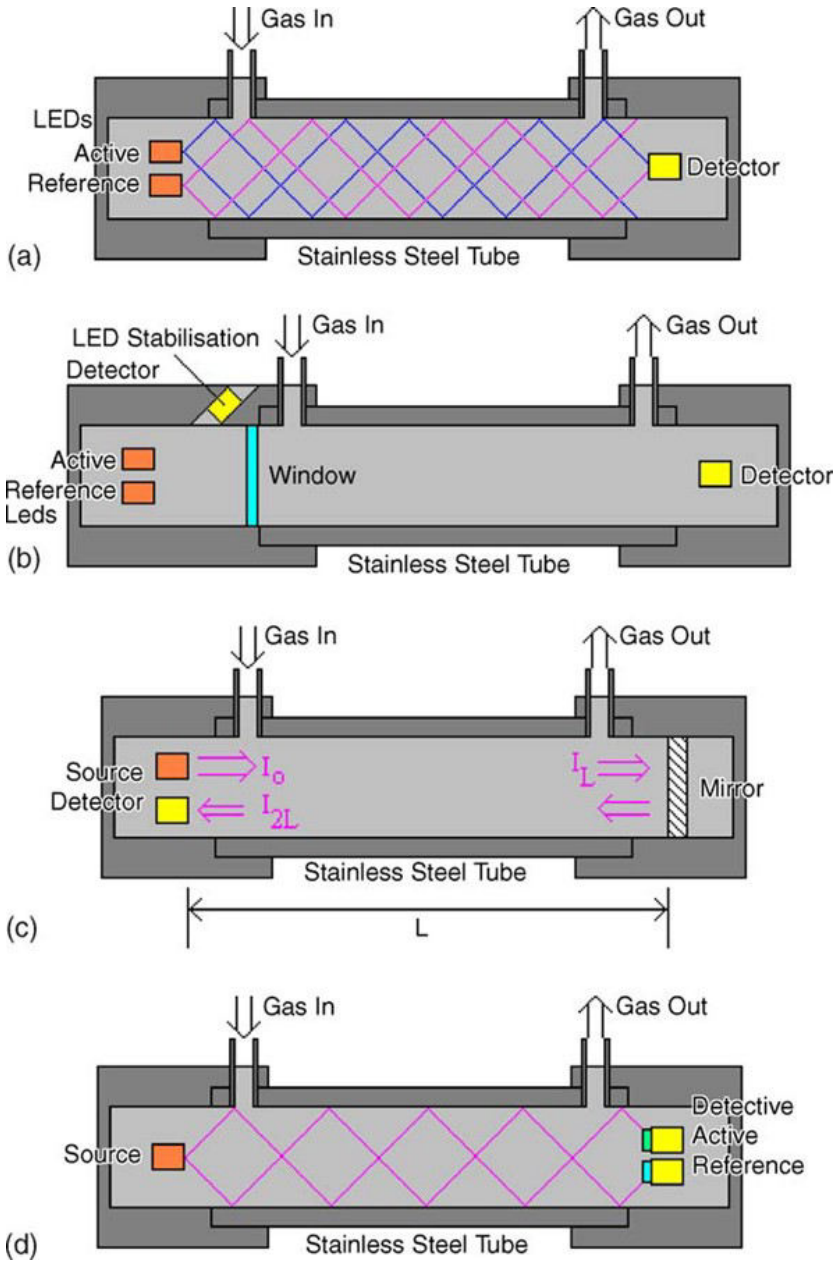

Figure 1.16 Various configurations for light source and detector layout in the NDIR gas sensor cell (a) Dual source, single detector (b) Dual source with stabilization detector; (c) Folded path; (d) single source, dual detector [98]

Light sources for NDIR gas sensors

Microbulbs. The spectral emission microbulbs are relatively higher (2 mW per steradian) than any conventional light sources and cost effective.[117] However, the

application is limited because of a number of inferior properties such as glass envelope, bulkiness and higher power consumption (500mW or more) and has slow transient times (typically operated around 2Hz.[34]

Diode laser. Diode lasers are very good source of IR radiation, both near (NIR) and mid IR (MIR) region.[118,119] Laser has the property of high power, narrow line width that assures better signal-to-noise-ratio (SNR) and tuneable at required wavelength.[120] Laser diode is best suited in TDLAS, whereas, it is considered as a less convenient light source in NDIR.[34] Besides, MIR laser needs cryogenic cooling leading it to be expensive one and although NIR laser could operate in room temperature has lower sensitivity.[121] This situation leads to development of new enhanced light source with spectral efficiency to use in NDIR spectroscopy.[119]

LED. As an emitter solid-state light sources (SSLS) like light emitting diodes (LED) covers a broad spectral range from UV-VIS to MIR[122] and act as a quasi-monochromatic emitting source[122] which enable them to work on specific gas of interest. Light emitting diode has already established its efficacy in mid IR region from 1.7- 4.8 μm[121], 3-5 μm[123] and 3-10 μm.[119] Popov et al.[121] manufactured some powerful LEDs and recommended these for atmospheric pollution monitoring of methane gas. Besides, Malyutenko et al.[124] have upheld LED as a better optical scene projector than diode laser in mid IR region.

The spectral efficiency of LEDs is excellent and matches with the absorption spectra of individual gases[125] (shown in Figure: 1.17), moreover these operate at room temperature with low power and are inexpensive.[121]Their optical outputs are stable and best match as an optopair with photodiodes.[126] Being smaller in size, they are very suitable for any

portable analytical device and lead to construct miniaturisation of instrument and enhance the performance during in- situ measurement.

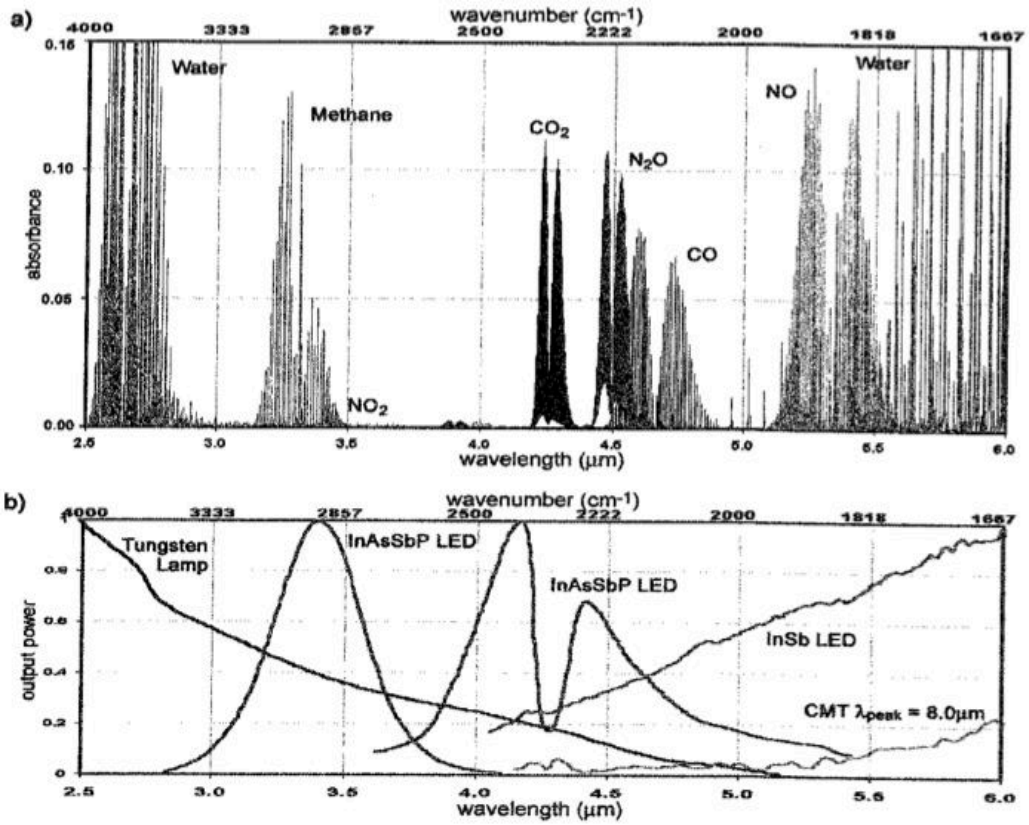

Figure 1.17 a) Spectra of the commonly sensed molecules in the atmospheric window bounded by water vapour in MIR region (HITRAN) b) The emission spectra of various emission sources in the same region[119]

Figure 1.17 reveals that the emission spectra of InAsSbP LED matches with that of CH_4 spectra in the same IR region which makes it the best candidate to detect CH_4.[127] Although the performance of LED in MIR region is temperature dependant (shown in Figure 1.18), there are some advances in the development of room temperature efficient LEDs in that region.[128] Moreover, Smith et al[119] have listed a number of room temperature LED in MIR region (3-10 μm).

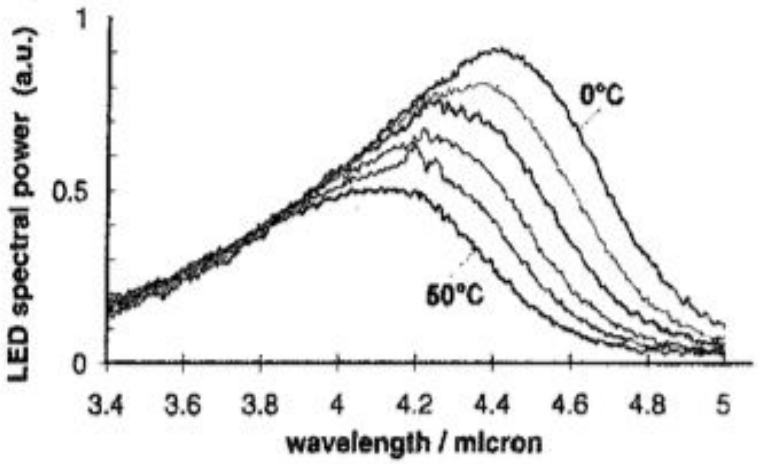

Figure 1.18 The temperature dependence of MIR infrared LED outputs[119]

1.10 LED based gas sensors

In 1991 the first IR LED based gas sensor that employed MIR LEDs for CO_2 and CH_4 sensing in a closed chamber was introduced.[33] For open path CH_4 sensing, Lugovskaya et al. were the first to employ IR LEDs.[13] Christoph et al.[128] asserted that NDIR based gas sensing is the most extensive for CO_2 and GC with FID is mostly used for CH_4 sensing. Nonetheless, a number of research groups presented CH_4 sensors that incorporated LEDs with NDIR spectroscopy.[130,131] For example, Zheng-jie, et al.[132] introduced NDIR spectroscopy based CH_4 sensor in close gas cell using IR LED and a pyroelectric detector as well as Fanchenko, et al.[133] used IR LED and photodetector based CH_4 sensor (in natural gas) for closed system. An open path CH_4 sensor was also developed by Fanchenko, et al.[133] using IR LEDs at 2.3 μm. Since LED in NIR wavelength range facilitates better thermal management than that of MIR LEDs, a number of research groups employed NIR LED based CH_4 sensors alongside with MIR LED, such as Massie et al.,[98] Roy et al.[135] and Okajima, et al.[136] used NIR LED at λ_{max} = 1.66, 1.653 and

1.65 μm, respectively. The LED based gas sensors offer portability of the sensor due to no requirement of additional cooling systems, low power consumption and small size and weight. All the abovementioned LED based CH_4 sensors are comparatively facile than any other TDLAS, FTIR based gas sensors. Additionally, better signal-to-noise ratio can be achieved from the IR LED based sensors when they are operated in pulsed mode and with shorter pulse width better optical resolution is delivered which consequently increases the sensing precision.[137]

1.11 Microcontrollers in gas sensing system

To achieve comprehensive optical output from IR LEDs, it is essential to operate them in pulse mode.[138] A number of commercial LED pulse signal generator with fixed rating are available to provide with this purpose.[139,140] These fixed rated pulse signal generators need additional pulse data acquisition and processing unit (DAQ).[141] However most of these signal generation unit and DAQ are unable to meet the rapid, large data processing requirements due to their fixed controlling and inadequate sampling frequency, respectively. In this context, microcontrollers (μC) are better alternative to fulfil these purposes. A number of μCs such as GSM,[142] MSP430F169[143] ATMEGA16[142] were used to develop CH_4 sensors. However, due to lower analog to digital conversion (ADC) rate (10 Kbit/sec) they are not pertinent for large data handling precisely in timely manner. Recently introduced portable μC with field-programmable gated array (FPGA), which enhances the processing capabilities of existing microprocessors, is capable of large data processing.[144] Cadena-Pereda et al.[145] used FPGA based binary gas mixture (CO_2-CH_4) sensor for automated sensing and Wang et al.[112] used FPGA in diode laser photoacoustic CH_4 sensor for continuous monitoring of gases. However, these FPGA based CH_4

sensors were not applied for real-time on-the-fly (live) data handling in in-field conditions utilising LEDs in portable analytical systems to date.

1.12 Summary

After reviewing the existing literatures, in Part A, we observe that LEDs are being used as an appropriate emitter for many portable miniaturised analytical instruments since last two decades. Although its utilization in analytical chemistry is enormous, little attention have been given to analysis the radiometric characterisation of them in a simplistic way. The existing techniques are somehow expensive, laborious, and involve complex geometry and algorithm.

From Part B, we found from literatures that continuous sensing of CH_4 in indoor and outdoor is not only worthwhile but also obligatory in some circumstances where there is a possibility of emission or leakage. We also identified that among the gas sensing techniques, optical gas detection technique is the most sensitive, fast responsive, non-destructive and simplest technique. FTIR and other optical methods have been utilised since many years back, however, most of them are suitable as stationary applications. On the other hand, NDIR spectroscopy based gas detection technique can overcome this gap by making the detection system portable, facile and cost effective.

There are a number of NDIR spectrometric absorption techniques, which are used in gas detection technique at specific wavelength. Most extensively used techniques are Tuneable Diode Laser Absorption Spectroscopy (TDLAS), Raman spectroscopy (RS) and Photoacoustic Spectroscopy (PAS). Higher sensitivity, specificity and fast responses are

possible to achieve through TDLAS, nevertheless, to operate them high electrical power and cooling systems are needed which make them inappropriate for portable design. Besides, lasers suffer from Fabry-Perot interference fringes that reduce their sensitivity. Similarly, RS and PAS require complicated instrumental design and additional cost is incurred to achieve higher resolution, selectivity, and reliability for gas sensing. In this context, it is possible to design a simple CH_4 sensor using NDIR based optical absorption spectroscopy using inexpensive light sources such as LEDs. However, the following capability gaps have been identified in employing LEDs in NDIR spectroscopy to achieve portable and rapid data handling as well as on-the-fly continuous gas sensing:

- Lack of simplistic analysis of radiometric properties of LEDs in analytical chemistry area.

- None of the LED based gas sensing techniques has real-time, on-the-fly large data handling and processing capabilities

- Existing gas sensing techniques often possess complicated and costly optical design and not compatible with portable, real-time and continuous sensing requirements in field conditions

1.13 Aims of the project

1.13.1 General aim

Radiometric analysis of LEDs and development of NDIR spectroscopic sensor for continuous monitoring of selected atmospheric gases using rapidly pulsed NIR LEDs enabling portable, flexible, wireless, on-the-fly data processing capabilities at indoor and outdoor environment.

1.13.2 Specific aims

Aim 1: Radiometric analysis of LEDs as solid-state light source used in optical detection studies in analytical chemistry.

Aim 2: Investigation of rapid microsecond pulse generation for NIR LEDs and flexible on-the-fly large data processing using microcontroller system with field programmable gate array (μC-FPGA) and rapidly pulsed NIR LED for portable gas analysis.

Aim 3: Development of a simple low-cost NDIR spectroscopy based portable gas sensor using NIR LED with corresponding responsive photodiode optopair and open platform μC-FPGA with real-time data analysis capabilities for continuous sensing in indoor and outdoor environment.

1.14 REFERENCES

(1) *Techniques and Instrumentation in Analytical Chemistry* **1994**, *16C*, 13-47.

(2) Macka, M.; Piasecki, T.; Dasgupta, P. K. *Annu Rev Anal Chem (Palo Alto Calif)* **2014**, *7*, 183-207.

(3) Price, R. B.; Ferracane, J. L.; Shortall, A. C. *J Dent Res* **2015**, *94*, 1179-1186.

(4) Measurement of LEDs; 9 53.085.342; International Commission on Illumination Provided by IHS under license with CIE: Kegelgasse 27, A-1030 Vienna, Austria, 2007.

(5) Miller, C. C.; Ohno, Y. In *2nd CIE Expert Symposium on LED Measurement*: Gaithersburg, Maryland, USA, 2001, pp 45-48.

(6) *Department of Environment and Energy, Australia*. [cited 2018 22/01/2018]; Available from: http://www.environment.gov.au/climate-change/climate-science-data/greenhouse-gas-measurement/publications/review-methods-unconventional-gas

(7) Jeremysharp. *Radiometric Calibration Using an Integrating Sphere*. Spectroscopy: Tips and Tutorials for Owners of Ocean Optics Spectrophotometers 2009 [cited 2015 12/12/2015]; Available from: http://www.spectroscopytv.com/radiometric-calibration-using-an-integrating-sphere/

(8) Lim, S.-R.; Kang, D.; Ogunseitan, O. A.; Schoenung, J. M. *Environmental science & technology* **2010**, *45*, 320-327.

(9) Michaels, P. J. e. a. *World Climate Report. Methane Matter*. 2007 [cited 2013; Available from: http://www.worldclimatereport.com/index.php/2007/04/13/methane-matters/

(10) Butler, J. H.; Montzka, S. A., National Oceanic & Atmospheric Administration: NOAA, U. S. D. o. C., Ed.; Earth System Research Laboratory: R/GMD, 325 Broadway, Boulder, CO 80305-332, 2014.

(11) Narendran, N.; Gu, Y.; Freyssinier‐Nova, J.; Zhu, Y. *physica status solidi (a)* **2005**, *202*, R60-R62.

(12) Leis, J.; Buttsworth, D.; Snook, C.; Holmes, G. *IEEE Transactions on Instrumentation and Measurement* **2014**, *63*, 3088-3095.

(13) Lugovskaya, A. I.; Login, S. A.; Balashov, O. B.; Kuznetsov, A. A.; Vasiliev, E. V.; Chernyak, E. Y. *Products and Systems. Control, monitoring, diagnostics* **2003**, *6* 55-59.

(14) Nakamura, S. *MRS Bulletin* **2009**, *34*, 101-107.

(15) Mokkapati, S.; Jagadish, C. *Materials Today* **2009**, *12*, 22-32.

(16) Bush, S. In *Electronics Weekly*; Metropolis Media: London, UK, 2010.

(17) Akasaki, I.; Amano, H.; Nakamura, S. *Nobel Prize Lecture. Stockholm: The Nobel Foundation. Available at* http://www. *nobelprize. org/nobel_prizes/physics/laureates/2014/popular-physicsprize2014. pdf (accessed 13 February 2015)* **2014**.

(18) Shur, M. S.; Gaska, R. *IEEE Transactions on electron devices* **2010**, *57*, 12-25.

(19) Chen, X.; Man Ching Ng, A.; Fang, F.; Hang Ng, Y.; Djurišić, A. B.; Lam Tam, H.; Wai Cheah, K.; Gwo, S.; Kin Chan, W.; Wai Keung Fong, P.; Fei Lui, H.; Surya, C. *Journal of Applied Physics* **2011**, *110*, 094513.

(20) Rose, J.; Jarnestad, J. In *The Royal Swedish Academy of Sciences*, Sara Gustavsson, L. B., Per Delsing, Anne L'Huillier and Olle Inganäs, the Nobel Committee for Physics, Ed.; The Royal Swedish Academy of Sciences: Stockholm, Sweden 2014, p 1.

(21) Yuan, L.; Liu, S.; Chen, M.; Luo, X. In *Electronic Packaging Technology, 2006. ICEPT'06. 7th International Conference on*; IEEE, 2006, pp 1-5.

(22) Steigerwald, D. A.; Bhat, J. C.; Collins, D.; Fletcher, R. M.; Holcomb, M. O.; Ludowise, M. J.; Martin, P. S.; Rudaz, S. L. *IEEE Journal of Selected Topics in Quantum Electronics* **2002**, *8*, 310-320.

(23) Bui, D. A.; Hauser, P. C. *Analytica Chimica Acta* **2015**, *853*, 46-58.

(24) Tan, J. K. S.; Baker, J. A.; Jones, D. A.; Google Patents, 1989.

(25) Kraiczek, K. G.; Bonjour, R.; Salvadé, Y.; Zengerle, R. *Analytical Chemistry* **2014**, *86*, 1146-1152.

(26) Fonseca, A.; Raimundo Jr, I. M. *Analytica Chimica Acta* **2004**, *522*, 223-229.

(27) Piasecki, T.; Breadmore, M. C.; Macka, M. *ELECTROPHORESIS* **2010**, *31*, 3737-3744.

(28) Trojanowicz, M.; Worsfold, P. J.; Clinch, J. R. *TrAC Trends in Analytical Chemistry* **1988**, *7*, 301-305.

(29) Macka, M.; Andersson, P.; Haddad, P. R. *ELECTROPHORESIS* **1996**, *17*, 1898-1905.

(30) Xiao, D.; Yan, L.; Yuan, H.; Zhao, S.; Yang, X.; Choi, M. M. *Electrophoresis* **2009**, *30*, 189-202.

(31) Ryvolová, M.; Macka, M.; Brabazon, D.; Preisler, J. *TrAC - Trends in Analytical Chemistry* **2010**, *29*, 339-353.

(32) Li, Y.; Nesterenko, P. N.; Paull, B.; Stanley, R.; Macka, M. *Analytical Chemistry* **2016**.

(33) Johnston, S. F. *Measurement Science and Technology* **1992**, *3*, 191.

(34) Hodgkinson, J.; Tatam, R. P. *Measurement Science and Technology* **2013**, *24*, 012004.

(35) Fowles, M.; Wayne, R. P. *Journal of Physics E: Scientific Instruments* **1981**, *14*, 1143.

(36) Aoyagi, Y.; Takeuchi, M.; Yoshida, K.; Kurouchi, M.; Araki, T.; Nanishi, Y.; Sugano, H.; Ahiko, Y.; Nakamura, H. *Journal of Environmental Protection* **2012**, *3*, 695.

(37) Degner, M.; Damaschke, N.; Ewald, H.; Lewis, E. In *Sensors, 2008 IEEE*; IEEE, 2008, pp 973-976.

(38) Žukauskas, A.; Vitta, P.; Kurilčik, N.; Juršenas, S.; Bakiene, E. *Optical Materials* **2008**, *30*, 800-805.

(39) Vitta, P.; Kurilčik, N.; Juršenas, S.; Žukauskas, A.; Bakiene, E.; Zhang, J.; Katona, T.; Bilenko, Y.; Lunev, A.; Hu, X.; Deng, J.; Gaska, R. In *Proceedings of SPIE - The International Society for Optical Engineering*, 2005.

(40) Technology insight report: :ED technology in lighting Gridlogics Technologies Pvt. Ltd.: Pune, India, 2010.

(41) *Celebrating the 50th Anniversary of the LED*. 2012 [cited 2017 15 March]; Available from: http://www.gelighting.com/LightingWeb/na/solutions/technologies/led/50th-anniversary-led.jsp.

(42) *Getting to Know LEDs, Applications and Solutions*. 2012 [cited 2017 10 April]; Available from: http://www.dialight.com/Assets/Application_Notes/Indication/Getting%20To%20Know%20LEDs.PDF.

(43) Björn, L. O. *Photobiology*; Springer, 2008.

(44) Leighton, W. G.; Forbes, G. S. *Journal of the American Chemical Society* **1930**, *52*, 3139-3152.

(45) Kuhn, H.; Braslavsky, S.; Schmidt, R. *Pure and Applied Chemistry* **2004**, *76*, 2105-2146.

(46) Hatchard, C. G.; Parker, C. A. *Proceedings of the Royal Society of London A: Mathematical, Physical and Engineering Sciences* **1956**, *235*, 518-536.

(47) Rahn, R. O. *Photochemistry and Photobiology* **1997**, *66*, 450-455.

(48) Wegner, E. E.; Adamson, A. W. *Journal of the American Chemical Society* **1966**, *88*, 394-404.

(49) A, S.; Nanver, L. K.; Veen, G. v.; Kooijman, K.; Vogelsang, P.; Scholtes, T. L. M.; Boer, W. d.; Wien, W. H. A.; Milosavljevi, S.; Heerkens, C. T. H.; Knezevic, T.; Spee, I. In *Electron Devices Meeting (IEDM), 2010 IEEE International*, 2010, pp 31.34.31-31.34.34.

(50) Jou, R. Y.; Lee, P. H. In *Energy Procedia*, 2014, pp 1261-1265.

(51) Shaw, P.-S.; Li, Z.; Arp, U.; Lykke, K. R. *Applied Optics* **2007**, *46*, 5119-5128.

(52) Say, C.; Young, R. *Optics and Photonics News* **2008**, *19*, 12-13.

(53) Hanssen, L. *Applied Optics* **2001**, *40*, 3196-3204.

(54) Pleijel, G.; Longmore, J. *Journal of Scientific Instruments* **1952**, *29*, 137.

(55) Weston, E. T.; Paix, D. *Journal of Scientific Instruments* **1960**, *37*, 359.

(56) Jou, R.-Y.; Lee, P.-H. *Energy Procedia* **2014**, *61*, 1261-1265.

(57) Kärhä, P.; Manninen, P.; Hovila, J.; Seppälä, L.; Ikonen, E., Available in: http://www.pmodwrc.ch/newrad2005/pdfabstracts/Newrad044.pdf

(58) Thorpe, Thomas Edward. Quantitative Chemical Analysis. J. Wiley & sons, 1893.

(59) Taylor, B. N.; Kuyatt, C. E. In *United States Department of Commerce Technology Administration, National Institute of Standards and Technology (NIST)Technical Note 1297, 1994 Edition*, 1994, p 24.

(60) Department of Environment, A. G., Ed.; Commonwealth of AUstralia: Canberra ACT 2610, Australia, 2014.

(61) *Department of Environment and Energy, Australia*. [cited 2017 02 February, 2017]; Available from: http://www.environment.gov.au/protection/air-quality/air-pollutants.

(62) In *Techniques and Instrumentation in Analytical Chemistry*, Valcárcel, M.; Luque de, C., Eds.; Elsevier, 1994, pp 13-47.

(63) *Air pollutants*. [cited 2017 5 January]; Available from: http://www.environment.gov.au/protection/air-quality/air-pollutants.

(64) Harmsen, J. *Chemical Engineering and Processing: Process Intensification* **2010**, *49*, 70-73.

(65) In *Training For the health Sector*; World Health Organization, 2008, p 67.

(66) Suh, H. H.; Zanobetti, A.; Schwartz, J.; Coull, B. A. *Environ Health Perspect* **2011**, *119*, 1421-1428.

(67) Agency, U. S. E. p., Ed.; Environmenta Protection Agency, UAS, 2014.

(68) Choi, E.; Heo, J.-B.; Hopke, P. K.; Jin, B.-B.; Yi, S.-M. *Water, Air, & Soil Pollution* **2010**, *215*, 67-82.

(69) Khoder, M. I. *Atmospheric Environment* **2007**, *41*, 554-566.

(70) Huang, S.; Shao, M.; Lu, S. H. *Huan Jing Ke Xue* **2008**, *29*, 3326-3330.

(71) Sarigiannis, D. A.; Karakitsios, S. P.; Gotti, A.; Liakos, I. L.; Katsoyiannis, A. *Environ Int* **2011**, *37*, 743-765.

(72) Kin Fai Ho, S. S. H. H., Shun Cheng Lee, Peter Kwok Keung Louie, ; Junji Cao, W. D. *Aerosol and Air Quality Research* **2013**, *13*, 1331-1347.

(73) Zhou, J.; You, Y.; Bai, Z.; Hu, Y.; Zhang, J.; Zhang, N. *Sci Total Environ* **2011**, *409*, 452-459.

(74) Massolo, L.; Rehwagen, M.; Porta, A.; Ronco, A.; Herbarth, O.; Mueller, A. *Environ Toxicol* **2010**, *25*, 339-349.

(75) Tiwari, V.; Hanai, Y.; Masunaga, S. *Air Qual Atmos Health* **2010**, *3*, 65-75.

(76) Agency, U. S. E. P., Ed.; Environmental Protection Agency: USA, 2012.

(77) LLC., F. C. I. In *Hazardous area Classifications and Protection*; Emerson Process Management: Marshalltown, Iowa 50158 USA, 2012, pp 10-18.

(78) Hiroyuki Kataoka; Yasuhiro Ohashi; Tomoko Mamiya; Kaori Nami; Keita Saito; and, K. O.; Takigawa, T. In *Advanced Gas Chromatography - Progress in Agricultural, Biomedical and Industrial Applications*, Mustafa Ali Mohd, I., Published: March 21, 2012 under CC BY 3.0 license, Ed.; In Tech, 2012, pp 161-184.

(79) Liu, Q.; Liu, Y.; Zhang, M. *Aerosol and Air Quality Research,* **2014**, *14*, 330–337.

(80) Atkinson, R.; Arey, J. In *International Conference on Atmospheric Chemical Mechanisms* Carter, B., Ed.; UC Davis, CA: Freeborn Hall, UC Davis, CA, 2006, pp 1-28.

(81) R. Moolla, S. K. V., C.J. Curtis & S.J. Piketh. In *WIT Transactions on The Built Environment: 5th International Conference*; WIT Press: Rome, Italy, 2013, pp 701-712.

(82) Tecklenburg, Z. In *KHSB 41 Action news*; Scripps Media, Inc: Kansas City, Missouri, USA, 2013.

(83) Saatchi, A.; Aghajani, A.; Alavi, F. *Materials performance* **2006**, *45*, 52-55.

(84) Jonathan Thompson Jan. 18. In *High Country News*; Paul Larmer: Paonia, Colorado, US, 2016.

(85) Clarence, J.; Google Patents, 1959.

(86) Azad, A.; Akbar, S.; Mhaisalkar, S.; Birkefeld, L.; Goto, K. *Journal of the Electrochemical Society* **1992**, *139*, 3690-3704.

(87) Li, S.; Zhang, Y.; Koscica, T.; Cui, H.-L. In *Proc. SPIE 6299, (September 01, 2006); doi:10.1117/12.680947*, Chu, A.; Szykman, J.; Kondragunta, S., Eds.; The International Society for Optical Engineering: San Diego, California, USA | August 13, 2006, 2006, pp 62990Q-62990Q-62998.

(88) *Principles of Gas Detection* 2013; Available from: http://www.honeywellanalytics.com/en-GB/gasdetection/principles/Pages/gasprinciples.aspx#infrared.

(89) Iino, A.; Kato, N.; Google Patents, 1989.

(90) Bogue, R. *Sensor Review* **2015**, *35*, 133-140.

(91) Liu, X.; Cheng, S.; Liu, H.; Hu, S.; Zhang, D.; Ning, H. *Sensors (Basel)* **2012**, *12*, 9635-9665.

(92) McDonagh, C.; Burke, C. S.; MacCraith, B. D. *Chem Rev* **2008**, *108*, 400-422.

(93) Kleeby, M. In *Separation Science*, Kelsey, J., Ed.; Eclipse Business Media Ltd, England, : No. 06513189, 2 Clarendon Road, Ashford, Middlesex TW15 2QE, United Kingdom, .

(94) Hinshaw, J. V. In *Chromatograghyonline.com*; LCGC North America: North America, 2005.

(95) Yang, C.; Li, X.; Xu, T.; Qu, W.; Liu, Y. In *3rd International Symposium on Mine Safety Science and Engineering*, 2016, pp 616-621.

(96) Chou, J. *Hazardous gas monitors: a practical guide to selection, operation and applications*; McGraw-Hill Professional Publishing, 2000.

(97) Dakin, J. P.; Chambers, P. In *Optical Chemical Sensors*; Springer, 2006, pp 457-477.

(98) Massie, C.; Stewart, G.; McGregor, G.; Gilchrist, J. R. *Sensors and Actuators B: Chemical* **2006**, *113*, 830-836.

(99) Rothman, L. S.; Gordon, I. E.; Barbe, A.; Benner, D. C.; Bernath, P. F.; Birk, M.; Boudon, V.; Brown, L. R.; Campargue, A.; Champion, J. P.; Chance, K.; Coudert, L. H.; Dana, V.; Devi, V. M.; Fally, S.; Flaud, J. M.; Gamache, R. R.; Goldman, A.; Jacquemart, D.; Kleiner, I., et al. *Journal of Quantitative Spectroscopy and Radiative Transfer* **2009**, *110*, 533-572.

(100) Ingle Jr, J. D.; Crouch, S. R. **1988**.

(101) Colby, J.; Footer, T.; Crawford, P. In *EPA Handbook: Optical Remote Sensing for Measurement and Monitoring of Emissions Flux* Mike, D. K.; Merrill, R., Eds.; Environmental Protection Agency: North Carolina, 27711, United States, 2011, p 210.

(102) Griffith, D. W. T.; Jamie, I. M. In *Encyclopedia of Analytical Chemistry*, Meyers , R. A., Ed.; ohn Wiley & Sons, Ltd, 2010.

(103) Li, Y.; Sun, Y.; Wang, L. C. *Applied Mechanics and Materials,* **2011**, *vol. 63*, 878-881.

(104) Adler, F.; Masłowski, P.; Foltynowicz, A.; Cossel, K. C.; Briles, T. C.; Hartl, I.; Ye, J. *Optics express* **2010**, *18*, 1-12.

(105) Collins, J. F.; Shepherd, P.; Durbin, T. D.; Lents, J.; Norbeck, J.; Barth, M. *Environmental Science & Technology* **2007**, *41*, 6554-6561.

(106) Tanahashi, T.; Toda, M.; Miyashita, H.; Ono, T. In *17th International Conference on Solid-State Sensors, Actuators and Microsystems, TRANSDUCERS and EUROSENSORS 2013*; IEEE: Barcelona; Spain, 2013, pp 2509-2512.

(107) Lackner, M. *Reviews in Chemical Engineering* **2007**, *23*, 65-147.

(108) Tittel, F. K.; Lewicki, R.; Jahjah, M.; Foxworth, B.; Ma, Y.; Dong, L.; Griffin, R.; Krzempek, K.; Stefanski, P.; Tarka, J. *Springer, NATO Science for Peace and Security Series* **2013**, 1-13.

(109) Werle, P. W. In *Laser in Environmental and Life Sciences*; Springer, 2004, pp 223-243.

(110) Werle, P. W.; Mazzinghi, P.; D'Amato, F.; De Rosa, M.; Maurer, K.; Slemr, F. *Spectrochimica Acta Part a-Molecular and Biomolecular Spectroscopy* **2004**, *60*, 1685-1705.

(111) Frish, M. B.; Wainner, R. T.; Green, B. D.; Laderer, M. C.; Allen, M. G. In *SPIE Optics East*; Society of Photo-Optical Instrumentation Engineers: Boston, MA, 2005, pp 2-10.

(112) Wang, J.; Wang, H.; Liu, X. *Sensors* **2016**, *16*, 1551.

(113) Ngai, A. K. Y.; Persijn, S. T.; von Basum, G.; Harren, F. J. M. *Applied Physics B* **2006**, *85*, 173-180.

(114) *Laser Moisture-Technology*. 2014 [cited 2017 17 February]; Available from: http://www.servomex.com/gas-analyzers/technologies/laser-moisture.

(115) Masiyano, D.; Hodgkinson, J.; Tatam, R. P. *Applied Physics B* **2008**, *90*, 279-288.

(116) Luft, K. *Z. tech. Phys* **1943**, *24*, 97-104.

(117) Hodgkinson, J.; Smith, R.; Ho, W. O.; Saffell, J. R.; Tatam, R. P. *Sensors and Actuators B: Chemical* **2013**, *186*, 580-588.

(118) Smith, S. D.; Vass, A.; Karpushko, F.; Hardaway, H.; Crowder, J. G. *Philosophical Transactions of the Royal Society A: Mathematical, Physical and Engineering Sciences* **2001**, *359*, 621-634.

(119) Smith, S. D.; Crowder, J. G.; Hardaway, H. R. In *Novel In-Plane Semiconductor Lasers*, Meyer, J. R.; Gmachl, C. F., Eds.; SPIE--The International Society for Optical Engineering: San Jose, CA, 2002, pp 157-172.

(120) Magalhães, F. T. A. d. *Development of gas detection systems based on microstructured optical fibres Development of gas detection systems based on microstructured optical fibres* University of Porto, Rua Roberto Frias, s / n, 4200-465 Porto, Portugal, 2008.

(121) Popov, A. A.; Sherstnev, V. V.; Yakovlev, Y. P.; Baranov, A. N.; Alibert, C. *Electronics Letters* **1995**, *33*, 480-481.

(122) Stojanovic, R.; Karadaglic, D. *Journal of Physics: Conference Series* **2007**, *76*, 012054.

(123) Miyazaki, E.; Itami, S.; Tsutomu, A. *Review of Scientific instruments* **1998**, *69*, 3751-3754.

(124) Malyutenko, V. K.; Malyutenko, O. Y.; Zinovchuk, A. V. *Applied Physics Letters* **2006**, *89*, 201114.

(125) Aleksandrova, S.; Gavrilov, G.; Kapralov, A.; Karandashov, S.; Matveev, B.; Sotnikova, G.; Stus, N. In *Second International Conference on Lasers for measurement and information Transfer*, Privlov, V. E., Ed.; SPIE, 2002, pp 188-194.

(126) O'Toole, M.; Diamond, D. *Sensors* **2008**, *8*, 2453-2479.

(127) Krier, A.; Sherstnev, V. V. *J. Phys. D: Appl. Phys.* **2000**, *33*, 101-106.

(128) Smith, S. D.; Vass, A.; Karpushko, F.; Hardway, H.; Crowder, J. G. *Philosophical Transactions: Mathematical, Physical and Engineering Sciences* **2001**, *359*, 621-634.

(129) Zellweger, C.; Emmenegger, L.; Firdaus, M.; Hatakka, J.; Heimann, M.; Kozlova, E.; Spain, T. G.; Steinbacher, M.; van der Schoot, M. V.; Buchmann, B. *Atmospheric Measurement Techniques* **2016**, *9*, 4737.

(130) Tan, Q. L.; Tang, L. C.; Yang, M. L.; Xue, C. Y.; Zhang, W. D.; Liu, J.; Xiong, J. J. *Optics and Lasers in Engineering* **2015**, *74*, 103-108.

(131) Ahmed, A. S.; Kim, H. J.; Kim, J.; Hwang, K. S.; Kim, S. *Sensors* **2017**, *17*, 11.

(132) Zhao, Z. J.; Liu, D. X.; Zhang, J. L.; Wang, Z. B.; Li, X. A.; Tian, E. M. *Spectroscopy and Spectral Analysis* **2011**, *31*, 570-573.

(133) Fanchenko, S.; Baranov, A.; Savkin, A.; Sleptsov, V. In *IOP Conference Series: Materials Science and Engineering*; IOP Publishing, 2016, p 012036.

(134) Fanchenko, S.; Baranov, A.; Savkin, A.; Petukhov, A.; Kalinina, K.; Zhurtanov, B.; Velikotny, M.; Ieee. *2015 Ieee Workshop on Environmental, Energy and Structural Monitoring Systems (Eesms)* **2015**, 146-151.

(135) Roy, S.; Desikan, R.; Duttagupta, S. P. *arXiv preprint arXiv:1611.08797* **2016**.

(136) Okajima, H.; Kakuma, S.; Uchida, K.; Wakimoto, Y.; Noda, K. In *SICE-ICASE, 2006. International Joint Conference*; IEEE, 2006, pp 1652-1655.

(137) Gibson, D.; MacGregor, C. *Sensors* **2013**, *13*, 7079-7103.

(138) *Alfa Photonics, IR LEDs*. Available from: http://www.alfaphotonics.lv/.

(139) *LED micro sensor's D51 LED driver*. Available from: http://lmsnt.com/eldev/D51-LED-Driver/.

(140) *LED driver from roithner laser*. Available from: http://www.roithner-laser.com/led_pulsed_driver.html.

(141) *edaq web page*. 2014 11 Nov]; Available from: https://www.edaq.com/.

(142) Sood, A.; Sonkar, B.; Ranjan, A.; Faisal, A. *International Journal of Electrical and Electronics Research* **2015**, *3*, 264-269.

(143) Deng, P. In *Advanced Research and Technology in Industry Applications (WARTIA), 2014 IEEE Workshop on*; IEEE, 2014, pp 784-786.

(144) Scholl, S. **2016**.

(145) Cadena-Pereda, R. O.; Rivera-Munoz, E. M.; Herrera-Ruiz, G.; Gomez-Melendez, D. J.; Anaya-Rivera, E. K. *Sensors* **2012**, *12*, 10742-10758.

2 Chapter 2: Radiometric analysis of deep UV to near infrared LEDs enabling fast, accurate and facile radiometric measurements in photochemical systems

LEDs as quasi-monochromatic emitters cover broadband spectral range and provide satisfactory radiometric power outputs using steady current. Radiometric analysis of LEDs facilitates quantitative characterisation of the radiometric parameters and subsequent wavelength specific applications of LEDs. Therefore, the entire work in chapter two is undertaken to accomplish the first specific aim of this thesis which is: 'Radiometric analysis of LEDs as solid-state light source used in optical detection studies in analytical chemistry.'

Chapter 2 has been removed for copyright or proprietary reasons.

It has been published as: Noori, A., Mahbub, P., Dvořák, M., Lucieer, A., Macka, M., 2018. Radiometric analysis of UV to near infrared LEDs for optical sensing and radiometric measurements in photochemical systems. Sensors and actuators B: Chemical, 262, 171-179.

3 Chapter 3: Portable Device for Continuous Sensing with Rapidly Pulsed LEDs – Part 1: Rapid On-the-fly Processing of Large Data Streams using an Open Source Microcontroller with Field Programmable Gate Array

The maximum radiometric power output from a NIR LEDs can obtain when they are operated in rapid pulsed mode. Flexibility in the rapid pulse generation to drive IR LEDs is the prerequisite for investigating and optimising the signal-to-noise (SNR) values in gas detection mechanisms in IR region. We designed a flexible system using microcontroller (μC) with field programmable gate array (FPGA) to generate rapid pulse signal (ca. 2 μs pulses with a typical repetition rate of 1 kHz) for NIR LEDs as well as for the on-the-fly large stream of data acquisition and processing with custom-made programme and investigate signal to noise ratio values (SNR) as the crucial performance characteristics of the system. Therefore, the work of this chapter is to accomplish the second specific aim of this thesis which is 'Investigation of rapid microsecond pulsed generation for NIR LEDs and flexible on-the-fly large data processing using microcontroller system with field programmable gate array (μC-FPGA) and rapidly pulsed NIR LED for portable gas analysis.'

Portable Device for Continuous Sensing with Rapidly Pulsed LEDs – Part 1: Rapid On-the-fly Processing of Large Data Streams using an Open Source Microcontroller with Field Programmable Gate Array

Ansara Noori[†], Parvez Mahbub[†], John S. Parry[‡], John Davis[‡], Arko Lucieer[§], Mirek Macka[†]*

[†] Australia Centre for Research on Separation Science (ACROSS) and School of Physical Sciences- Chemistry, University of Tasmania, Tasmania, Australia

[‡] Central Science laboratory, University of Tasmania, Private Bag 74, Hobart 7001, Australia

[§] *School of Land and Food, University of Tasmania, Tasmania, Australia.*

KEYWORDS. Red Pitaya microcontroller with FPGA, On-the-fly data acquisition and processing, IR LED, Rapid microsecond pulsing.

ABSTRACT: Infra-red light emitting diodes (IR LEDs) operated in a rapid pulsed mode are suitable for portable low-cost optical sensing of gases with the transmitted light detected by a IR sensitive photodiode. We design a portable system using an open source micro controller (μC) with built-in field programmable gate array (FPGA). The system is used for rapid pulse generation (ca. 2 μs short pulses with a typical repetition rate of 1 kHz) to drive the IR LED as well as for the optical sensing data acquisition and on-the-fly processing of large data streams of ca. 2 Gbit/s. The flexibility and performance of the system is demonstrated by investigating instrumental signal to noise ratio values (SNR) as the crucial performance characteristics of the system governing the limit of detection values. Digital data filtering is accomplished first by repetitive smoothing (averaging a number of raw data pulses usually 10 - 10,000), followed by boxcar averaging and Savitzky-Golay (2^{nd} degree polynomial regression) based smoothing. Repetitive smoothing resulted in SNR improvement by a factor of $\sqrt{n}$ (n is the number of repetitive pulses averaged). Then, for measuring the pulse height to determine the detected pulsed signal attenuation, three different statistical methods applied to the corresponding data points at the baseline and at the pulse top were compared: simple averaging, linear regression, and 2^{nd} degree polynomial regression. Finally, each of the digitally processed signal pulses yields one data point of analytical signal in time as a quasi-continuous data stream produced at a rate between 1000 and 0.1 Hz (1 point every 1 ms to 10 s, depending on the level of repetitive smoothing). The minimum measurable absorbance corresponding to the highest SNR for n=1000 resulting in quasi-continuous data points at 1 Hz was found 10^{-4} a.u. This microcontroller–based portable open source platform is then implemented in the accompanying paper on on-the fly data acquisition and processing and wireless transfer of analytical signal enabling continuous gas sensing in real-time in indoor and outdoor environment.

3.1 Introduction

For analytical measurements where the sample property can change at a fast rate, such as in case of atmospheric monitoring of trace gases, rapid digital sampling and analysis techniques are required.[1] This is well satisfied with optical analytical platforms, such as infrared (IR) spectrometers, supplemented with adequately fast electronics and data handling capability. Although IR spectroscopy based gas detection is a well-established technique,[2] designing small low-cost low power consumption analytical platforms for portable and remote analysis presents number of challenges.[3] One of them is rapid on-the-fly processing of continuous and live data streams in a flexible custom-defined manner. Additionally, low-cost, small-size-weight and low-power analytical platforms capable of rapid, on-the-fly and custom-defined data processing are required in number of field deployment modes including portable hand-held devices and remote sensing devices such as on-board unmanned aerial vehicles (UAVs).

Most gaseous analytes of environmental or industrial significance have strong absorption bands in the infrared (IR) spectral range.[4] Most commercially available instruments for the analysis of gases employ sophisticated and expensive spectrometers that provide measurements solely in a laboratory setting.[5,6] In this context, the use of LEDs with photodiodes (PDs) in the IR spectral range has enabled development of portable low-cost sensors.[7-9] However, most of the commercially available LED drivers for pulse signal generation (in μs pulses with 1kHz frequency) have fixed setting and need addi-

tional electronics for signal collection and data acquisition.[10,11] In most cases an oscilloscope or standard electronic data acquisition (eDAQ) system can be a good option. However, the maximum sampling rate for data acquisitions of a typical eDAQ is only 1 kHz which is by far not adequate for acquisition of data generated by microsecond pulses.[12] Expensive digital oscilloscopes with a sampling rate in excess of 100 mega samples/sec can be implemented for data acquisition and collection, however, acquisition of large data streams (in our case 125 MHz at 16bit yielding 2 Gbit/s) will exhaust the memory of a typical 16 GB SD card in only ca.1 min.[13]

Nowadays, computers are omnipresent as an interface with analytical instruments for online digital data acquisition, processing, storage and display.[14,15] Some are capable of handling large data stream precisely in modern laboratory based (not portable) analytical instruments such as Raman spectrometry.[16] However, for miniaturized portable analytical instruments, modern powerful microcontrollers (μC) are ideal where on-the-fly (live data) data processing is needed.[17,18] Recently Hauser group published a review covering the use of μC for portable analysis.[17] Although a number of μC based commercial devices including those for detection of methane are available,[19] these lack flexibility and give no insight into the way analytical signal is produced ('black box'), so that it is in principle impossible to make a judgement on the data processing.

Currently, open source μC systems, such as Arduino are popular due to its programmable options,[20] however, they can handle only one operation at a time and the maximum sampling rate of its in-built analog-to-digital converter (ADC) is only 10 kHz.[21] Another popular open source μC, Raspberry pi, has no built-in analog input, which then has to be implemented using an additional ADC.[22] Conventional ADC does single conversion at a time which results in a random lag between analog signal acquisition and data processing, making it difficult to generate synchronised data.[23] Importantly, even with very fast ADC, Raspberry pi is not capable of processing the data in a rapid manner due to the speed limit of its processor. Regarding the most important parameter in respect to this work, namely on-the-fly large data stream data processing, both Arduino and Raspberry pi would not be able to handle data streams in excess of 50 kHz at 16 bit yielding maximum 0.1 MB/sec.[24]

To the contrary, recently introduced portable microcomputer with field-programmable gated array (FPGA, which enhances the processing capabilities of existing microprocessors) 'Red Pitaya' (technology spin-off from Instrument Technologies as the makers of Libera family devices*[25]) is capable of on-the-fly processing of large data volumes without any lag, thanks to the FPGA responsible for data synchronization.[26] FPGA allows for the integration of ADC interface, input/output (I/O) interface, memory and processing units in a single chip.[27] FPGA-based devices are specially used in particle colliders for high-energy physics (HEP),[28] gamma radiation spectroscopy, real vision imaging and many other reconfigurable high performance virtual instrumentation.[29] Although FPGA based devices offer real-time data handling capability of large data without any lag, other than the fields of nanosecond pulse generation,[30] computational chemistry[31] and simulated mass spectroscopy (MS),[32] the application of μC system with FPGA in analytical chemistry to the best of authors' knowledge, has not been presented in analytical literature.

Therefore, we aimed to investigate flexible data acquisition and on-the-fly fully automated data processing through developing in house data processing routine capable to handle large and live data using μC system with FPGA in a rapid manner. This creates capability to generate rapid pulsed signal and process in real time large volume of data per second (2 Gbits/sec at 125 MHz with 16bit ADC), where implementation of miniaturized μC with FPGA for IR LED based optical gas sensing offers portability, and at the same time maximum flexibility for implementing codes for specific analytical scenarios such as portable and remote analysis of gases.

3.2 EXPERIMENTAL SECTION

3.2.1 Instrumentation.

3.2.1.1 Microcontroller with field programmable gate array. A microcontroller (μC) system (Red Pitaya V1.1, RS Components Pty Ltd, Wetherill Park. NSW. 1851, Australia) shown in Figure 1 is an open source platform, based on ARM Cortex A9 processor plus a Zynq μC system on chip (SoC) field programmable gate array (FPGA) in the same device (component A in Figure. 1) with 512MB of DDR3 RAM (component B in Figure. 1). The operating μC system is based on Linux (version 2015.1 from Xilinx) supporting network connection (WIFI, LAN and USB), which allows it to operate remotely. The ARM CPU functions as data analyser to evaluate the collected data by high-speed ADC. The sampling capability of this μC system through RF output and input (component C and D in Figure. 1) has four different options from 2-125 MHz. The buffer size (maximum data capture capacity) of the FPGA-μC system is 16,384. The input and output buffer of the FPGA-μC system was self-triggered using its external triggering facilities in the GPIO (shown as component E in Figure. 1).

Insert figure 1

3.2.1.2 In-house electronics: Voltage to current converter and resistor-capacitor circuit or RC filter. We developed a voltage to current conversion unit (V-to-I) and a resistor-capacitor circuit as RC filter in house with off the shelf electronics. The voltage pulsed from the operational amplifier (op amp) of V-to-I circuit was converted into pulsed forward current to drive the LED and functions as LED driver.

In the RC filter, there are two 1 ohm resistor and 390 μf capacitor. There is also a dummy load resistor 27 ohms connected across the output. The dummy load is necessary so that the power bank does not switch off if the load becomes too small. The filter is supplying the LED driver (V-to-I) so that the

* Libera is a product family delivering electronics to the particle accelerator project such as CERN ("Conseil Européen pour la Recherche Nucléaire", or European Council for Nuclear Research) project.

2 amp pulse is not affecting the detector which is supplied power from the same power bank. See in the supplementary information (SI) Figure. S1 A&B for detailed circuit diagram of V-to-I and RC filter).

3.2.1.3 LED and photodiode (PD). We used IR LED with an emission maximum wave length λ_{max} = 1.65 μm, (Lms16LED-R, Alfa Photonics, Latvia) and IR sensitive photodiode (PD) (Lms24-05-PA, Alfa Photonics, Latvia) having a spectral response over the range from 1.1 to 2.3 μm equipped with embedded preamplifier.

3.2.1.4 Power supply. We employed rechargeable portable power bank (CY1767PBCHE, Cygnett, Australia) to supply 5 volt DC power to the μC system, V-to-I conversion circuit and the preamplifier circuit of the IR PD.

3.2.2 Methods.

3.2.2.1 Pulse generation. We employed the microcontroller (μC) system to generate voltage pulses which were subsequently converted into current pulses with the help of voltage to current converter (V-to-I) unit to drive the IR LEDs in pulse mode. The shape of the pulse is generated stepwise digitally in a flexible way and details are described in the result and discussion section.

After receiving the radiation from the pulsed IR LED, optical pulses from the IR PD were acquired by μC system through its input channel 1 as analog voltage pulses. 800 mm long and 7.5 mm inner diameter electro polished aluminium tube was used as a sample cell for portable analysis, which also housed the IR LED and IR PD (shown in Figure. 2 in Results and Discussion section).

3.2.2.2 Fast data acquisition and on-the-fly data processing. The analog voltage pulses from the IR PD which were collected by the μC system through the RF input high speed ADC (input channel 1) we call 'raw pulses' for the sake of better understanding. We constructed data processing programme for the ARM cortex A9 processor of μC system and performed digital smoothing on raw pulses by applying three techniques: repetitive smoothing (averaging a number of consecutive pulses) alone, and with additional to the repetitive smoothing boxcar averaging or Savitzky-Golay (a special form of 2nd polynomial regression based smoothing). After applying the smoothing techniques, the smoothened pulses were termed as 'processed pulses' (described more in Fig. 4).

The baseline and pulse top of each processed pulses were evaluated using three different statistical operations: averaging, linear regression, 2^{nd} degree polynomial regression. From the evaluated values of baseline and pulse-top, height of the pulse was calculated (by subtracting), which ended up with one data point for each processed pulse and termed as 'final signal values'(S). After acquiring additional quasi-continuous final signal values from arbitrary number of pulses 'digital data signal' (S) in volt was formulated and by taking negative natural logarithm (base e) of each data stream' values, digital data stream was converted into 'final analytical signal' (A) in absorbance unit (A.U) (described more in Figure. 4). The total calculation time for the μC was ~20 ns.

Baseline noise was evaluated by observing the distribution pattern of all the data points in the baseline of each pulses for random and fixed instrumental noise in our detection system. Distribution pattern for the final digital signal was also tested on obtained results using the two different statistical evaluation techniques: simple averaging and linear regression. Both instrumental and analytical signal-to noise ratio was calculated and the obtained result was optimized by comparing one another.

3.3 RESUTLS AND DISCUSSION

3.3.1 Design of Pulse Generation for IR-LED.

Radiometric power output of LEDs increases proportionally with the magnitude of applied current.[33] However, temperature across the chip of the LEDs rises significantly when it is driven at higher applied current[34] which causes efficiency droop (i.e. efficiency of LED decreases while operating it with higher electric current) due to overheating across the semiconductor material of the LED chip.[33]

Therefore, to minimize the effect of overheating of the semiconductor materials used in IR LED, the LEDs have to be operated either in quasi continuous wave (QCW) mode (duty cycle = 50%) or in pulsed mode (switched on for very short time, usually in microseconds). The maximum driving current in QCW for the IR LED is 250mA,[35] whereas in pulse mode the driving current can be up to 2A,[35] which yields higher radiometric power output during the pulse[33] and this in turn yields in better performance of the optical measurement due to lower minimum absorbance values that can be measured by absorbance-based analytical detection.[14,36]

In rapid pulsing mode, the duty cycle (the percentage of the 'on' time) is retained significantly shorter which helps to reduce the thermal effect. In our work, the IR LED was in "on" mode only for 2 μsec with duty cycle = 0.2%, so the LED was in "off" mode for comparatively longer period (998 μsec), which allows sufficient time to cool down and protect the LED from efficiency drooping. The corresponding pulse repetition frequency (PRF) in our study was 1 kHz which helps to produce a higher number of pulses within a short period of time with resulting maximum radiometric power output.

Further to demonstrate the flexibility of this approach with custom-defined data processing, we developed a computer programme written and compiled in C in Linux OS environment to generate the voltage pulses in required shape with the help of the μC system. This programme was employed to forward an array of voltage values with amplitude between 0 – 1 volt step wise from the μC system to the voltage-to-current converter (V-to-I) circuit shown in Figure. 2. Since LEDs are current driven, we applied the in-house voltage-to current (V-to-I) converter circuit to transform the voltage pulsed signal generated (Vin) by the μC system into current signal pulse (I_{in}) for the IR LED.

Insert Figure 2

As mentioned before generated pulses could be in arbitrary shape i.e. any time duration (pulse width or duty cycle), frequency and forward voltage are possible to apply simply by changing the parameters to the programme. The stepwise-generated pulses by the μC are shown in Figure. 3A (i) as continuous stream and in Figure. 3B (i) as single pulse which

was constructed by 500 steps with 0 volt to achieve the base line, 20 steps to achieve 0.9 volt, 180 steps to make the pulse top with 0.9 volt, 20 steps to bring the pulse signal down to 0 volt and the remaining steps to fill the buffer at 0 volt and 1 step = 10ns. The pulse generated was repeated with 1 kHz frequency and the total time duration depends on the number of pulse data need to be processed. The corresponding converted current pulsed from the V-to-I conversion unit is measured in channel 2 of the μC are shown in Figure. 3 A (ii) and 3 B (ii) was used to drive the IR LEDs in pulse mode. IR radiation from the LED was detected by the IR PD and transformed in to optical pulse signal to voltage pulses (V_{out}) as measured in channel 1 of the μC shown in Figure 3A (iii) and 3B (iii). This voltage pulsed signal was collected by the μC system as raw pulsed signal and employed for further processing.

Insert Figure 3

From Figure 3 B i) it is observed that the stepwise generated pulse from the μC system which follows smooth shape, sharp rise and fall as it was generated. However, when it was converted into current pulses by the V-to-I conversion circuit the LED has a rise time of 200 ns to generate ultimate optical output (~2A). After detecting the response from the IR LED, the IR PD, has "rise time" and "fall time" of 250 ns a shown in Figure 3 B. The response delay appears due to inherent property of the semiconductor material of the IR LED and IR PD and response of the embedded PA in it and therefore, cannot be controlled by the user.

3.3.2 Data Acquisition and on-the-fly Data processing with μC system.

By default, Red Pitaya FPGA performs data acquisition in continuous mode, which may result overwriting and loss of necessary data for further processing in pulsed mode. Therefore, buffer size of data acquisition was fixed through a command to the FPGA to acquire the buffer size of points as an array of digital number. The external triggering sets the initiation of data acquisition and acquire 16384 elements after the initiation which allowed the μC system to collect only the informative part from the raw signal that includes the baseline and the entire pulse.

To eliminate time lag between data acquisition and data processing, input and output buffer of the μC were synchronized using self-triggering. Self-triggering was done by employing external triggering facility of the FPGA where the digital output from the GPIO (component E in Figure 1) was feedback as the external trigger. It was programmed by rising the pin from low (0 volt) to high (3.3 volt), kept high for 5 μsec then back to low, triggering both RF input and output to function simultaneously.

3.3.2.1 Digital filtering by repetitive smoothing, boxcar averaging and Savitzky-Golay. In order to achieve smooth pulses from the acquired raw pulses, we incorporated three digital filtering techniques namely, repetitive smoothing, boxcar averaging, and Savitzky-Golay through C programming in the CPU of the μC. When digital filtering software's are incorporated in commercially available analytical instruments, analysts lose the flexibility of investigating different digital filtering techniques with variable input data according to specific analytical requirements.[14] Our digital filtering approach with μC system allowed us to select flexible number of raw pulses starting from time zero (triggered on) to perform the repetitive smoothing by averaging consecutive pulses,[37] boxcar averaging and Savitzky-Golay (S-G) methods 14 using pointwise data from repetitive smoothing and produced smoothed processed pulses. Selection criteria for large number of raw pulses for processing are described in ESI.

In the data processing programme, we started repetitive smoothing of different number of raw pulses (10, 100, 1000, and 10,000) (Shown in Figure 4A). We then employed Boxcar averaging and Savitzky-Golay methods on 1000 pulses already smoothed by repetitively smoothing to investigate whether further smoothing after repetitive smoothing is required (discussed in section 3.3.2).

In order to obtain the final signal (height of the pulses) from both raw and processed pulses we applied three different statistical operations: simple averaging, linear regression and 2nd degree polynomial regression in the programme to evaluate the base line and pulse top (shown in Figure 4B). We selected 125 data points (discarding the pulse rise and fall) from the pulse top and 150 data points from the base line (before the rise) for each statistical operation. The difference between the pulse top and baseline i.e. pulse height is considered as final signal value for each individual pulse. Schematic representations of final evaluated signal as pulse height and the ultimate obtained stream of quasi-continuous data are shown in Figure 4C.

Insert Figure 4

3.3.2.2 Baseline noise evaluation and instrumental signal-to-noise (SNR) from the processed pulses. *A. Baseline noise evaluation.* Theoretically Gaussian (white) noise attenuates with square root of the number of repetitive pulses, while other types of noise will not. Similarly the additional Boxcar and Savitzky-Golay smoothing along with the repetitive smoothing will not be equally beneficial as well (noise will not attenuate with square root of the number of repetitive pulses). Therefore, to assess the nature of the noise of the processed data, we have conducted statistical analysis based on histogram of the baseline data point values. The histograms were constructed using 150 data points in the base line of processed pulses using repetitive smoothing for A=1000, Boxcar and repetitive smoothing for A=1000+Savitzky-Golay shown in Figure 5A. From the histograms in Figure 5A we observed that the baseline signals follow normal distribution for repetitive smoothing and for repetitive smoothing + Boxcar, while the repetitive smoothing + Savitzky-Golay resulted a distribution skewed to the right. The characteristic appearance of the normal distribution of the baseline data values in this study confirms that the baseline signals resulting from repetitive smoothing as well as repetitive smoothing with Boxcar averaging methods include only white noise.[38,39]

We determined the baseline noise of the processed pulses after repetitive smoothing by multiplying the standard deviation (σ) of 150 baseline data points by 5 following classical noise evaluation technique in analytical chemistry for flow-through detection and found a good agreement with theoretical noise values as shown in SI Figure S2 A also confirms the Gaussian nature of the baseline noise in the processed pulses through

repetition smoothing. The baseline noise values after applying three different smoothing techniques are shown in SI Figure S2 B where A=1000. As expected, the repetitive smoothing followed by additional smoothing techniques resulted in lower white noise in the baseline Boxcar averaging (7%) and Savitzky-Golay (5%).

The flexibility in this type of baseline noise evaluation with the μC system provides the users with the capability to choose from a variety of digital filtering by smoothing techniques. And so, we have chosen repetitive smoothing only for further investigation in this study with a view to provisioning of rapid data processing with the proposed μC based detection system.

Instrumental signal-to-noise (SNR). The quality of an analytical method is very often quantified by analyzing signal-to-noise ratio (SNR). We determined the instrumental SNR for each resulting signal values (pulse height) and baseline noise obtained from each processed pulse after employing different smoothing techniques. In Fig. 5B we compared the SNR values obtained after employing repetitive smoothing as a function of number of pulses being averaged (A) using three different statistical methods. We observed that the SNR improves as the number of pulses being averaged (A) increase. The enhancement of SNR follows the theory where SNR improves linearly by a factor of $\sqrt{A}$ (shown in Fig. 5C).[39] However, different statistical operations have no observable effect on the SNR values. All the measurements were reproducible since the standard deviations were too little to notice the error bars for 10 repetitions of each result.

Insert Figure 5

3.3.2.3 Determination of the digital data stream.

A. Pulse top and baseline signal distribution. In order to select the best suitable statistical method to determine the pulse top and baseline signal values for each subsequent pulse signal (pulse height), we investigated the distribution of the pulse top and baseline signal values applying simple averaging and linear regression for both cases. We omitted 2nd degree polynomial as we did not observe any significant differences in the SNR values using simple averaging, linear intercept or 2nd degree polynomial methods as illustrated in Figure 6A. In Figure S 3A of ESI we have shown the baseline and pulse top signal values obtained from evaluating 10,000 consecutive raw pulses (without implying any digital smoothing) using simple averaging and linear regression. We constructed the histogram using these data values (10,000 baselines and pulse tops) as shown in Figure S 3B and C, where we observed that the simple averaging method resulted smaller standard deviations (51% for baseline and 43% for pulse top) and normal distributions compared to linear regression for both evaluations of baselines and pulse tops.

B. Final quasi-continuous data stream. From the distribution pattern of baseline and pulse top signal values (Figure S3 B&C) it is evident that the simple averaging has less deviation while using it for signal evaluation. Therefore, we considered the simple averaging method to investigate the final signal (pulse height) distribution while averaging consecutively increased number of pulses for repetitive smoothing and referred to it as final digital data stream as shown in Figure S4. The distributions of ultimate pulsed signal (height of the pulse) became smooth and as expected the analytical noise (in voltage) of final data stream suppressed while increasing the number of consecutive pulses being averaged for repetitive smoothing.

C. *Evaluation of analytical signal by converting the voltage signal into absorbance signal.* Since, the ultimate usage of the proposed optical system is analytical sample detection based on absorbance principle, we converted each voltage signal of the final data stream (Figure S 3) into absorbance unit (a.u.). By taking the negative natural logarithm (base e) of final signal (pulse height) values, minimum measurable absorbance was determined[40] and referred to as the final analytical signal for this proposed absorbance based detection system. In Figure 6 the final absorbance signal is shown with corresponding analytical noise values (ΔA in a.u.). It is evident that as the number of repetition of pulses for smoothing increases the noise drops down by a factor of square root of number of pulses, which consequently, helps to improve the performance of any analytical detection. However, while the number of repetitive pulses increases, time required for processing each pulse increases simultaneously and the rapid instantaneous processing capability of the system goes down thereby. Hence, where fast data processing is principal focus, the number of repetitive pulses being smoothed needs to be optimized.

Insert Figure 6

Optimization. In this section, the number of pulses to be averaged for repetitive smoothing are optimized for the proposed IR detection system using on-the-fly data processing which will be exercised further in field for real sample analysis. For this, the analytical signal-to-noise ratio (ratio of averaged absorbance values obtained from Figure 6 to the corresponding absorbance noises (A/ΔA)) were compared with the instrumental signal-to-noise ratio (SNR) shown in Figure 7A. The analytical or absorbance noises (ΔA) were also compared with the instrumental or baseline noises (N) of each processed pulse as shown in Figure 7B. In both cases, the signal-to-noise ratio increased as the number of pulses being averaged were increased and almost same pattern was followed although they were appraised independently for different data set following different approach of evaluation. From Fig 8B, we observed that the analytical and instrumental noise values merged each other at A=10000 (for repetitive smoothing) which is the consequence of fixed instrumental noise only and the pulse being almost smoothed. Although at A=10000 gives the optimal result in terms of noise elimination and signal-to-noise ratio enhancement, however the time needed for each pulse being smoothed for A=10000 takes 10 secs, which in some cases may not be ideal in terms of rapid data processing. Therefore, to keep the system response fast enough for most real-time sensing scenarios, A=1000 (1 s for each data point) is used further for on-the-fly data processing in-field real sample analysis.[41]

Insert Figure 7

3.4 Conclusions

This study demonstrates the prospects of rapid data processing of large data streams on modern portable μC systems such as here with field-programmable gate array – FPGA, for on-the-fly and large data processing in rapidly changing sample sce-

narios. Further it shows the benefits of flexibility and full insight based on custom defined data handling routine implemented in an open source μC system with FPGA. The ability of user-defined data processing thus acquired and implemented through the μC system in a flexible manner also allows to generate the required pulsed driving signal for the LED in a desired shape, duration, frequency, and amplitude. The user can define and adapt as needed any data processing software and apply it in a flexible way as required. By using such miniaturized μC-FPGA system interfaced with custom made data processing routine for on-the fly and large data processing that results quasi-continuous analytical signal with high reproducibility allows analytical sensing of rapidly changing samples such as atmospheric gases a real and relatively low-cost possibility.

SUPPLEMENTARY INFORMATION

Detail of the in-house made instruments and figure for baseline noises, Pulse top and baseline signal values, constructed histograms and quasi-continuous digital data stream using two different statistical methods and command line parameter with program code are given in the SI.

AUTHOR INFORMATION

Corresponding Author

*mirek.macka@utas.edu.au.

ACKNOWLEDGMENT

MM acknowledges his ARC Future Fellowship Level 3 (FT120100559).

3.5 REFERENCES

(1) Leis, J.; Buttsworth, D.; Snook, C.; Holmes, G. IEEE Transactions on Instrumentation and Measurement 2014, 63, 3088-3095.
(2) Dang, J. M.; Fu, L.; Yan, Z. H.; Zheng, C. T.; Chang, Y. C.; Chen, C.; Wang, Y. D. Spectroscopy and Spectral Analysis 2014, 34, 2851-2857.
(3) Fanchenko, S.; Baranov, A.; Savkin, A.; Sleptsov, V. IOP Conference Series: Materials Science and Engineering 2016, 108, 012036.
(4) Rothman, L. S.; Gordon, I. E.; Babikov, Y.; Barbe, A.; Chris Benner, D.; Bernath, P. F.; Birk, M.; Bizzocchi, L.; Boudon, V.; Brown, L. R.; Campargue, A.; Chance, K.; Cohen, E. A.; Coudert, L. H.; Devi, V. M.; Drouin, B. J.; Fayt, A.; Flaud, J. M.; Gamache, R. R.; Harrison, J. J., et al. Journal of Quantitative Spectroscopy and Radiative Transfer 2013, 130, 4-50.
(5) Kim, K.-H.; Pandey, S. K.; Pal, R. J. Sep. Sci 2009, 32, 549-558.
(6) Lawrence, N. S. Talanta 2006, 69, 385-392.
(7) Massie, C.; Stewart, G.; McGregor, G.; Gilchrist, J. R. Sensors and Actuators B: Chemical 2006, 113, 830-836.
(8) Park, G.-t.; Park, K.-c.; Lyu, G.-j.; Kwon, J.-r.; Kim, Y.-g.; Ryou, B.-j.; Park, J.-i. In 24th World Gas Conference in October 2009: Buenos Aires, Argentine Republic, 2009.
(9) de Lima, K. M. G. Microchemical Journal 2012, 103, 62-67.
(10) http://msnt.com/eldev/D51-LED-Driver/, (accessed date: 20 February, 2017
(11) http://www.roithner-laser.com/led_pulsed_driver.html, (accessed date: 16th June 2016)
(12) https://www.edaq.com/, (accessed date: 15 January 2017)
(13) www.tek.com/digital-oscilloscope, (accessed date: 25 January 2017)
(14) O'Haver, T. A Pragmatic Introduction to Signal Processing; Lulu Enterprises Incorporated, 2016.
(15) Capitán-Vallvey, L. F.; Lopez-Ruiz, N.; Martinez-Olmos, A.; Erenas, M. M.; Palma, A. J. Analytica chimica acta 2015, 899, 23-56.
(16) Lauwers, D.; Brondeel, P.; Moens, L.; Vandenabeele, P. Philosophical Transactions of the Royal Society a-Mathematical Physical and Engineering Sciences 2016, 374, 10.
(17) Bui, D. A.; Hauser, P. C. Analytica chimica acta 2015, 853, 46-58.
(18) Suzuki, Y.; Takahashi, T.; Takayanagi, T.; Motomizu, S.; Kawakubo, S. Bunseki Kagaku 2010, 59, 125-130.
(19) http://www.tmgtestequipment.com.au/products/, acessed date
(20) Koenka, I. J.; Sáiz, J.; Hauser, P. C. Computer Physics Communications 2014, 185, 2724-2729
(21) Teikari, P.; Najjar, R. P.; Malkki, H.; Knoblauch, K.; Dumortier, D.; Gronfier, C.; Cooper, H. M. Journal of neuroscience methods 2012, 211, 227-236.
(22) Gandhi, V.; Heda, S.; Anand, R.; Zarin, A.; Upadhyay, A.; Chakraborty, A. L. In Microwave and Photonics (ICMAP), 2015 International Conference on; IEEE, 2015, pp 1-2.
(23) Abdallah, M.; Elkeelany, O.; Alouani, A. In 2009 41st Southeastern Symposium on System Theory, 2009, pp 360-362.
(24) Scholl, S. 2016. In https://kluedo.ub.uni-kl.de/frontdoor/index/index/docId/4442
(25) Kosicek, A. In Particle Accelerator Conference, 2005. PAC 2005. Proceedings of the; IEEE, 2005, pp 4284-4286.
(26) https://redpitaya.com/, (accessed date:7 March 2017)
(27) Zhu, H; Sun, L.; Wang, Z.; Nie, Z.; Liu, H. Journal of Applied Optics 2014, 35, 890-894.
(28) Pozniak, K. T. Measurement Science and Technology 2010, 21, 062002.
(29) Gazzano, J. D. D.; Crespo, M. L.; Cicuttin, A.; Calle, F. R. Field-Programmable Gate Array (FPGA) Technologies for High Performance Instrumentation; IGI Global, 2016.
(30) Zhu, Y.; Wang, L. M. In Proceedings of the 2015 International Conference on Electronic Science and Automation Control, Liu, C., Ed.; Atlantis Press: Paris, 2015, pp 323-326.
(31) Berces, A.; Feher, B.; Szanto, P.; Pechan, I.; Lajko, L.; Runyo, Z.; Laczko, P.; Lazanyi, J. Abstracts of Papers of the American Chemical Society 2010, 240, 1.
(32) Pascoe, C.; Box, D.; Lam, H.; George, A.; Ieee. In 2012 Symposium on Application Accelerators in High Performance Computing; IEEE Computer Soc: Los Alamitos, 2012, pp 111-120.
(33) Energy, U. S. D. O., Ed.; Office of Energy Efficiency & Renewable Energy: Washington, DC 20585, 2013.
(34) Lawler, J. V.; Currano, J. In Technologies for Synthetic Environments: Hardware-in-the-Loop Testing XIII: Orlando, FL, 2008.
(35) http://www.alfaphotonics.lv/, accessed date
(36) Geng, X. H.; Wu, D. P.; Wu, Q.; Guan, Y. F. Talanta 2012, 100, 27-31.
(37) Wahab, M. F.; Dasgupta, P. K.; Kadjo, A. F.; Armstrong, D. W. Anal Chim Acta 2016, 907, 31-44.
(38) Palmer, J. M.; Grant, B. G. The Art of Radiometry, 2009.
(39) Wentzell, P. D.; Brown, C. D. In Encyclopedia of Analytical Chemistry, Meyers, R. A., Ed.; Ó John Wiley & Sons Ltd, Chichester, 2000, pp 9764–9800.
(40) Hodgkinson, J.; Tatam, R. P. Measurement Science and Technology 2013, 24, 012004.
(41) Mittleman, D. M.; Jacobsen, R. H.; Neelamani, R.; Baraniuk, R. G.; Nuss, M. C. Applied Physics B 1998, 67, 379-390.

3.6 FIGURES

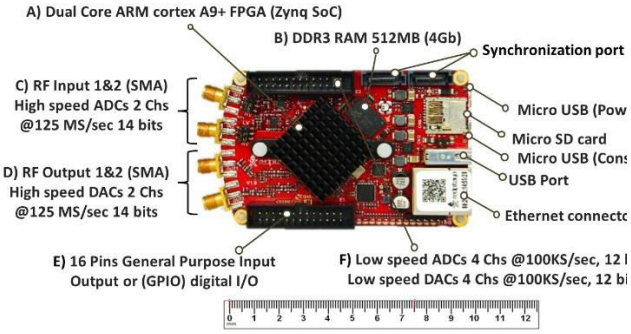

Figure 1. µC system (Red Pitaya) showing the principal components A) µC system Processor + FPGA B) RAM High speed & resolution ADC input C) High speed and resolution ADC input D) High speed and resolution DAC output E) General Purpose input and output (GPIO) which provides external self-triggering facilities F) High speed ADC input and DAC output

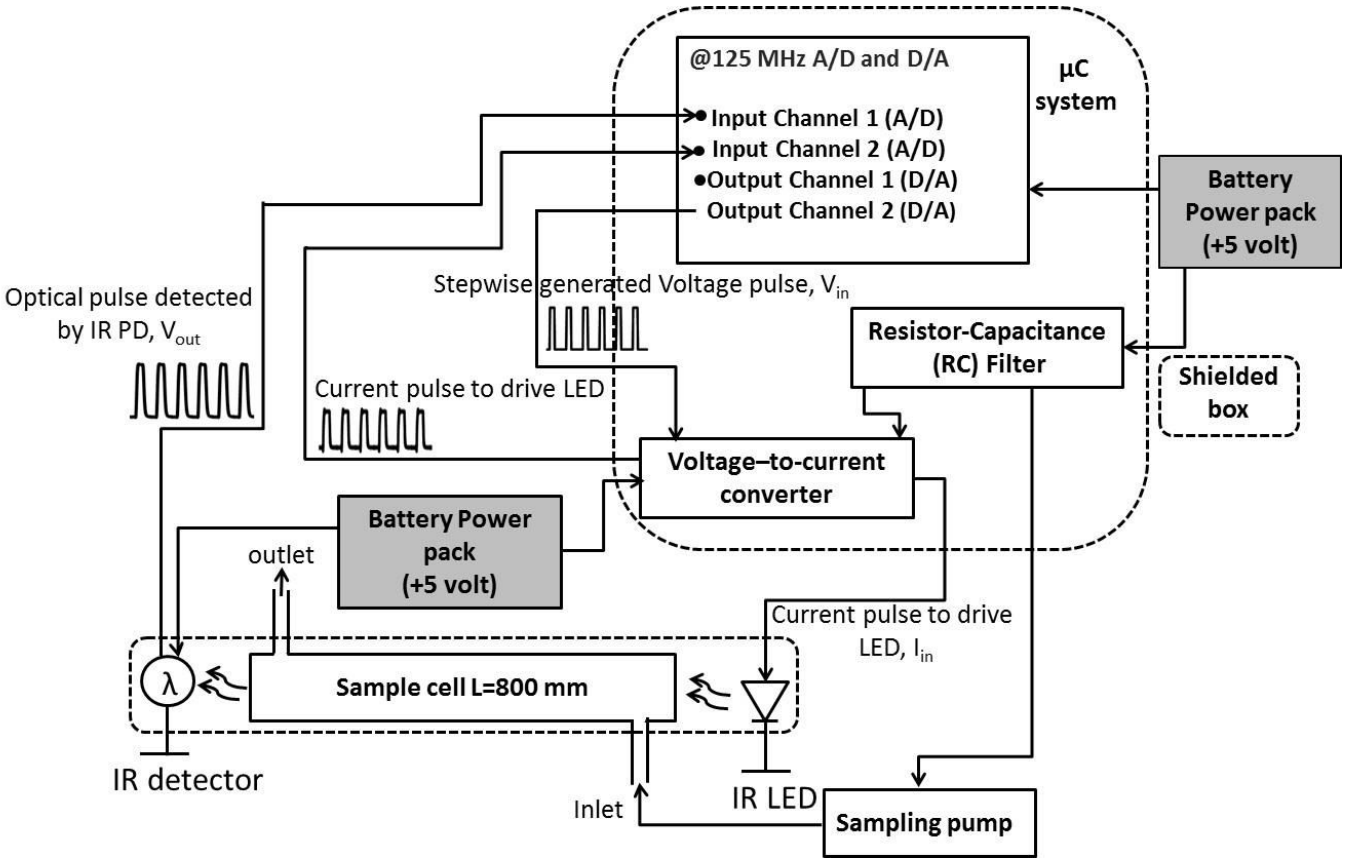

Figure 2. Schematic representation of the IR detection associated with µC system as pulse generation and data collection system

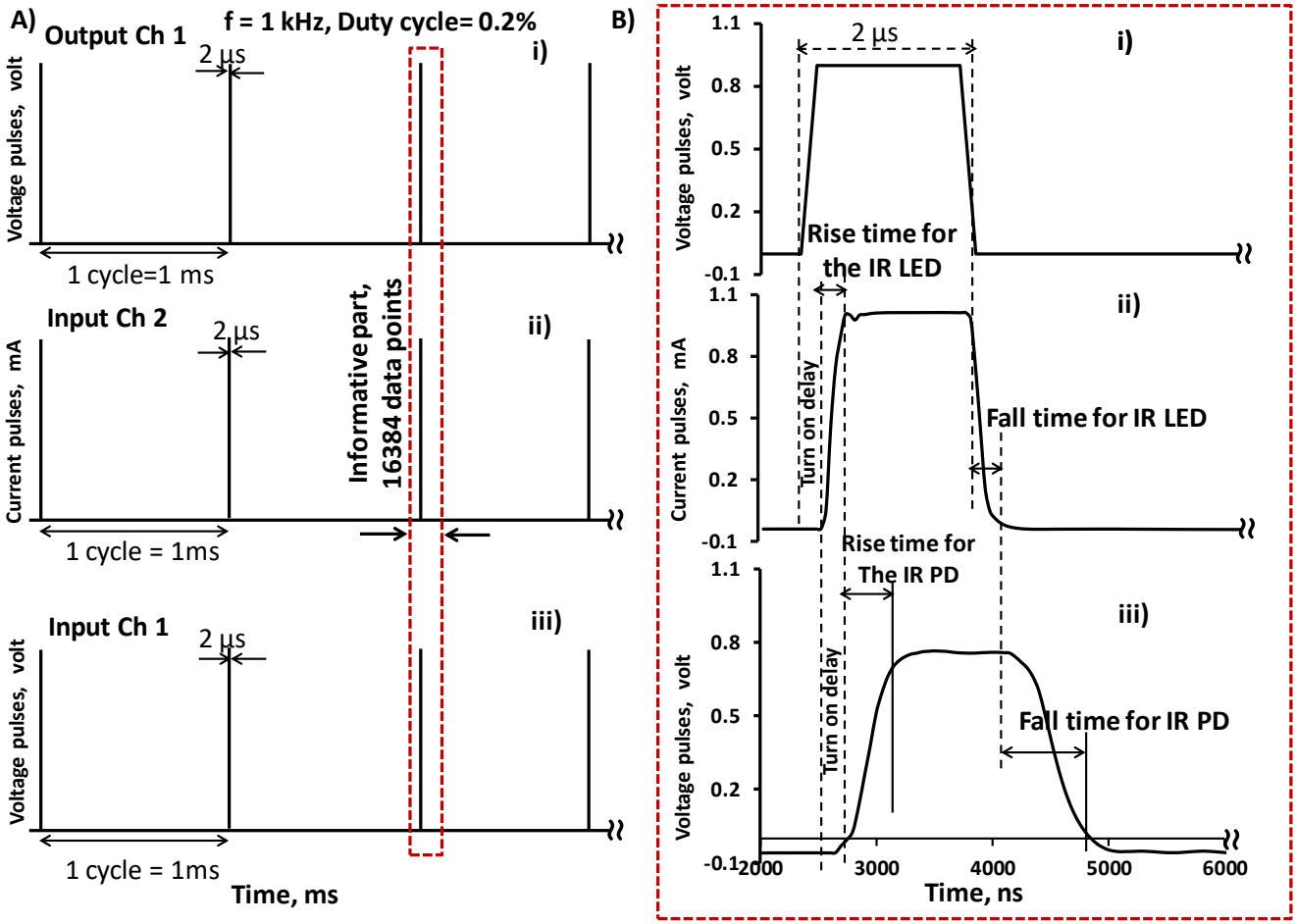

Figure 3 A) Schematic representation of three types of pulsed signals generated and measured through i) output channel 1, ii) input channel 2 and iii) input channel 1 of the micro-controller system, informative parts (buffer size data points) are shown within the red dash lined rectangle B) detail of each pulsed signal: (i) Step wise generated pulse defined by the µC system (Red Pitaya); (ii) current pulse to drive the IR LED, and (iii) the corresponding optical output pulses from the IR LED detected by the IR PD

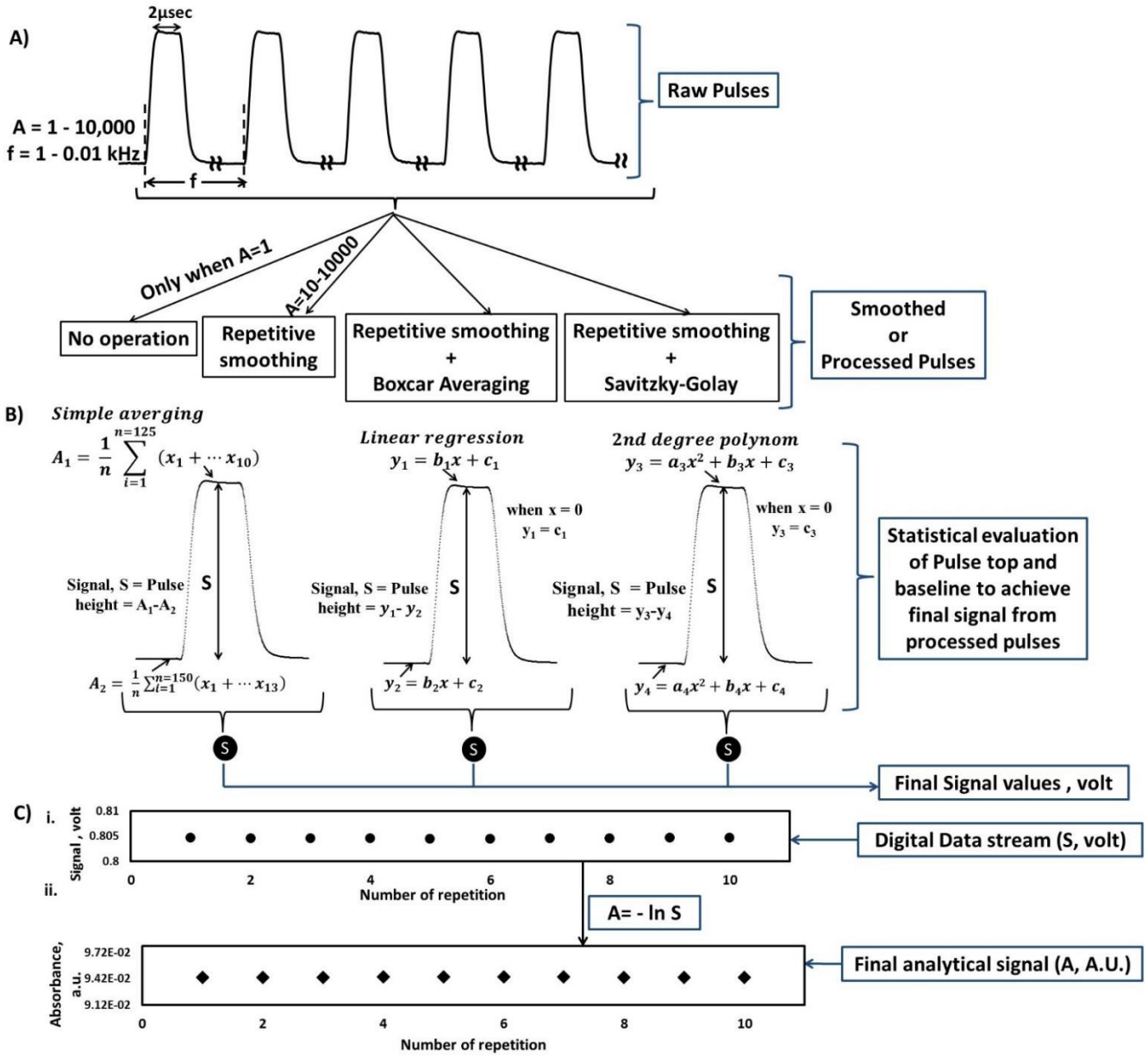

Figure 4 Schematic representation of data processing methods A) repetitive smoothing and two additional digital smoothing techniques: Boxcar averaging and Savitzky-Golay applying on pointwise obtained data from repetitive smoothened pulses B) evaluation of baseline (from 150 data points) and pulse top (from 125 data points) of each processed pulse applying three different statistical methods to obtain final signal values (height of the pulses, S) C) Final data i. digital data stream in volt and ii. analytical signal in absorbance unit (A.U.) from each individual pulse after the statistical evaluation of pulse top and baseline

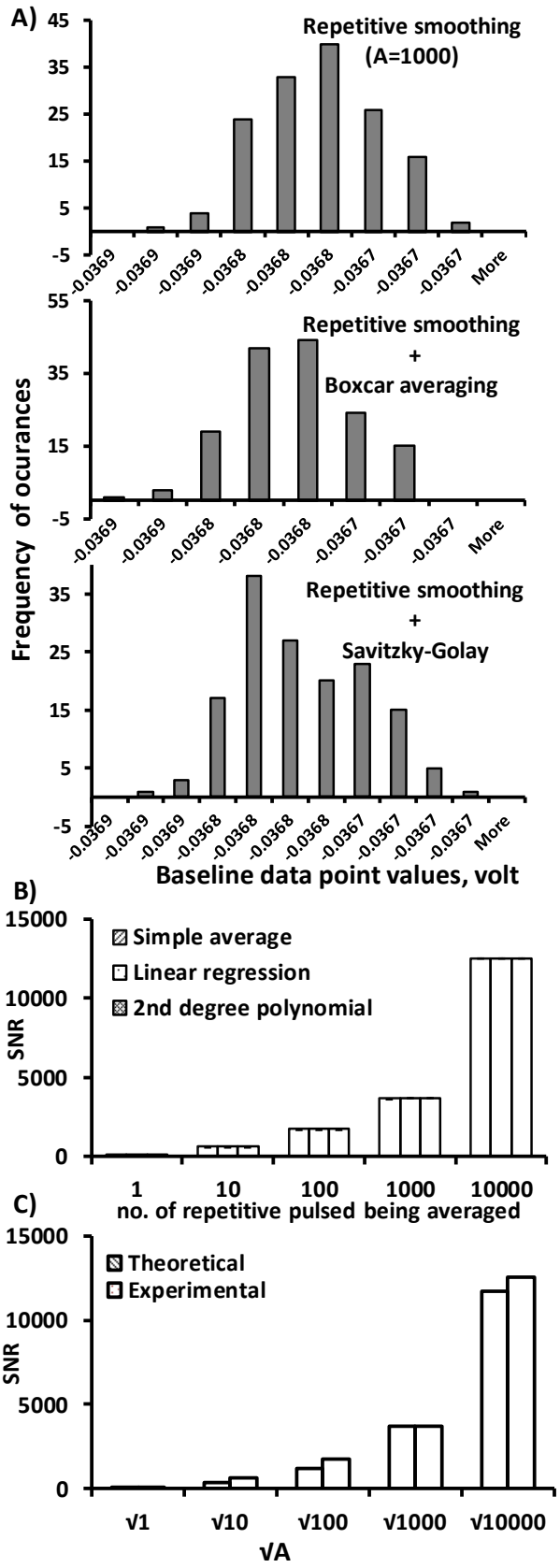

Figure 5 A) Histograms of the baseline data points. Legend: value of the baseline data points was obtained by binning the baseline data values, difference between each bin values were = (max baseline – min baseline)/6 and covers the whole range of baseline data point values B) Signal-to noise ratio obtained by applying three different statistical methods after smoothing raw pulses by repetitive smoothing and **C**) comparison of experimental SNR with theoretical values where SNR should increase by a factor of √A

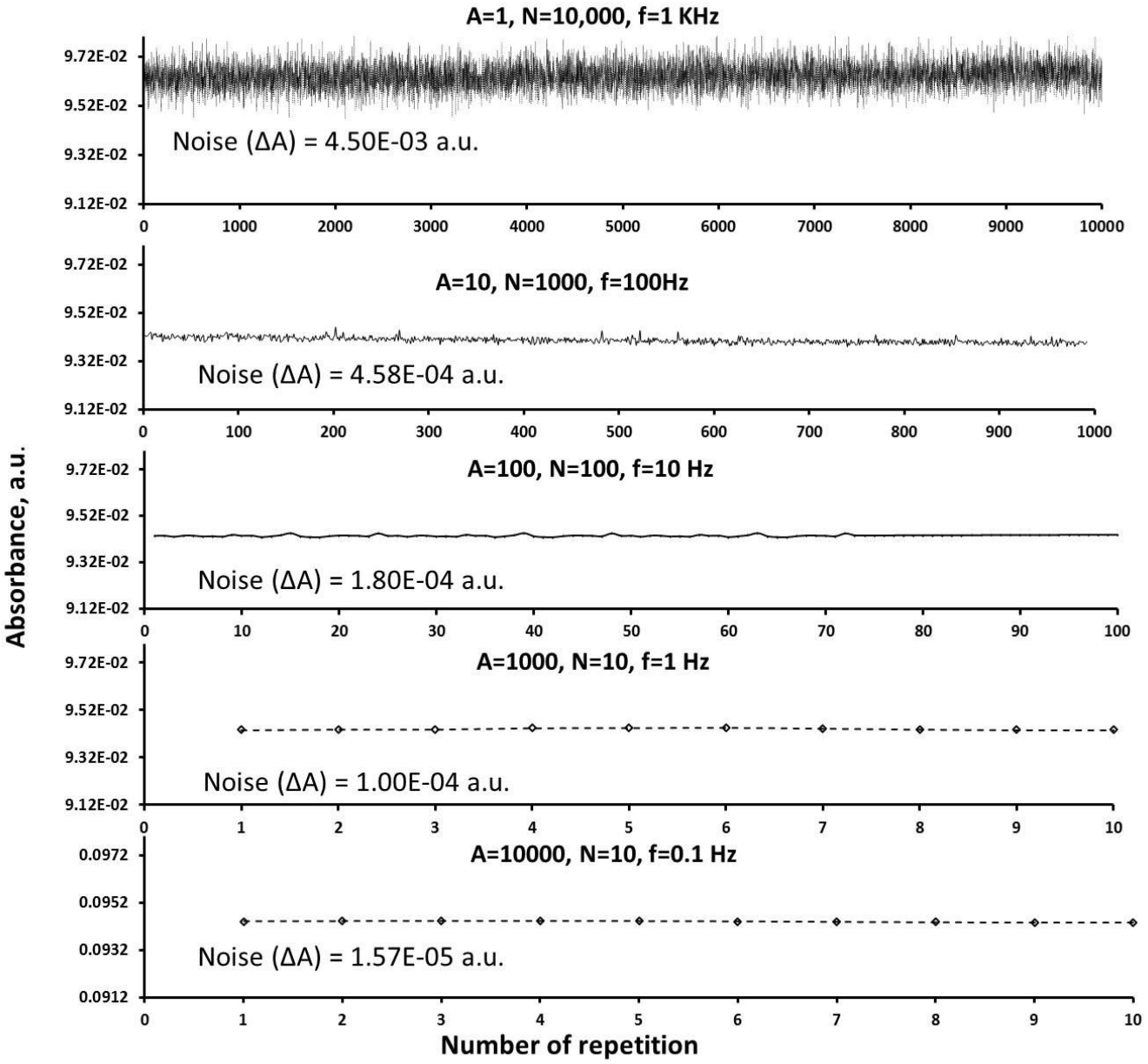

Figure 6. Ultimate analytical signal in absorbance unit (A.U.) as negative natural logarithm of each signal values with corresponding noise values

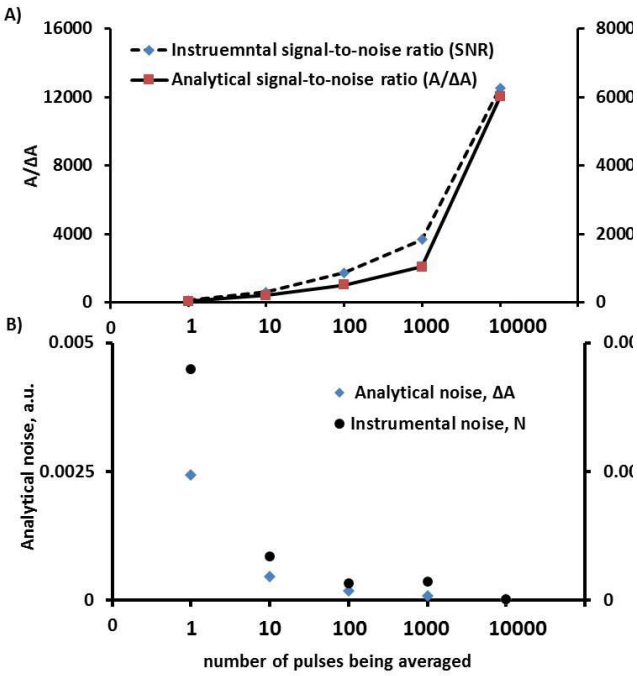

Figure 7. Comparison of analytical and instrumental A) signal to noise ratio (A/ΔA) and (SNR) respectively, calculated for different set of acquired data at different start time B) noises (noise = 5*σ) of same set data as A

FOR TOC ONLY

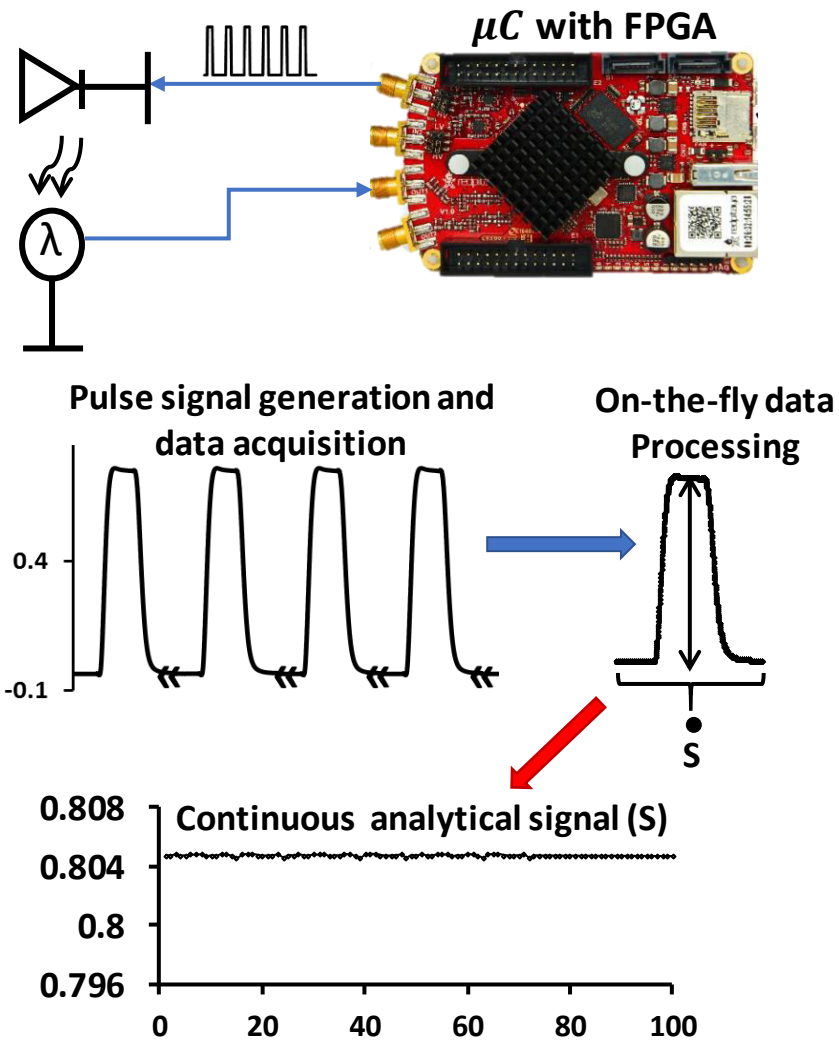
μC with FPGA
λ
Pulse signal generation and data acquisition
On-the-fly data Processing
0.4
-0.1
S
0.808
0.804
0.8
0.796
Continuous analytical signal (S)
0
20
40
60
80
100

Supplementary Information

Portable Device for Continuous Sensing with Rapidly Pulsed LEDs – Part 1: Rapid On-the-fly Processing of Large Data Streams using an Open Source Microcontroller with Field Programmable Gate Array

A. Noori [a], P. Mahbub [a], J. S. Parry [b], J. Davis [b], A. Lucieer [c], M. Macka [a*]

[a] *Australian Centre for Research on Separation Science (ACROSS) and School of Physical Sciences University of Tasmania, Private Bag 75, Hobart 7001, Australia*
[b] *Central Science laboratory, University of Tasmania, Private Bag 74, Hobart 7001, Australia*
[c] *School of Land and Food, University of Tasmania, Private Bag 76, Hobart 7001, Australia*

1. Voltage-to-current conversion

The amplified output voltage from pin 6 of the op amp turns on the Mosfet (Fig. S1 A Q1) allowing current to flow through the LED (Fig. S1 D2) and resistors R10, R11. The voltage increased across the resistors until it is equal to the voltage applied to pin 3. This voltage is fed back to the op amp (D) through pin 2 which holds the current constant until the voltage applied to pin 3 changes to a different value

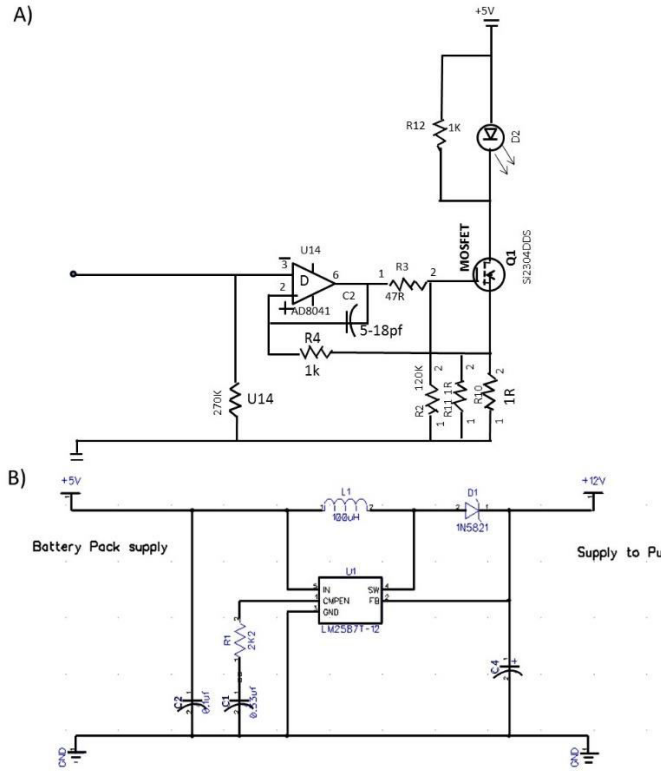

Fig. S 1 Block diagram of the in-house made **A)** voltage-to-current (V-to-I) conversion circuit **B)** resister-capacitor (RC) filter

2. Other Figures

Figure for baseline noises, Pulse top and baseline signal values, constructed histograms and quasi-continuous digital data stream using two different statistical methods are given in Figure S2, S3, S4 respectively.

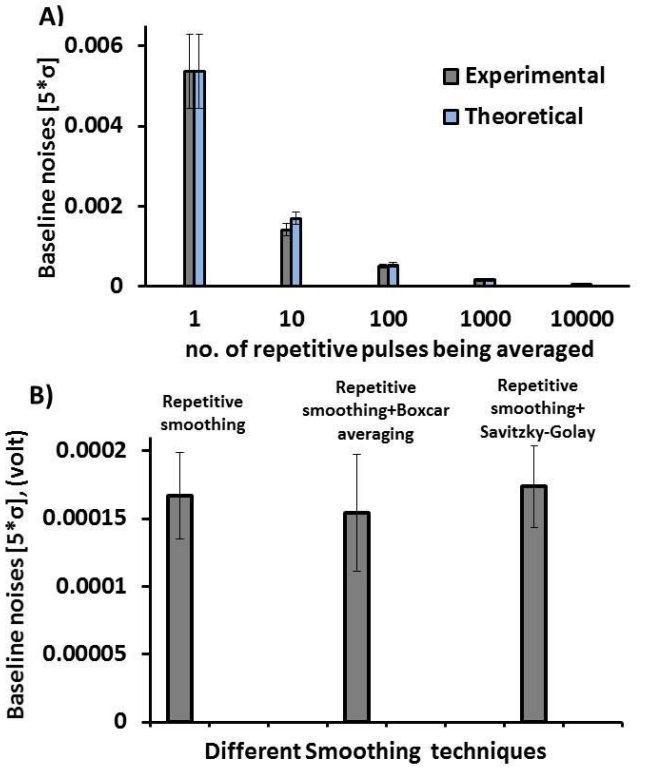

Fig S 2 A) Baseline noise values of raw and repetitive smoothing pulses compared with theoretical values B) Comparison of baseline noise values obtained after three different smoothing techniques

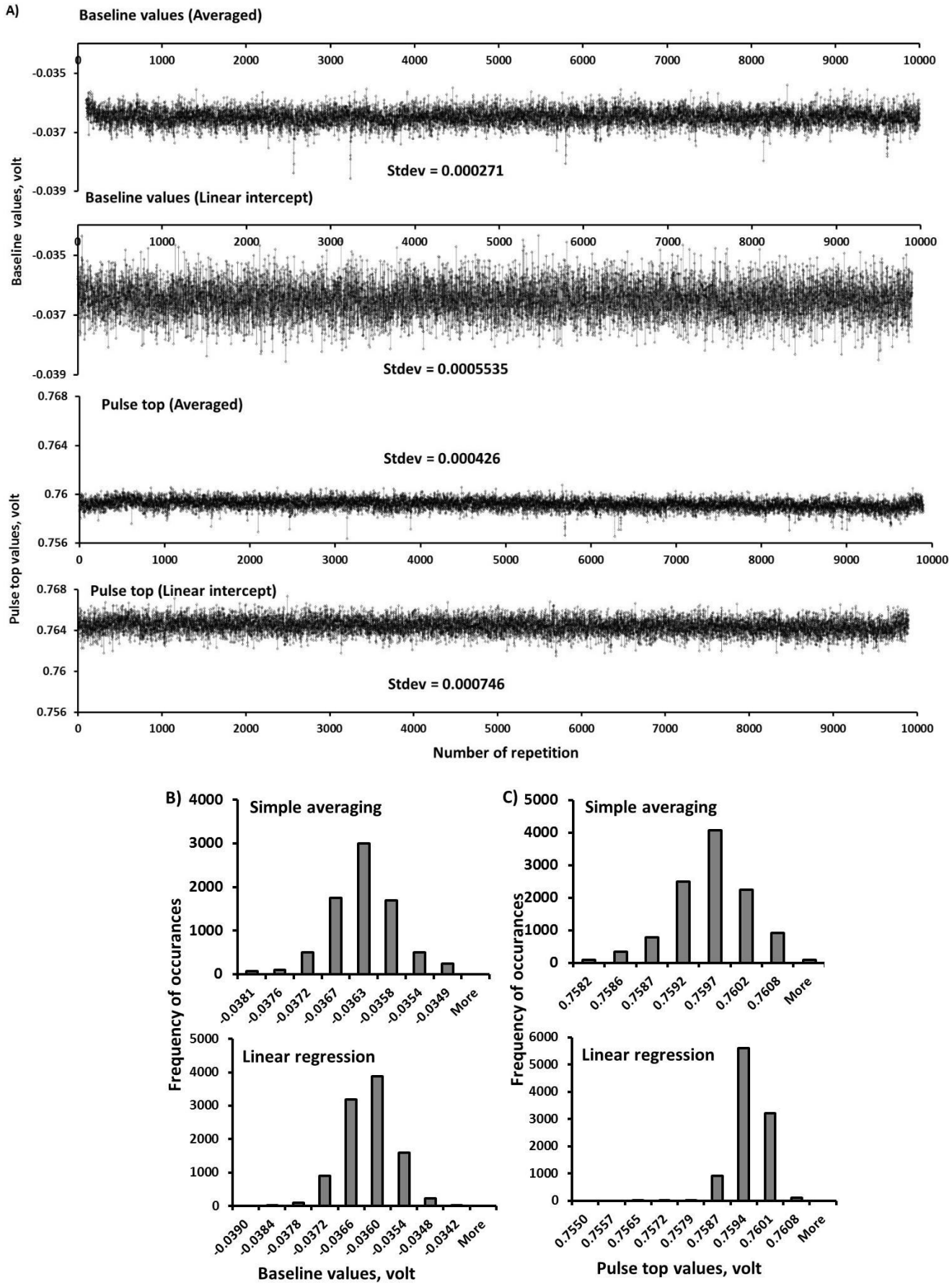

Fig S 3 A) Pulse top and baseline signal values of respective optical voltage pulses, constructed histogram **B)** pulse top data values **C)** Baseline data values obtained from 10,000 consecutive raw pulses after applying two different data evaluation statistical methods simple averaging and linear regression

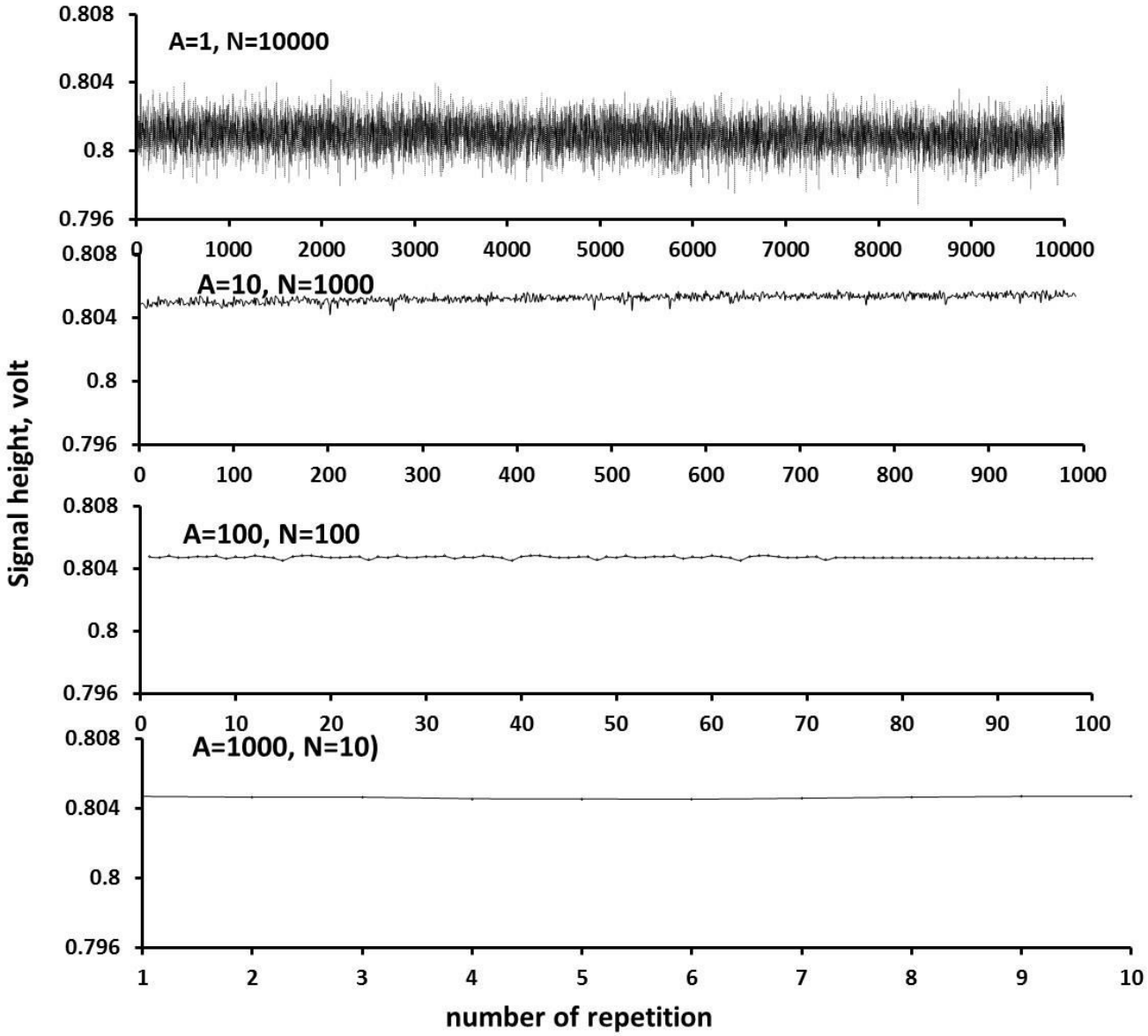

Fig. S 4 Analytical signal from each digitally processed signal pulses of processed data point as a quasi-continuous data stream using two different statistical methods A) simple averaging and B) Linear regression applied on of the pulse top (125 data points) and base line (150 data points)

3. Command line parameters and code in C language

Command line parameters for the RedPitaya peakshape program (note that lower case letters in the commands below refer to a number chosen by the user):

t,v Time (t) and voltage (v) pair. Time is in 0.01 micro seconds or steps, Voltage is in volts. Each pair specifies the next step in generating the voltage graph to be sent from the red pitaya, taking t steps to get from current voltage to desired voltage. For example, if the graph is currently at 0.4V and the parameter given is 4,0.6 then the next four steps in the graph will be 0.45V 0.50V 0.55V and 0.6V.

N=n Specifies how many samples to process. The pump will be turned on before each sample, x must be a whole number. The value of n must be a whole number greater than or equal to 1. A value less than 1 will be replaced by 1. If it is not specified the default is 10. If N=n is specified more than once then only the last one on the command line is used.

S=n Specifies how many sub groups of pulses are acquired for each sample. The pump will NOT be turned on between subgroups. If S=n is specified more than once then only the last one on the command line is used. If not specified, the default is 1, ie not sub group analysis.

A=n Specifies how many pulse are generated and acquired for each sub group which are averaged together. The total number of pulses generated / acquired and then averaged together for each sample is value of S x value of A. If A=n is specified more than once then only the last one on the command line is used.

P:s,t Specifies the speed (s) and time (t) that the pump will operate between the analysis of each sample. The value of s must be between 0.5 and 1.8, if the value is less than 0.5 the pump will not turn on, if the value is greater than 1.8 the pump will turn on to 1.8. The second parameter is the time in milliseconds to turn the pump on. Example if P:0.9,4000 is specified the pump will be provided with 0.9 volts for 4 seconds between each sample. The pump cannot be turned on for less than 500 milliseconds and any value less than 500 will be taken as 500. Example if P:1.1,0 is specified the pump will turn on the 500 milliseconds. You cannot turn the pump off by specifying no time, you must specify no voltage or not include the parameter. If this parameter is not present, the default is not to turn the pump on. . If P:s,t is specified more than once then only the last one on the command line is used.

R=Y Record the time when the pump is turned on and also turned off.

C:s,f Specifies a calculation zone within the recorded averaged pulse. The calculation preformed and a simple average, linear regression, polynomial regression, boxcar smoothing with simple average, linear regression and polynomial regression along with s-k smoothing with simple average, linear regression and polynomial regression. Up to 10 calculation zones can be specified.

B:n Specifies how many points to average together in the box car analysis.

V:s,f:v Not yet implemented.

D=N Specifies to only read and process fast analogue input channel 1 rather than both channel 1 and channel 2.

F=Y Specifies that the input signals should be collected at 125 MHz instead of the default 15.625 MHz.

Z=N Specifies to not zero the calculation array between samples. This parameter should rarely be used if ever.

O=N Specifies that the sequence of averaged pulses should NOT be written to the output.

O=n Specifies how many steps of each averaged pulse should be output, default if not specified is 1000. If O=n is specified more than once then only the last one on the command line is used.

T=Y Specifies that timing information should be provided to the user on standard streams. The information produced is how long is spent in each routine on every call, which can be used to improve the program performance or determine how long a particular run is going to take. This parameter should rarely be used.

W=Y Indicates that the program should wait for a signal (button being pushed) before collecting and analysing each sample.

W=S Indicates that the program should initially wait for a signal (button being pushed) before starting to collect samples.

Code: Program codes are available in the appendix 1 of the thesis

4 Chapter 4: Portable Device for Continuous Sensing with Rapidly Pulsed LEDs – Part 2: Continuous Real-time Methane Sensing with Wireless Analytical Signal Transfer using IR LEDs for Indoor and Outdoor Monitoring of Gases

Rapidly pulsed IR LEDs with corresponding IR sensitive photodiode are an appropriate combination for low-cost portable optical sensing of gases. We designed a low-cost portable non-dispersive infrared (NDIR) spectroscopy based CH_4 sensor using rapidly pulsed NIR LED and the μC-FPGA with user defined programme developed in the previous chapter for real-time, continuous atmospheric CH_4 sensing in indoor and outdoor environments. The design of chapter 3 is to accomplished specific aim 3 which is 'development of a simple low-cost NDIR spectroscopy based portable gas sensor using NIR LED with corresponding responsive photodiode optopair and open platform μC-FPGA with real-time data analysis capabilities for continuous sensing in indoor and door out environment.'

Portable Device for Continuous Sensing with Rapidly Pulsed LEDs – Part 2: Continuous Real-time Methane Sensing with Wireless Analytical Signal Transfer using IR LEDs for Indoor and Outdoor Monitoring of Gases

Ansara Noori[†], Parvez Mahbub[†], John S. Parry[‡], John Davis[‡], Arko Lucieer[§], Mirek Macka[†]*

[†] Australia Centre for Research on Separation Science (ACROSS) and School of Physical Sciences- Chemistry, University of Tasmania, Tasmania, Australia

[‡] Central Science laboratory, University of Tasmania, Private Bag 74, Hobart 7001, Australia

[§] School of Land and Food, University of Tasmania, Tasmania, Australia

* Corresponding author: Email: mirek.macka@utas.edu.au Fax: +61-3-6226-2858

KEYWORDS: Near infrared light emitting diodes (NIR LED); Non-dispersive Infrared (NDIR) spectroscopy; continuous methane gas sensing, wireless data transfer; On-the-fly Automated Data processing, Real-time facile monitoring of gas

ABSTRACT: Continuous measurements of fugitive emission of gases in portable and remote conditions in indoor and outdoor environments are challenging due to the technical requirements for small size and low weight and the need of on-the-fly processing of large data streams. In this work, we design a facile, low-cost and weight nondispersive infrared (NDIR) spectroscopy based system for continuous sensing of atmospheric methane (CH_4) with rapidly pulsed near-infrared light emitting diode (NIR LED) at 1.65 µm. It uses a microcontroller with field programmable gate array (µC-FPGA) enabling on-the-fly and wireless streaming and processing of large data streams (~2Gbit/s). The investigated NIR LED detection system offered favourable limit of detection (LOD) of 300 ppm (0.03%) CH_4.and precision of ±5% (RSD). All the generated raw data were processed automatically on-the-fly in the µC-FPGA and transferred wirelessly via network connection. The sensing device was then deployed in portable sensing of atmospheric CH_4 at a local landfill, resulting in quantified concentrations within the sampling area (ca 400 m^2) in the range from 0.5% to 3.35% CH_4 and was cross-validated with GC-MS (2.1% CH_4). This NIR LED based sensor system offers a facile low-cost solution for continuous real-time, quantitative and direct measurement of CH_4 concentrations in indoor and outdoor environments, and possesses future potential for remote monitoring of gases directly from mobile platforms such as, smartphones and unmanned aerial vehicles (UAV).

4.1 INTRODUCTION

Industrialization and rapid population growth are adversely affecting the ambient and indoor air quality particularly in urbanized areas throughout the world. Monitoring of flammable and explosive alkane gases such as, methane (CH_4) and ethane (C_2H_6) is obligatory in industrial applications involving high temperatures, in filling stations, petrochemicals industries, in mine excavating and at many indoor (home, hospitals, livestock barns) or outdoor (gas pipelines, gas storage, landfills) areas to ensure safety from fire and explosion, as well as to maintain health and wellbeing of the population.[1,2] Additionally, ¡ndustrial process such as, pharmaceutical production, where humidity may affect the product quality, water vapor (H_2O) monitoring is compulsory.[3,4] Strict quality control measures are also undertaken at CH_4 gas plants where biogases are upgraded to high quality biomethane.[5] Therefore, the applications of gas detection and monitoring is wide-ranging from air quality control and monitoring, healthcare to fire and explosion prevention, production and process control, personal exposure to analytical application.[6,7]

CH_4 is the most abundant hydrocarbon in the atmosphere.[8] Additionally, CH_4 is the main constituent of natural gas (NG).[9] Now-a-days, NG has become the most dominant domestic and industrial fuel. CH_4 is not only a vital player in global warming but also is extremely explosive in nature. The explosion limit of CH_4 concentration is between 5% (Lower Explosion Limit, LEL) to 15% (Upper Explosion Limit, UEL).[10] Gas explosions in coal mines where CH_4 is the main accountable constituent are frequent events causing life and property losses.[11,12] Fire and explosions are also the two most common hazards in manufacturing industries where CH_4 plays significant role.[13] Additionally, inhalation of CH_4 (even short time exposure in a confined area) may cause acute pulmonary injury with a restrictive ventilator defect.[14] Therefore, real-time, fast and accurate sensing of CH_4 is worthwhile to ensure safety, prevent invaluable life and material loss as well as to ensure quality control during upgrading biogas to biomethane.

Although analytical instruments based on gas chromatography (GC), Nuclear magnetic resonance (NMR) spectroscopy and gas chromatography with mass spectroscopy (GC-MS) are the most precise techniques for quantitative analysis of gaseous

contaminants, they need laboratory based non-portable costly instrumentations and expert handling.[15] To employ these laboratory based instruments, laborious sampling procedures are required.[16] However, in areas where sample characteristic changes frequently, sampling of the field samples for subsequent laboratory based analysis can never mimic the real-world condition.[17] Therefore, for real time in-field gas analysis, portable and robust instruments capable of fast data handling enabling continuous sensing is needed.

Some of the stationary analytical instruments (GC and GC-MS) have been upgraded to portable versions but yet to achieve better quantification, limit of detection (LOD) and sensitivity than laboratory conditions.[16,18] A wide range of commercial gas sensors based on interaction with a chemical indicator, or surface of a semiconductor metal oxide[19] and high temperature ceramic layer,[20] electrochemical, catalytic combustion (pellistor) are low-cost and field deployable, however, possess short life time, susceptible to burn out easily and have poor sensitivity.[21]

On the other hand, non-dispersive infrared (NDIR) based optical gas sensors which employ absorption, emission or Raman scattering principles in specific spectral region, are comparatively fast responsive, highly selective towards the gases and provide good precision with high sensitivity.[22] Broadband light sources such as, xenon lamps are used for open path optical gas detection*.[23] However, it needs additional optical filters to use a particular wavelength, higher electrical energy and environmental protection,[24] whereas lasers and laser diodes provide tuneable amenities and being monochromatic they have wavelength selective facilities.[25] However, low pressure and longer optical pathlength (more than 1m) is needed to achieve high sensitivity for tuneable lasers which make the spectroscopic design and measurement incredibly complex and expensive.[26] Moreover, tuneable diode lasers suffer from interference fringes in the optical path which limit their detection sensitivity.[24,27] Recently, interband and quantum cascade lasers (ICL and QCL) in mid infrared employed for measuring atmospheric CH_4 have demonstrated lower detection limits than NDIR.[28-30] However the inherent property of the QCL and ICL is that they need high electrical power supply to operate in pulse or continuous wave (CW) mode which makes them unfeasible to employ in portable devices.[28] Additionally, similar to diode lasers, QCL and ICL need cooling system to minimize the thermal rise and maintain proper functioning, as well as more than several meter pathlength to achieve reasonable sensitivity.[31] The intensity of QCL varies from pulse to pulse while operating in nanosecond pulse regime and needs faster data acquisition facilities to read the pulse signal precisely.[28,32] Although, Murata et al[33] claim to develop low power consumption QCL for atmospheric CH_4 analysis with impressive LOD, lack of real field validation, applicability of these sensors are questionable. Moreover, the proposed QCL based technique possesses longer pathlength (76 m) with complex optical design and needs cooling system for heat dissipation.[33] All these features make the QCL based detection system expensive and comparatively more convoluted than the simple NDIR spectroscopy based detection system and limits their application in portable real world measurement. Although a new generation of hollow waveguides called substrate-integrated hollow waveguide (iHWG) offers smaller pathlength for gas sensing in MIR region[34] , the requirement of minute sample (few microliters) [31] and complexity of the design and cost involved[34] diminishes their usability as a facile gas sensor. Some research group for instance, Ribessi, et al[35] also used heart shaped iHWG for CH_4 sensing in NG using two integrated NIR radiation sources (909.1–1676.2 nm and 1558.8–2169.4 nm). The resulting overlap of the hydrocarbons in the absorption spectra of NG required additional multivariate analysis. [35] Moreover, none of the gas sensors based on iHWG shown its applicability in the in-field condition in a real-time manner.

In this context, quasi-monochromatic light emitting diodes (LEDs) are available in wide spectral range with spectral matched photodiodes, are environmentally friendly, less energy consuming, compact, robust and emits high optical power while operating in pulsed mode.[36] IR LED based portable gas detection system was first reported by Johnston in 1992[37] who used MIR LEDs (3.3-3.4 μm) for CH_4 and carbon dioxide (CO_2) (at 4.5 μm) detection in a closed chamber. In 2003, Lugovskaya, et al.[38] assembled the first open path IR LED based hydrocarbon gas detector. Until now numerous IR LED and photodiode optopair were explored for CH_4 detection using NDIR spectroscopic technique.[39-42] Among the IR LEDs, NIR LED (1.3-2.3 μm range) has better thermal management capability than that of mid IR LEDs (3.3-5 μm range) due to the higher energy gap of NIR semiconductor materials (SM) than MIR SM.[43] Therefore, use of NIR LEDs for gas sensing has advantages over MIR specially for applying them in room temperature and also selectivity towards CH_4 (around 1.65 μm CH_4 has no cross-sensitivity with other gases).[44,45] Numerous research groups, for instance, Massie et al.,[46] Roy et al.[47] and Okajima, et al.[48] used NIR LED at λ_{max} = 1.66, 1.653 and 1.65 μm, respectively. However, none of the MIR and NIR LED based CH_4 sensors are competent with continuous sensing of CH_4 that requires handling of large data streams on-the-fly and rapid data processing wirelessly at indoor and outdoor environments. Although the abovementioned NIR LED based CH_4 sensors are portable, they were not employed in real field rapidly changing sample scenarios. Several commercial NDIR gas sensors are also available which are portable and field deployable,[49] however, they demonstrated poor detection limits.

This paper aims to present a simple low-cost design for a NIR LED based portable gas sensing system, on NDIR technique using open platform μC-FPGA for the first time with real-time data analysis capabilities using NIR LEDs at λ_{max} = 1.65 μm and corresponding responsive photodiode (PD) optopair. This enabled for the first time the continuous sensing using open platform μC-FPGA with rapidly pulsed NIR LED based on NDIR spectroscopy for CH_4 sensing in indoor and outdoor environments.

4.2 EXPERIMENTAL SECTION

4.2.1 Theory

CH_4 has absorbance spectral line in the IR range, therefore, when the IR radiation of certain wavelength passes through CH_4 gas, attenuation of the IR radiation occurs. The intensity

* detecting gas anywhere along the path of the IR beam.

of light passing through the gas sample relates to the gas concentration and initial light intensity I_0 and can be expressed according to Beer-Lambert Law as follows,

$$A = \ln(\frac{I_0}{I}) = \sigma_\nu CL \quad (1)$$

where, A is the gas absorbance, I_0 is the reference signal in volt (without sample) and I is the transmitted signal after getting absorbed by the sample gas in volt, L is the length of the gas cuvette in cm, C is the concentration of the gas under test in molecule.cm^{-3}, and σ_ν is the absorption cross-section in cm^2.molecule^{-1} of the CH_4 at frequency ν (cm^{-1}). Note that, unlike liquid phase samples, in gas sensing, natural 'e' based logarithm has been used instead of 10 base logarithm which results 2.3 times lower value than 10 base logarithm.[24] We can rewrite eqn. 1 as follows:

$$A = lnI_0 - ln\, I \quad (2)$$

In our work, we mathematically zeroed the blank signal ($i.e., lnI_0$=$lnI_{\text{blank}} = 0$) and hence, eqn. 2 becomes,

$$A_{sample} = -\ln(I_{sample}) \quad (3)$$

where, I_{sample} is the signal in volt when the light passes through the sample and adjusted with the zeroed blank signal.

4.2.2 Instrumentation and chemicals.

Details about the commercially procured instruments (NIR LED, IR PD, microcontroller) and in-house made electronics (voltage to current conversion unit, resistor-capacitor circuit), and other instrumentations are provided in our adjoining work (part A: rapid and on-the-fly optical data processing paper). Three electronic circuits: microcontroller (µC), voltage to current conversion unit (V-to-I) and resistor-capacitor (RC) filter were housed in shielded box (190 × 110 × 60 mm), internally coated with nickel acrylic with surface resistivity <1.5Ω/0.025mm^2 which provides shielding towards electromagnetic interference (EMI) and resistant towards chemicals and weathering impact) (BIM2006/16-EMI/RFI, RS, Sydney, AU). A 5 V and 1.3 W DC axial fan, (50×50×10 mm, 22 m³/h capacity), is used to keep all the electrical circuits cool while running.

The ultra-high purity (UHP) (99.995%), compressed CH_4 gas (BOC Limited, NSW, Australia) was used as standard sample to calibrate the proposed CH_4 sensor and GC-MS instrument (Varian 3800 Gas Chromatograph coupled to a Bruker 300-MS triple quadrupole mass spectrometer). 25.4×25.4 cm Gas bags (ALTEF, LECO Australia Pty Ltd), equipped with a single polypropylene combo valve and septum, 1 eyelet with maximum 3L capacity, were used to prepare CH_4 calibration standards. 800 mm long and 7.5 mm internal diameter electropolished aluminium tube is used as gas cuvette (sample cell) which holds the NIR LED and IR PD in correct alignment (shown in Figure 1 A and B). To pump gas (compressed air, standard CH_4 gas and CH_4 rich atmospheric air in the landfill) to the gas cuvette, a vacuum diaphragm pump (1420DP BLDC, Gardner Denver Thomas GmbH, Munich, DE) with maximum flow rate of 11l/min was employed.

4.2.3 Methods.

4.2.3.1 Design and major operation of NDIR CH_4 detection system.

The configuration of NDIR detection system is shown in Figure 1 A and B which is comprised of shielded box containing three circuit boards, gas cuvette holding the IR LED and IR PD, a vacuum pump and two battery power packs. Detail about the sensor construction is given in the ESI.

Insert Figure 1

The vacuum pump used in this system is controlled by the µC with required flow rate by employing defined voltage (1.3 volt with resultant flow rate 2 l/min) and on for 3 s which provides adequate volume of gas to flush the 80 cm gas cuvette with ca. 35 cm^3 of internal volume, 3 times once it is on. Another in house made electrical circuit RC filter is used to filter out noise generated from the op-amp of the V-to-I converter unit. In this same circuitry board, a 5 to 12 volt converter is assembled to run the pump with its required power. While the pump is running, the pulse generation is activated and again starts after 4 s (additional 1 s is required to average 1000 raw pulses being averaged, described in the part one as an accompanying paper to this article). Once the system is on we can collect flexible number of data points (in this case 50 data points) as digital data stream which are processed on-the-fly and transfer wirelessly with network connection.

4.2.3.2 Baseline construction and calibration of the NDIR detection system.

For baseline construction, the NDIR detection system was run without any sample in four different circumstances: in the lab, walking around, roof top and in the landfill. In all four situations, fresh compressed air was pumped through the gas cuvette connecting the inlet (suction) of the pump with the valve of the gas bag full of that air. The stable base lines obtained in each condition was considered as zero absorbance (result shown in Figure 4 in Result and Discussion section).

The constructed detection system was calibrated in the lab using standard CH_4 gas samples before and after the real sample analysis in the landfill site. Six different concentration of CH_4 gas (1%, 2%, 3%, 4%, 5%, and 6%) was prepared with the 99.995% UHP compressed CH_4 gas mixing with compressed clean air in gas bags using airtight gas syringes and flow meter.

4.2.3.3 Field measurements.

For atmospheric CH_4 gas analysis using the NDIR detection system, a sampling location was chosen in the landfill site at the McRobies Gully Waste Management Centre of Hobart City Council, Tasmania. Marking pegs were installed in the ground to identify the sampling site and repeat the analysis in the same area. The detection system was carried by hand and analysis of CH_4 gas in the air of the landfill site was undertaken by walking through the defined sampling path. During the analysis in the field, the GPS coordinate values (northing, easting, altitude) of each marking peg and exact sampling time were recorded and stored as comma separated value (CSV) files by using a proprietary GPS mobile app (GPS Receiver HD). All the processed real-time data were transferred wirelessly through network connection.

4.2.3.4 Cross validation with GC-MS analysis.

For GC-MS analysis, the field sample was collected in the gas bags by walking through the sampling site to attain the identical air sample as analyzed in the landfill site using the proposed NDIR detection system. GC calibration was done with different concentrations UHP (99.995%) compressed CH_4 gas using the GC-MS instrumental facilities in Central

Science Laboratories(CSL), University of Tasmania (UTAS). Then the collected air sample from the landfill site was analyzed and the process was repeated five times to test the reproducibility of the measurement. Detail about the GC-MS experimental conditions are provided in the ESI.

4.3 RESULTS AND DISCUSSIONS

4.3.1 General considerations.

Part 1 of this work already illustrates how a micro controller (μC) with field programmable gate array (FPGA) (known as Red Pitaya) was used to step wise generation of micro pulse signal for the IR LEDs (λ_{max} = 1.65 μm) which is a prerequisite for this type of LEDs. At the same time, the μC with FPGA was used for data acquisition and data processing purpose by constructing suitable algorithm and custom-made programme for it. The pulse signal generation and data processing was done simultaneously without any lag. Detail about the pulse generation, data processing program and reason behind selection of this μC with FPGA are described in part 1 of this article and outcome of part 1is used in this work.

In NIR region CH_4 has 3 sets of absorption lines, P (at 1.1 μm), Q (at 1.33 μm) and R (at 1.65 μm). In 1.65 μm region the absorption coefficients are larger and the spectral widths are broader than those P and Q bands[50,51] because the absorption lines has overtone (i.e. combination of rotational and vibrational modes), in this spectral region.[46] Moreover, it has the advantage of not overlapping with water and other gaseous absorptions that can interfere with the CH_4 response.[27,52] In Figure 2 the relative spectra of NIR LED (λ_{max} = 1.65 μm), the spectral response of the IR PD and absorption lines of CH_4 gas in the same wavelength range are shown.

Insert Figure 2

From Figure 2 we observe that CH_4 absorption band overlapped with the emission spectrum of our deployed NIR LED and the spectral responsivity of the IR PD. Since, LEDs are quasi-monochromatic light sources, its optical power is spread over the emission spectra. However, the maximum emission wavelength of the deployed LED matches the maximum absorption spectral line of CH_4 within this band and relatively high pulsing frequency (1 kHz) with 0.02% duty cycle offers substantial higher optical output (ca.5 times higher than in continuous wave mode) as well as provides thermal stability while operating in lower duty cycle. Although the spectral responsivity of the IR PD of our deployed system is completely flat across the gas absorption band, having no other interfering gas in this spectral range gives advantage of free from any interference and error due to over estimation.

4.3.2 Design considerations.

4.3.2.1 Optimization of the length of the gas cuvette.

Absorbance is related to gas concentration and the pathlength through which light travel across. (eqn. 1). Longer pathlength facilitates higher absorbance and hence, lower LOD of the detection system, because it provides better absorbance of the IR radiation within the gas cuvette allowing more time for interaction and gives advantage for very low concentration measurement.[53] Moreover, NDIR gas sensing relies on the strength of optical absorption in the IR region and the absorption strength of CH_4 in NIR region is nearly two order of magnitude smaller than that in the mid IR (MIR).[24] Eventually, effective interaction of the gaseous molecules with NIR radiation is slower and longer time is needed to provide better resolution of gaseous molecular interaction with NIR radiation and increased sensitivity of gas detection.[54] Hodgkinson and Tatam reported that maximizing the pathlength also enables to overcome the detector noise limit.[54]

To investigate the maximum optimized pathlength for our proposed NDIR detection system, we used different length of electropolished aluminium tubes (Al has 99% reflectivity in NIR region) from 10 to 100 cm, and scrutinized the optical output (mV) and corresponding signal-to-noise ratio (SNR) of the employed LED applying two different pulsed forward current, 0.2 A and 1.8 A. The obtained results are shown in Figure 3. From Figure 3 we observe that up to certain pathlength the optical output signal remains saturated using two different applied current because of the overshooting (beyond the response limit) of the IR PD. While applying 1.8 A current (the highest possible forward current for this type of NIR LED), the signal got saturated up to 60 cm whereas while lower current (0.2 A) was applied, the signal endures saturation up to 30 cm. The highest optical output with maximum applied current was obtained at 80 cm pathlength without being saturated. We also attained the maximum SNR (9120) while using 80 cm length polished Al-tube by applying highest possible current 1.8 A. Hence, we selected 80 cm as the optimized pathlength for our NDIR detection system for resultant highest signal with highest SNR to utilize the maximum radiometric power output from the NIR LED while keeping the path length long enough to provide prolonged interaction period amongst the gaseous molecules and the incident IR radiation.

Insert Figure 3

4.3.2.2 Instrumental Design.

In Figure 1A and B, the photograph and scheme the NDIR based gas detection system is shown respectively. The advantage of using μC as pulse generator is manifold, such as, the commercially available LED pulse generators provides some fixed provision for applied current, duration of the pulse (duty cycle %) and frequency of pulse current, whereas in our system any shape, duration and applied current is allowed to produce in a flexible manner. Thermal rise is a vital issue for IR LEDs which is minimized using small 0.2% duty cycle with 1 kHz frequency (2 μsec on time and 980 μsec off time). The mounting technique for the LED and the detector with the gas cuvette are shown in the red rectangular in Figure 1B which are designed to provide the inlet and outlet for the gas sample in an elegant but simple way. The inner surface of the Al-tube was electropolished to capture maximum light by reflecting back to the PD. However, our primary aim at this point is not to achieve perfect waveguiding for our system, but the simplicity and efficiency of our system. Sometimes waveguidings such as iHWG are employed for IR active gas sensing.[34] However, the channel dimensions of these types of waveguides are relatively narrow (ca. 2 mm which are suitable for directional and coherent emitter such as lasers),[31] while efficient coupling of incoherent sources like LEDs poses additional challenges that may render the sensor design more complex.[50] Moreover, coupling the iHeart (heart shape iHWG) did not produce superior LOD values for methane in NG (LOD for methane was 0.42% at 1700 nm and 0.49% at 2200nm).[35]

4.3.3 Baseline considerations and linearity.

From the digital signal data stream in volt, the absorbance was directly calculated on-the-fly as the negative logarithm (base 'e') of the signal which at the end was considered as final analytical signal using eqn (3).

$$A = -\ln S \quad (4)$$

where S is the value of each data point in volt and A is the absorbance in absorbance unit (a.u.).

When only clean air was pumped through the gas cuvette, the analytical signal was regarded as baseline. Since absorbance is a relative measurement we considered the obtained absorbance values as zero absorbance for the baseline. Therefore, the upsurge of absorbance from this zeroed value is considered as the presence of CH_4 gas (S_{sample}). To check the stability of the proposed system, baseline of this system is established in four different environmental conditions: i) in the laboratory, ii) while walking outside the lab, iii) in the roof top and iv) in the landfill site. The result of the obtained zeroed base line values in all four conditions are shown in Figure 4A and B. In Figure 4A it shows that all the four baselines in different conditions coincided each other. However, when the scale was zoomed by 2 orders of magnitude we can see that four baselines are not completely identical. Baselines in the laboratory and walking around outside the laboratory have stable signal and are moderately identical to each other while the roof top base line has slightly increased stable signal, but the landfill site baseline obtained some instability. Nevertheless, none of the baseline exceeded the upper limit of 95% confidence interval as shown in Figure S1 in the supplementary information (SI).

In order to test the linearity of the system, 6 different standard concentration of CH_4 was pumped through the gas cuvettes, which were prepared in the 3 L capacity gas bags. The obtained continuous absorbance signal (50 data points) for 200 s is shown with the baseline signal in Figure 4B. From the Figure 4 it is found that as the concentration of the CH_4 gas increases the absorbance signal rises from the baseline. Concentration verses absorbance calibration curve is shown in the Figure S2 in the SI. The calibration was done before and after the field measurement and reproducibility of the result was obtained within $\pm 5\%$ RSD which approves the reliability and robustness of this NDIR based sensor.

The obtained result shows that the LOD of our detection is 300 ppm (0.03%) (shown in SI as Figure S2) which is around 160 times lower than the LEL) of CH_4 gas (LEL= 5%), however, in the atmosphere which is ~ 2 ppm and acquired by exploiting Annual Greenhouse Gases Index (AGGI) over the year.[55]

Insert Figure 4

4.3.4 Field deployment.

Once the baseline stability without sample and linearity of the absorbance data with standard sample in the laboratory was achieved, the detection system was tested in the real-field application. The landfill site was chosen as it is one of the most obvious regions which produce huge amount of CH_4 gas mainly through anaerobic decomposition of different types of organic materials[56] and it contributed 22% of atmospheric CH_4.[57] In Figure 5A and B, the 3D spatial map of CH_4 concentration along the selected sampling area and the location of the sampling path at the landfill are presented, respectively. Distance between each sampling points were ~10 meter and the detection system was carried in hand while walking along the sampling path. The concentration of CH_4 varied from one point to another and variation was between 0.5% to 3.35%. The RSD of measurements (six times) were within $\pm 25\%$ which is quite similar to other studies such as, Robinson, et al[58] where the agreement was within $\pm 20\%$. According to Slanina et al[59] measurement of CH_4 emission from its sources observe immense uncertainty and variation. Such variations can be attributed to the highly heterogeneous nature of the distribution of CH_4 emissions across any given site during the time of measurement, the content of the waste being landfilled, the route followed by the emitted CH_4 to reach surface as well as escape through faults in any gas control system or migration through geological features.[58]

From Figure 5A we observe a well-defined concentration pattern in the 3D spatial mapping varying with visible dumping sites at the landfill. The highest concentration was observed adjacent to the pile of dumped material (white circles in Fig. 5B) where continuous production of CH_4 gas due to the decomposition of organic material may trigger the elevated CH_4 concentrations. As the distance increases from the piles of dump materials, CH_4 starts diluting with ambient air, and consequently, lower percentage of CH_4 was acquired. From Figure 5A we also observe that low (0.5%-0.9%) CH_4 concentration profiles are at the high elevation sampling points (196 m), whereas, the highest concentration (3.35%) was obtained after 6 m below at the highest elevated sampling point (190 m). The concentrations remain relatively higher and unchanged (2.75%-3.35%) at 190 m elevation zone. This profile indicates gas concentration is influenced by the elevation of the surface and significance of surface level CH_4 emission measurement is substantiated. Now-a-days, Airborne Visible/Infrared Imaging Spectrometers (AVIRIS) have been used for mapping the CH_4 emission by measuring the reflected radiation spectrum.[60] However, many of these sensors fail to detect the lower surface emission over heterogeneous surfaces and suffers from spatial resolution problem,[61] therefore needs huge thermal data simulation, to achieve fine spatial resolution.[62] To the contrary, our designed sensor, undertakes continuous sampling of CH_4 resulting accurate lower surface spatial mapping of CH_4 concentration in real time in a simplistic, facile manner while keeping the measurement sensitivity maximum.

Insert Figure 5

4.3.5 Validation of results with GC-MS and comparison with other sensing techniques.

As mentioned in the method section, the atmospheric air sample was collected in the 3L gas bags by walking through the same sampling path (shown in Figure 5B) for cross validation of the field measurements using our sensor with standard laboratory based GC-MS analysis. The results are shown in Figure S3 in the supplementary information with the GC-MS calibration curve obtained using standard CH_4 sample. 2.1% ($\pm 0.2\%$) CH_4 concentration was obtained in the field sample which represent the CH_4 concentration in the entire sampling area since the sample was collected by walking through the same sampling area. GC peak and MS spectrum of standard CH_4 gas and the fields sample are shown in Figure S 3A and B.

In Table 1, the comparisons amongst crucial performance parameters of existing gas sensors using different detection techniques and our designed sensor are illustrated.

Insert Table 1

From this table we observe that the CH_4 sensor we developed is the simplest in terms of optical design, thermal management and use of simple algorithm for data processing, faster (analysis time needed is shortest among the other technique), cost effective (electric energy consumption is lower, the NIR LED is order of magnitude cheaper than any other NIR sources for instance tunable diode laser, I/QCL and microbulbs, possesses on-the-fly data processing and wireless data transfer competencies enabling continuous sensing of CH_4 at indoor and outdoor with comparable LOD to other NDIR NIR LED based CH_4 sensors.[47,63]

4.4 CONCLUSIONS

We designed a simple low-cost NDIR spectroscopic CH_4 sensor using rapidly pulsed NIR LED with flexible, wireless and on-the-fly data handling capability in real-time manner, thus enabling continuous sensing of CH_4. The µC with FPGA system used in this sensor worked as signal generating, signal processing, wireless and on-the-fly data handling, storage and transfer unit as well as to control the pump for sampling. All these capabilities are provided in a flexible open platform manner, through custom made programme with specific command code. This portable sensor is capable of measuring the atmospheric CH_4 in a continuous basis without using any complex algorithm, costly instrumentations or data post-processing. The sensor demonstrated operational sensitivity, reliability and repeatability of the baseline over time.

Our simple optical design as well as fast data handling and data processing features subsequently enabled the sensor to deploy in real world sample analysis in a facile way and offers a genuine alternative to laser based optical sensing at lower cost and instrumental complexity. At a landfill site this sensor detected CH_4 selectively in real-time and continuous manner, and the result from cross validation using standard analytical method GC-MS in the laboratory demonstrates the authenticity of the sensor performance. Furthermore, such low cost continuous CH_4 sensor possesses future potential to integrate advanced software applications in remote sensing of gases using low cost mobile platforms such as smartphones or unmanned aerial vehicles (UAV) in a facile manner.

ACKNOWLEDGEMENTS

MM acknowledges his ARC Future Fellowship Level 3 (FT120100559). The authors have declared no conflict of interest.

SUPPLEMENTARY INFORMATION AVAILABLE

The linear relation of absorbance vs concentration with standard CH_4 sample as calibration curve for the proposed detection system, the calibration curve for GC-MS analysis with standard CH_4 sample and the GC-MS spectrum for standard CH_4 gas and field sample are shown.

4.5 REFERENCES

(1) Beaver, R. L.; Field, W. E. *J Agromedicine* **2007**, *12*, 3-23.
(2) Kucuker, H. *Occup Med (Lond)* **2006**, *56*, 144-146.
(3) Crouter, A.; Briens, L. *AAPS PharmSciTech* **2014**, *15*, 65-74.
(4) Rogers, B.; Setra Blog: Boxborough, MA 01719, USA, 2016.
(5) Knobelspies, S.; Bierer, B.; Perez, A. O.; Wöllenstein, J.; Kneer, J.; Palzer, S. *Sensors and Actuators B: Chemical* **2016**, *236*, 885-892.
(6) Rathgeb, F.; Gauglitz, G. In *Encyclopedia of Analytical Chemistry*; John Wiley & Sons, Ltd, 2006.
(7) Lakkis, S.; Younes, R.; Alayli, Y.; Sawan, M. *Sensor Review* **2014**, *34*, 24-35.
(8) Bianchi, F.; Barmet, P.; Stirnweis, L.; El Haddad, I.; Platt, S. M.; Saurer, M.; Lotscher, C.; Siegwolf, R.; Bigi, A.; Hoyle, C. R.; DeCarlo, P. F.; Slowik, J. G.; Prevot, A. S. H.; Baltensperger, U.; Dommen, J. *Atmospheric Environment* **2016**, *141*, 41-47.
(9) Faramawy, S.; Zaki, T.; Sakr, A.-E. *Journal of Natural Gas Science and Engineering* **2016**, *34*, 34-54.
(10) Gas, L. *Matheson gas products* **2013**, 22.
(11) Yang, C.; Li, X.; Xu, T.; Qu, W.; Liu, Y. In *3rd International Symposium on Mine Safety Science and Engineering*, 2016, pp 616-621.
(12) Ajrash, M. J.; Zanganeh, J.; Moghtaderi, B. *Journal of Loss Prevention in the Process Industries* **2016**, *40*, 207-216.
(13) Wu, S. Y.; Lin, N. K.; Shu, C. M. *Process Safety Progress* **2010**, *29*, 349-352.
(14) Jo, J. Y.; Kwon, Y. S.; Lee, J. W.; Park, J. S.; Rho, B. H.; Choi, W.-I. *Tuberculosis and respiratory diseases* **2013**, *74*, 120-123.
(15) Lawrence, N. S. *Talanta* **2006**, *69*, 385-392.
(16) Gałuszka, A.; Migaszewski, Z. M.; Namieśnik, J. *Environmental Research* **2015**, *140*, 593-603.
(17) Pawliszyn, J. *Sampling and sample preparation for field and laboratory: fundamentals and new directions in sample preparation*; Elsevier, 2002; Vol. 37.
(18) Harris, C. M. *Analytical chemistry* **2002**, *74*, 585 A-589 A.
(19) Capone, S.; Forleo, A.; Francioso, L.; Rella, R.; Siciliano, P.; Spadavecchia, J.; Presicce, D.; Taurino, A. *Journal of Optoelectronics and Advanced Materials* **2003**, *5*, 1335-1348.
(20) Akbar, S.; Dutta, P.; Lee, C. *International Journal of Applied Ceramic Technology* **2006**, *3*, 302-311.
(21) Shemshad, J.; Aminossadati, S. M.; Kizil, M. S. *Sensors and Actuators, B: Chemical* **2012**, *171-172*, 77-92.
(22) Dakin, J. P.; Chambers, P. In *Optical Chemical Sensors*; Springer, 2006, pp 457-477.
(23) Li, S. W.; Wen, M. H.; Dai, H. F.; Wang, J. T.; Li, P. F. *Guangdianzi Jiguang/Journal of Optoelectronics Laser* **2014**, *25*, 920-924.
(24) Hodgkinson, J.; Tatam, R. P. *Measurement Science and Technology* **2013**, *24*, 012004.
(25) Mao, X. F.; Zheng, P. C.; Wang, X. F.; Yuan, S. Z. *Sensors and Actuators B-Chemical* **2017**, *239*, 1257-1260.
(26) Werle, P. W. In *Laser in Environmental and Life Sciences*; Springer, 2004, pp 223-243.
(27) Shemshad, J.; Aminossadati, S. M.; Kizil, M. S. *Sensors and Actuators B: Chemical* **2012**, *171*, 77-92.
(28) Li, J.; Chen, W.; Fischer, H. *Applied Spectroscopy Reviews* **2013**, *48*, 523-559.
(29) Kosterev, A.; Wysocki, G.; Bakhirkin, Y.; So, S.; Lewicki, R.; Fraser, M.; Tittel, F.; Curl, R. F. *Applied Physics B* **2008**, *90*, 165-176.
(30) Manfred, K. M.; Hunter, K. M.; Ciaffoni, L.; Ritchie, G. A. D. *Analytical Chemistry* **2017**, *89*, 902-909.
(31) Tütüncü, E.; Nägele, M.; Fuchs, P.; Fischer, M.; Mizaikoff, B. *ACS Sensors* **2016**, *1*, 847-851.
(32) Gmachl, C.; Capasso, F.; Sivco, D. L.; Cho, A. Y. *Reports on progress in physics* **2001**, *64*, 1533.
(33) Murata, M.; Yoshinaga, H.; Mori, H.; Tsuji, Y.; Hashimoto, J.-I.; Iguchi, Y. *SEI TECHNICAL REVIEW* **2016**, 41.
(34) Wilk, A.; Carter, J. C.; Chrisp, M.; Manuel, A. M.; Mirkarimi, P.; Alameda, J. B.; Mizaikoff, B. *Analytical chemistry* **2013**, *85*, 11205-11210.
(35) Ribessi, R. L.; Neves, T. d. A.; Rohwedder, J. J.; Pasquini, C.; Raimundo, I. M.; Wilk, A.; Kokoric, V.; Mizaikoff, B. *Analyst* **2016**, *141*, 5298-5303.
(36) Yeh, P.; Yeh, N.; Lee, C.-H.; Ding, T.-J. *Renewable and Sustainable Energy Reviews* **2017**, *75*, 461-468.

(37) Johnston, S. F. *Measurement Science and Technology* **1992**, *3*, 191.
(38) Lugovskaya, A. I.; Login, S. A.; Balashov, O. B.; Kuznetsov, A. A.; Vasiliev, E. V.; Chernyak, E. Y. *Products and Systems. Control, monitoring, diagnostics* **2003**, *6* 55-59.
(39) Popov, A.; Stepanov, M.; Sherstnev, V.; Yakovlev, Y. P. *Technical Physics Letters* **1997**, *23*, 828-830.
(40) Matveev, B.; Aidaraliev, M.; Gavrilov, G.; Zotova, N.; Karandashov, S.; Sotnikova, G.; Stus, N.; Talalakin, G.; Il'inskaya, N.; Aleksandrov, S. *Sensors and Actuators B: Chemical* **1998**, *51*, 233-237.
(41) Krier, A.; Sherstnev, V. V. *Journal of Physics D: Applied Physics* **2000**, *33*, 101.
(42) Alexandrov, S.; Gavrilov, G. A.; Kapralov, A.; Karandashev, S. A.; Matveev, B. A.; Sotnikova, G. Y.; Stus, N. M. In *Second International Conference on Lasers for Measurement and Information Transfer*; International Society for Optics and Photonics, 2002, pp 188-194.
(43) Fanchenko, S.; Baranov, A.; Savkin, A.; Somov, A.; Calliari, L. In *IEEE 2nd International Smart Cities Conference: Improving the Citizens Quality of Life, ISC2 2016 - Proceedings*, 2016.
(44) Clark, R. N.; Curchin, J. M.; Hoefen, T. M.; Swayze, G. A. *Journal of Geophysical Research: Planets* **2009**, *114*.
(45) Hodgkinson, J.; Pride, R. D. *Measurement Science and Technology* **2010**, *21*, 105103.
(46) Massie, C.; Stewart, G.; McGregor, G.; Gilchrist, J. R. *Sensors and Actuators B: Chemical* **2006**, *113*, 830-836.
(47) Roy, S.; Desikan, R.; Duttagupta, S. P. *arXiv preprint arXiv:1611.08797* **2016**.
(48) Okajima, H.; Kakuma, S.; Uchida, K.; Wakimoto, Y.; Noda, K. In *SICE-ICASE, 2006. International Joint Conference*; IEEE, 2006, pp 1652-1655.
(49) *Drager Technology for Life*. [cited 2017 15 January, 2017]; Available from: https://www.draeger.com/en_aunz/Home.
(50) De Biasio, M.; Leitner, R.; Krall, C.; Krivec, M.; Wilk, A.; Mizaikoff, B.; Waldner, R.; Starmans, F.; Maier, D. In *SENSORS, 2016 IEEE*; IEEE, 2016, pp 1-3.
(51) Pfeiffer, P.; Meyrueis, P.; Patillon, D.; Bounaix, F. *IEEE Transactions on Instrumentation and Measurement* **2004**, *53*, 45-50.
(52) Jun, L.; Qiulin, T.; Wendong, Z.; Chenyang, X.; Tao, G.; Jijun, X. *Measurement* **2011**, *44*, 823-831.
(53) Leis, J.; Buttsworth, D.; Snook, C.; Holmes, G. *IEEE Transactions on Instrumentation and Measurement* **2014**, *63*, 3088-3095.
(54) Hodgkinson, J.; Smith, R.; Ho, W. O.; Saffell, J. R.; Tatam, R. P. *Sensors and Actuators B: Chemical* **2013**, *186*, 580-588.
(55) Butler, J. H.; Montzka, S. A., National Oceanic & Atmospheric Administration: NOAA, U. S. D. o. C., Ed.; Earth System Research Laboratory: R/GMD, 325 Broadway, Boulder, CO 80305-332, 2014.
(56) Li, Y.; Park, S. Y.; Zhu, J. *Renewable and sustainable energy reviews* **2011**, *15*, 821-826.
(57) EPA, U. S. *FINAL ORS Protocol* **2006**.
(58) Robinson, R.; Gardiner, T.; Innocenti, F.; Woods, P.; Coleman, M. *Journal of Environmental Monitoring* **2011**, *13*, 2213-2220.
(59) Slanina, J.; Warneck, P.; Bazhin, N. M.; Akimoto, H.; Kieskamp, W.; Khalil, M.; Calvert, J.; Matthews, E.; Barrie, L.; Wahlen, M. *Pure and applied chemistry* **1994**, *66*, 137-200.
(60) Roberts, D. A.; Bradley, E. S.; Cheung, R.; Leifer, I.; Dennison, P. E.; Margolis, J. S. *Remote Sensing of Environment* **2010**, *114*, 592-606.
(61) Frankenberg, C.; Aben, I.; Bergamaschi, P.; Dlugokencky, E.; Van Hees, R.; Houweling, S.; Van Der Meer, P.; Snel, R.; Tol, P. *Journal of Geophysical Research: Atmospheres* **2011**, *116*.
(62) Funk, C. C.; Theiler, J.; Roberts, D. A.; Borel, C. C. *IEEE transactions on geoscience and remote sensing* **2001**, *39*, 1410-1420.
(63) Fanchenko, S.; Baranov, A.; Savkin, A.; Sleptsov, V. In *IOP Conference Series: Materials Science and Engineering*; IOP Publishing, 2016, p 012036.
(64) McCurdy, M. R.; Bakhirkin, Y.; Wysocki, G.; Lewicki, R.; Tittel, F. K. *J Breath Res* **2007**, *1*, 014001.
(65) Picciaia, D.; Zazzeri, G.; Gimberini, M.; Andreussi, P. In *Proceedings Sardinia*, 2011.
(66) Frish, M. B.; Wainner, R. T.; Laderer, M. C.; Allen, M. G.; Rutherford, J.; Wehnert, P.; Dey, S.; Gilchrist, J.; Corbi, R.; Picciaia, D. In *SPIE Defense, Security, and Sensing*; International Society for Optics and Photonics, 2013, pp 87260C-87260C-87269.
(67) Schneising, O.; Burrows, J. P.; Dickerson, R. R.; Buchwitz, M.; Reuter, M.; Bovensmann, H. *Earth's Future* **2014**, *2*, 548-558.
(68) Richard, E.; Kelly, K.; Winkler, R.; Wilson, R.; Thompson, T.; McLaughlin, R.; Schmeltekopf, A.; Tuck, A. *Applied Physics B: Lasers and Optics* **2002**, *75*, 183-194.
(69) Frankenberg, C.; Thorpe, A. K.; Thompson, D. R.; Hulley, G.; Kort, E. A.; Vance, N.; Borchardt, J.; Krings, T.; Gerilowski, K.; Sweeney, C.; Conley, S.; Bue, B. D.; Aubrey, A. D.; Hook, S.; Green, R. O. *Proceedings of the National Academy of Sciences of the United States of America* **2016**, *113*, 9734-9739.
(70) Wolsey, W. C. *Qualitative Chemical Analysis (Harris, Daniel C.)*; ACS Publications, 1987.

4.6 FIGURES

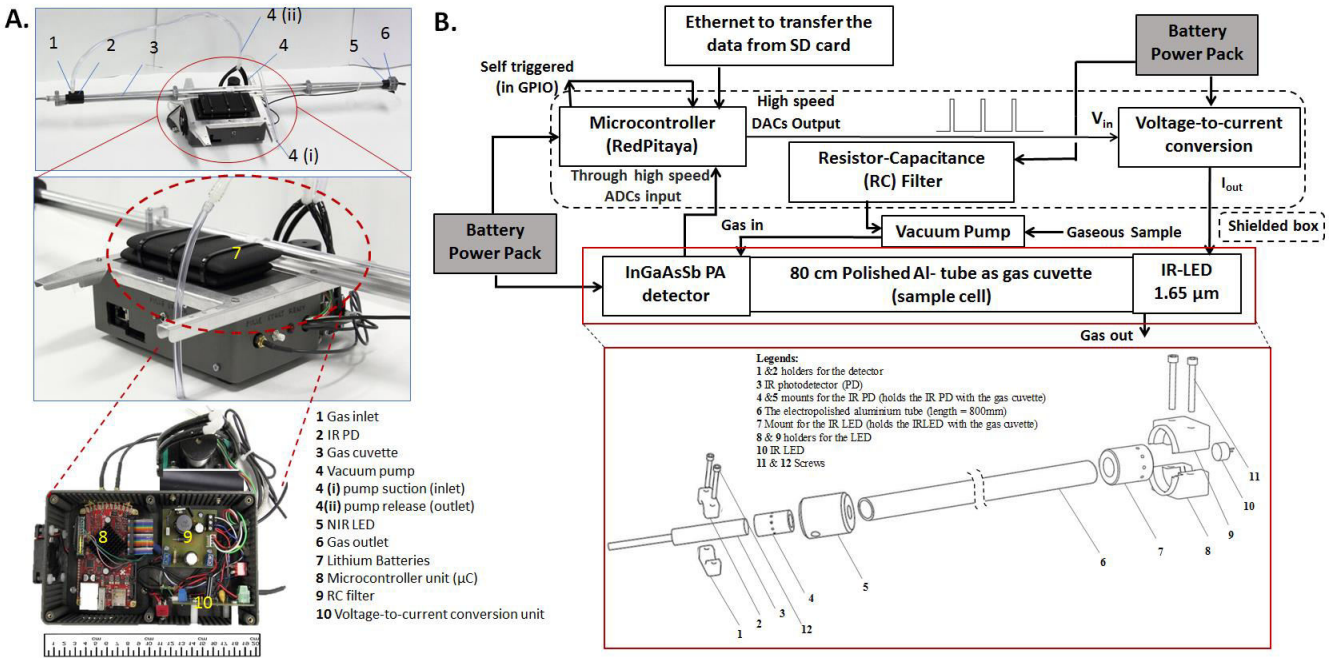

Figure 1A. Photograph of the proposed detection system B. The schematic diagram of the NDIR based CH_4 gas detection system. and the scheme for the arrangement of gas cuvette with the IR LED and PD optopair (in the red rectangle)

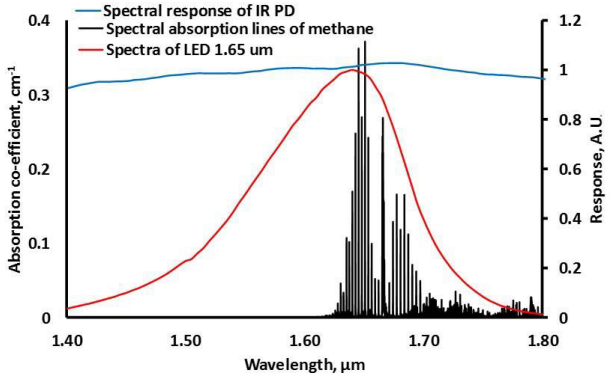

Figure 2. The absorption spectrum of CH_4 (source: hitran.org) and the vendor provided relative responsivity of the IR PD and the relative emission spectrum of the NIR LED (λ_{max} = 1.65 μm)

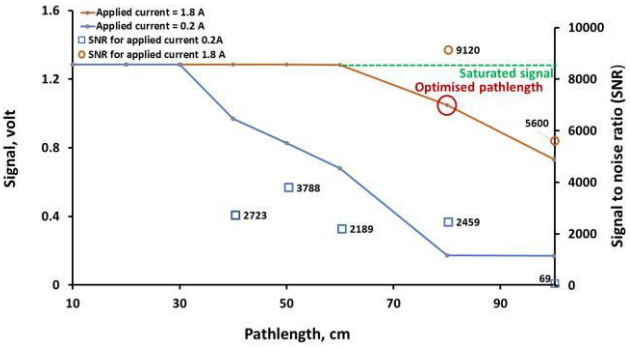

Figure 3. The obtained signal in the IR detector with increasing pathlength (length of the gas cuvette made of polished Al-tube) at two different applied current for the employed NIR LED with corresponding signal-to-noise ratio (SNR) for unsaturated signal

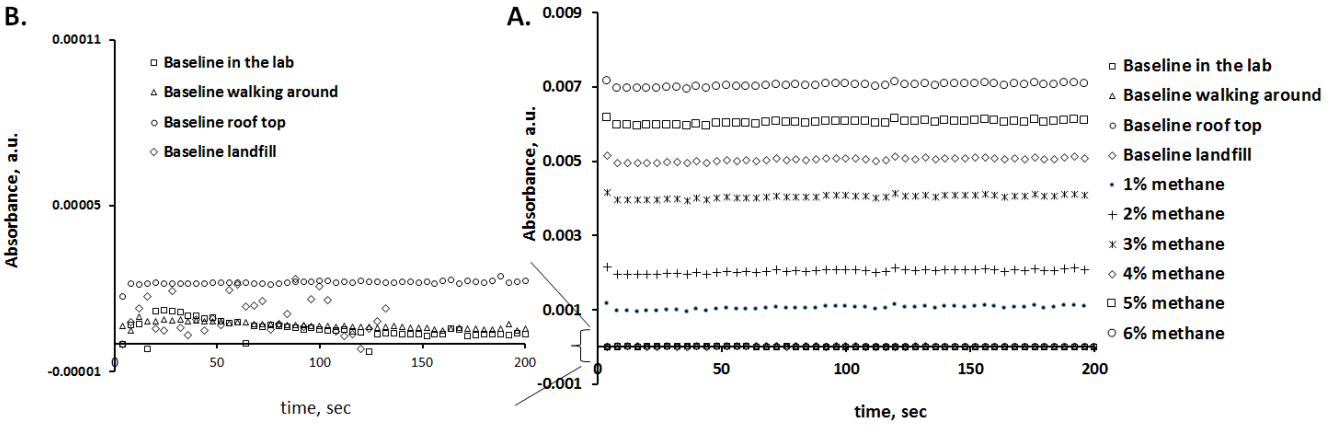

Figure 4A. Continuous absorbance values with different concentration of standard CH_4 gas B Baseline absorbance values in different indoor and outdoor conditions without any CH_4 sample

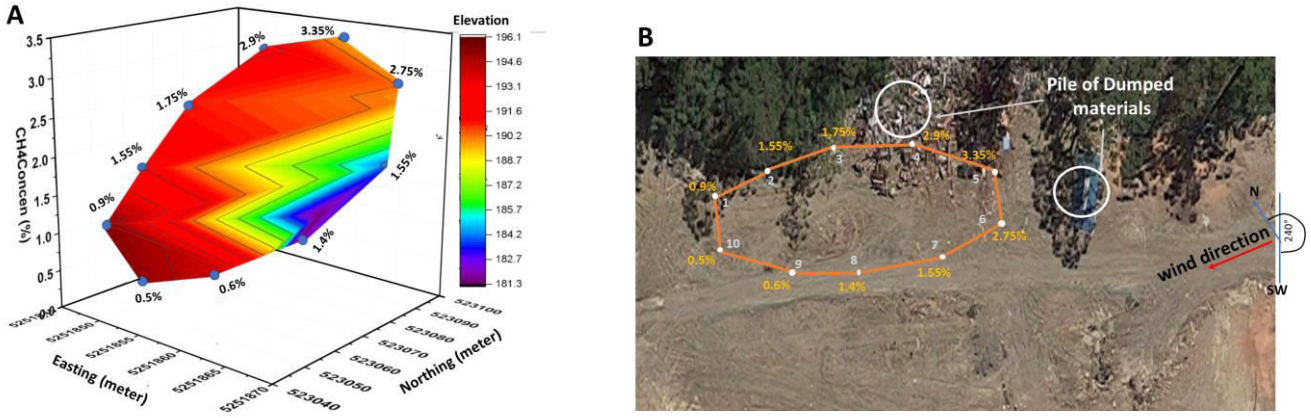

Figure 5 A. 3D spatial map of the CH_4 concentrations at 10 sampling points and B. the image of the landfill site (source: google maps) and the sampling path's position in it. Wind direction was observed from the Bureau of Meteorology (http://www.bom.gov.au/watl/wind/forecast.shtml) Forecast for 10:00 AEST on Tuesday 4 April 2017. 1, 2, 3, 4, 5, 6, 7, 8, 9 and 10 are 10 sampling points with GPS coordinate values in the sampling path where CH_4 concentration is measured. Easting, northing, elevation and time of measurement at each point were recorded and provided in Table S1 in SI

4.7 TABLE

Table 1. Comparisons amongst crucial parameters of our designed sensor and other gas sensors techniques

Features	NDIR based sensor		QCL[a]	LAS[b]	Image spectroscopy
	sensor developed in this study	Conventional NDIR sensors			
Thermal management	No cooling needed	Depends on the emitter	Cryogenic cooling[33]	Cryogenic cooling[24,60]	Depends on the emitter
Optical Filter or monochromator	No	Depends on the emitter	No[32]	No[64]	Depends on the emitter
Analysis Time	ca. 3 sec	<1min[33]	120 sec [33]	≥30 m[64]	Longer [65]
Optical pathlength	80 cm	4 cm – 4m[24]	<1m[28]	Varies be-tween cm to km[21,24]	Several meters to several km[65-67]
Electrical energy	>1 W	several Watt[33]	several Watt[28]	several Watt[28]	higher
Cost	1500 USD	moderate[33]	expensive[33]	expensive[24]	expensive[65,67]
Algorithm	Simple and flexible	moderate[33]	complex[32]	complex[24]	simulated[65-67]
Data processing	On-the-fly	Post processing[24]	Post processing[28]	Post processing[64]	Post processing[65-67]
Flexibility	yes	No	No[32]	No[64]	No[65-67]
Wireless	yes	No	No[28]	No[23]	No[65-67]

Continuous	yes	No	No[24]	No[24]	No[65,67]
Pulse	yes	yes	yes[33]	yes	yes[65,67]
LOD	300 ppm (at λ_{max}=1.65 µm)	<100 pm (at λ_{max}=1.66 µm)[46]	<17 ppb (at 7 µm)	<20 ppb (at 1.66 µm)[68]	2 kg/h[69]

[a] Quantum Cascade Laser
[b] Lasers absorption spectroscopy

4.8 FOR TOC ONLY

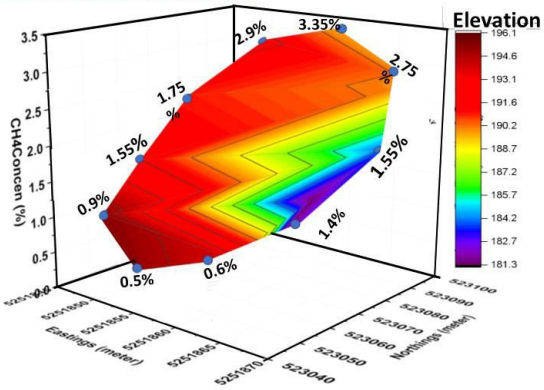

Supplementary Information

Portable Device for Continuous Sensing with Rapidly Pulsed LEDs – Part 2: Continuous Real-time Methane Sensing with Wireless Analytical Signal Transfer using IR LEDs for Indoor and Outdoor Monitoring of Gases

A. Noori [a], P. Mahbub [a], J. S. Parry [b], J. Davis [b], A. Lucieer [c], M. Macka [a*]

[a] *Australian Centre for Research on Separation Science (ACROSS) and School of Physical Sciences University of Tasmania, Private Bag 75, Hobart 7001, Australia*
[b] *Central Science laboratories, University of Tasmania, Private Bag 74, Hobart 7001, Australia*
[c] *School of Land and Food, University of Tasmania, Private Bag 76, Hobart 7001, Australia*

DETAIL CONFIGURATION OF THE NDIR BASED SENSOR

The IR LED and corresponding responsive PD were connected with the Al-tube using in-house made mount and screwed on an L-shaped Al-plate using holders which was further bolted on the top of the shielded box. All the mount, holders and screws were in house made and 3D printed. The mount for the PD allocates the option for gas inlet to the gas cuvette and therefore connected with the outlet of the pump with hose pipes and the LED mount provides the option for gas outlet. In Figure 3B the scheme of the arrangement of gas cuvette with the IR LED and PD optopair is shown.

The gas cuvette with the LED and PD, and two batteries were positioned on top of the shielded box, the vacuum pump on the longest side of the rectangular shielded box and the axial fan is bolted on one width side (shorter length side) of the shielded box. On the opposite width side of the box an indicator red LED with a press switch was installed to exhibit the readiness of the detection system with stabilization of program and wait for ran till the switch being pressed. An electrical switch was also installed to start the entire system with LED and pump on for taking the sample. Rest of the description about this system is already provided in our previous work as part A of this present work.

CALIBRATION CURVES IN THE LAB

In Figure S2 the calibration curve obtained in the lab is shown from where concentration of CH_4 was estimated in the landfill sample. From the calibration curve the limit of detection (LOD) of this detection system was calculated as equation (11) following [70]

$$LOD = \frac{3.3 \times SD\ of\ blank(S_{blank})}{Slope\ of\ the\ calibration\ curve} \qquad (11)$$

In figure S3 the calibration curve obtained in the GC-MS analysis with UHP CH_4 is shown, from where the concentration of the methane gas was estimated from the sample which was collected during the field measurement. For GC-MS analysis of the landfill sample we used Varian 3800 Gas Chromatograph coupled to a Bruker 300-MS triple quadrupole mass spectrometer. The GC column was Agilent DB-5 30m x 0.25mm; 0.25µm phase where carrier gas was Helium and its slow rate was 1.0 mL/min. Injection temperature of GC was 200°C and was operated in split mode at 50:1 ratio whereas in the transfer line the temperature was 290° C. The initial oven temperature was 35°C which held for 2 min and at the end it rose to 100°C at the rate of 20°C/min.

In the MS electron impact ionization was done at 70eV with simultaneous full scan (FS) over (m/z) from 10 to 70 whereas single ion monitoring (SIM) was done at (m/z) 16.

All the GC-MS data was processed using Bruker MS Work-station Version 7 software

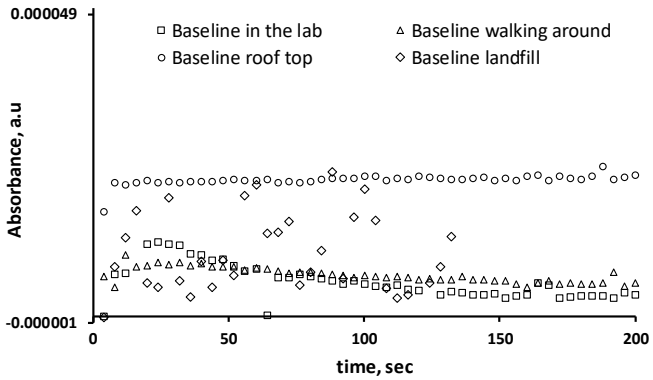

Figure S1 Baseline in three different conditions

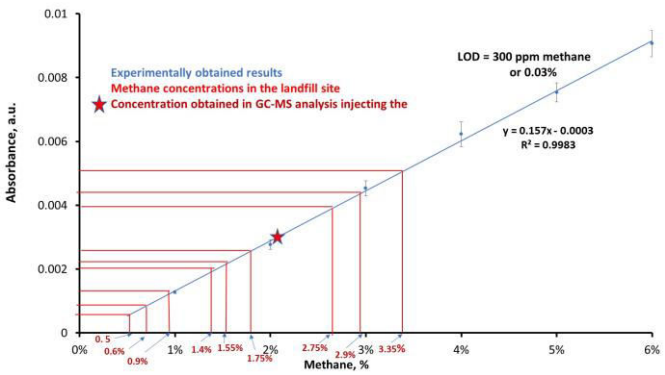

Figure S2 Calibration curve of CH_4 standard and concentration obtained from the field sample

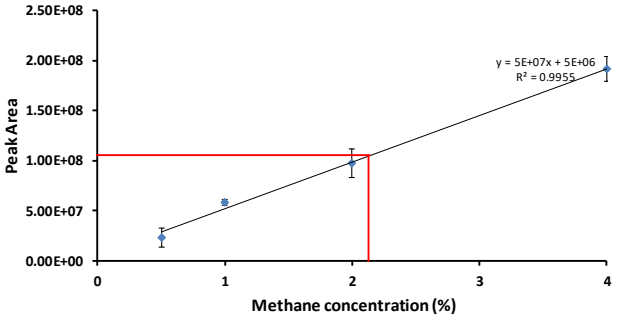

Figure S3 Calibration curve obtained in GC-MS analysis and the subsequent CH_4 concentration in the landfill sample

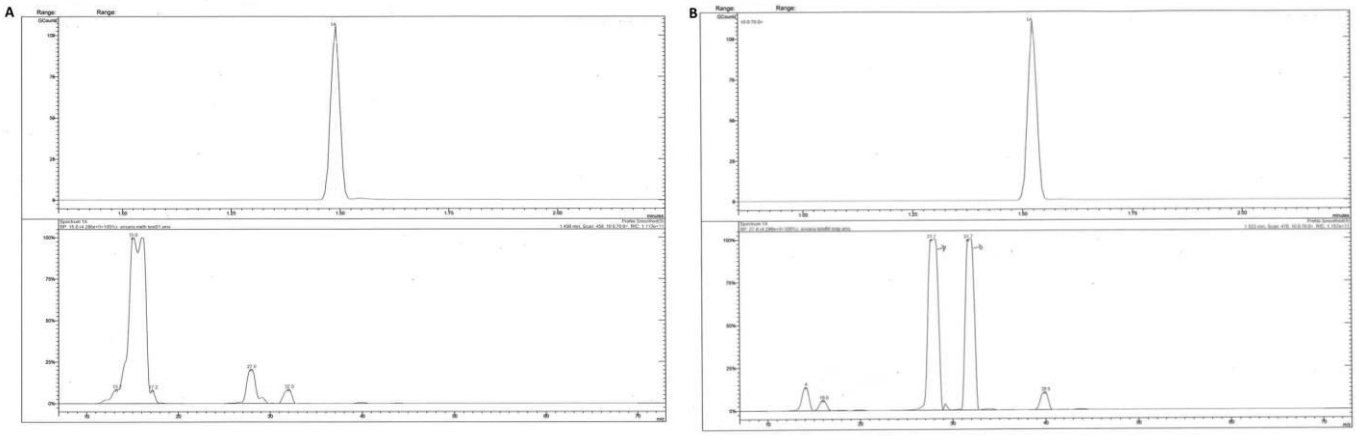

Figure S4 The CH_4 peak from GC and the spectrum of MS A for the CH_4 standard and B the field sample

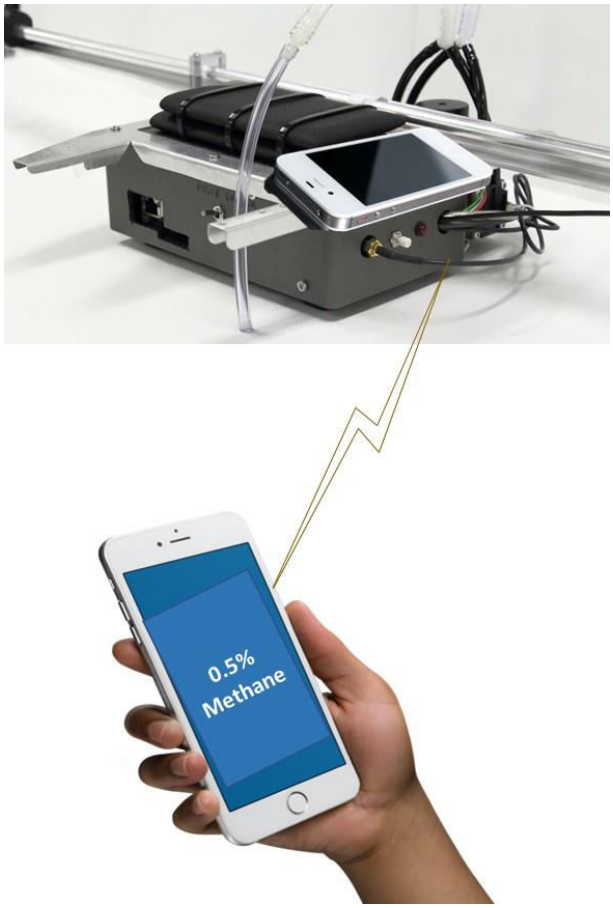

Figure S 5. Current work as a future direction of this project

Video link of the landfill sampling and CH_4 measurement is available in the following youtube link:

https://www.youtube.com/watch?v=XzxoBCvawvk&feature=youtu.be

Table S1 Easting, northing, elevation, speed and time of measurement at each point of 10 sampling points in the sampling area

North (m)	East (m)	Zone	Altitude (m)	Horizontal Accuracy (m)	Vertical Accuracy(m)	Time (AEST)	Course	Speed(kph)
5251862	523045	55G	181.71	10	12	2017-04-04T11:34:00+1000	327.66	1.3
5251864	523056	55G	181.25	5	6	2017-04-04T11:34:11+1000	69.96	3.31
5251868	523065	55G	183.97	5	8	2017-04-04T11:34:23+1000	15.82	3.89
5251868	523079	55G	189.79	5	6	2017-04-04T11:34:36+1000	113.55	3.35
5251866	523093	55G	186.94	5	6	2017-04-04T11:34:52+1000	90.35	2.92
5251855	523092	55G	191.89	5	6	2017-04-04T11:35:06+1000	228.87	3.06
5251851	523083	55G	190.93	5	6	2017-04-04T11:35:24+1000	196.88	4.82
5251850	523071	55G	191.65	5	6	2017-04-04T11:35:41+1000	297.42	2.74
5251849	523062	55G	195.32	5	8	2017-04-04T11:35:53+1000	269.65	2.77
5251849	523051	55G	196.08	10	8	2017-04-04T11:36:03+1000	260.16	3.13
5251860	523049	55G	193.62	10	8	2017-04-04T11:36:14+1000	134	356.13

5 Chapter 5: General Conclusions and Future Directions

The work presented in this thesis comprises of three major sections presented in chapters 2, 3 and 4: (1) radiometric analysis of LEDs, (2) on-the-fly rapid large data stream processing for portable analytical systems, and (3) development of a NIR LED based methane sensor for continuous indoor and outdoor sensing. While the work in Chapter 2 has wide ranging implications for broad areas of optical methods in analytical chemistry, the work in Chapter 3 established capability for portable rapid on-the-fly large data stream processing, which then enabled the work in Chapter 4 in portable continuous sensing.

We established a comprehensive radiometric analysis of wide range of LEDs from deep UV (λ_{max} = 255 nm), visible to NIR (λ_{max} = 950 nm) using a large area silicon photodiode by assigning straightforward geometry and calculations. This method results not only a facile, rapid and inexpensive radiometric analysis of LEDs but also accurate radiometric parameters namely, absolute emission spectra as spectral radiant power (W/nm), radiometric power output (W), irradiances (W/cm^2), radiant efficiencies (%) as well as uncertainties (%) demonstrated for a wide spectral emission range of commercial LEDs. The accuracy of the measurements was validated using two completely independent methods: chemical actinometry and spectrophotometry. This method for radiometric characterization of the LEDs was further demonstrated to be useful for calculating quantum yield and fluence measurement of actinometric systems. The significance of this work rests in wide-ranging implications to broad areas of analytical chemistry where light sources are used and that need to be properly characterised.

The knowledge gained in the first experimental chapter was utilized in the further two experimental chapters of this thesis where a portable NIR LED based optical sensor was designed and implemented in real world atmospheric gas sensing. In the first experimental chapter, we characterised LEDs up to NIR spectral region at λ_{max} = 950 nm, and then we used NIR LEDs at λ_{max} = 1.65 μm for our further work in Chapters 3 and 4. The radiometric analysis of LEDs inspires purposeful employment of LEDs in analytical chemistry in a broader sense and was further used in this work for portable in field gas sensing.

To adopt rapid pulsing of NIR LEDs (2 μs, with 1 kHz repetition frequency) in an optical sensor, the prime prerequisite is to have a correspondingly rapid data acquisition capability. When acquisition is done precisely (without any loss of data) in a rapid manner it generates very large data streams. Consequently, to handle on-the-fly that large data streams, fittingly capable continuous on-the-fly data processing is needed in real-time, allowing no lag between data acquisition and processing.

IR LEDs in rapid pulsed mode (delivering maximum radiometric power output within the pulse) are appropriate for low-cost optical sensing of gases employing corresponding IR sensitive photodiode as an optopair. However, when extremely short pulses are applied (~2 μs), it presents a challenge that render the use of conventional data acquisition system with lower sampling rate inapplicable. Therefore, in the second experimental chapter we demonstrate an open source portable microcontroller (μC) system with field-programmable gate array (FPGA) for rapid on-the-fly real-time data processing of large data streams (125 MHz@16bit, resulting in 2 Gbit/sec). The μC with FPGA is not only used for data processing purpose but also allows to generate the required pulsed signals for the NIR LED in a desired shape, duration, frequency, and amplitude. This miniaturised μC-FPGA based system offers portability and at the same time ultimate open source flexibility, as

demonstrated by implementing codes written for specific analytical purposes, such as in this work portable, continuous and real-time sensing of gases.

In the third experimental chapter, we designed a low-cost portable non-dispersive infrared (NDIR) spectroscopy based CH_4 sensor using rapidly pulsed NIR LED and the μC-FPGA with user defined programme developed in the previous chapter. A favourable limit of detection (LOD) of 300 ppm (0.03%) CH_4 was achieved. Then we deployed this portable sensor at a local landfill site where CH_4 sensing was conducted continuously in real-time. The in-field results were cross validated using GC-MS. This NIR LED based CH_4 sensor presents a facile low-cost approach offering a flexible, open platform with on-the-fly data handling and wireless transfer of data in real-time, enabling continuous sensing of atmospheric CH_4 for indoor and outdoor applications.

The relatively low cost of LEDs makes a promise for their increasing use in optical sensing in the future. Similarly, rapid advances in μC technology can be expected to enhance the capability of on-the-fly handling of rapid large data streams. However, radiometric characterisation of LEDs and the feasibility studies of μC technology in terms of software integration and mobile platform installation are not yet common in wide areas of portable analysis and remote sensing. As a result, low-cost sensors possess future potential to integrate accurately characterised LEDs as well as custom-made software for portable analysis and remote sensing, including of gases using low cost and weight mobile platforms such as on smartphones or unmanned aerial vehicles (UAV).

Appendix

The computer programme coding given in the appendix is generated according to the project's specific requirements with the help of IT support, Central Science Laboratories (CSL), University of Tasmania (UTAS). And the copyright of this written programme code belongs to the University of Tasmania. The candidate have frequently consulted with her supervisors as well as with the IT support, CSL, UTAS, John Parry, during the algorithm development stage of these codes to ensure that the codes are generating correct and meaningful results and debugged as required during the implementation of the gas sensing.

```
//*************************************************************************/
//*                                                                       */
//*         Central Science Lab - Red Pitaya software.                    */
//*                                                                       */
//*         Program:                    PeakShape.                        */
//*         Programmer :                John  S.  Parry.                  */
//*         Date :                      September 2016.                   */
//*         Language :                  C.                                */
//*         Machine :                   RedPitaya.                        */
//*                                                                       */
//*         Copyright (C) 2016,   Central Science Lab                     */
//*                               University of Tasmania                  */
//*                               Churchill Avenue                        */
//*                               Sandy Bay                               */
//*                               Tasmania  Australia                     */
//*                                                                       */
//*************************************************************************/
//*                                                                       */
//* This program is the property of the University of Tasmania.  Use of the    */
//* program without permission is forbidden.  No warranty is provided with     */
//* software with this software.                                          */
//*                                                                       */
//*************************************************************************/
//*                                                                       */
//* This program uses the fast analog input and output of the red pitaya to    */
//* form a pulse and then reads the current though an LED and the amount of    */
//* light detected.                                                       */
//*                                                                       */
//*************************************************************************/

#include <stdio.h>
#include <stdlib.h>
#include <unistd.h>
#include <math.h>
#include <time.h>
#include <sys/time.h>
#include "redpitaya/rp.h"

void WaitUntilSignal ( ) ;                          //* This routine turns on the ready LED and waits for the start button to be pressed.
void OutputTime ( ) ;                               //* The routine outputs the time since program start or time of day.
void TurnPumpOn ( float, int ) ;                    //* This routine turns on the pump by supplying the provided voltage (parameter 1)
                                                    //* for the specified time (parameter 2, in milli seconds)
void SetupGeneration ( ) ;                          //* This routine load the output wave into the FPGA.
int GenerateAcquire ( ) ;                           //* This routine generates the output wave and acquires the responses.
void Accumulate ( ) ;                               //* This routine takes the acquired data and accumulates it into an accumulation
                                                    //* buffer.
```

```
void OutputRawData ( ) ;
void Calculation ( ) ;


struct timeval RunStart ;

int  OutputSize ;
int  MaxCalculation ;


int  DoCodeTiming ;
```

```
//* This routine output to a text file comma separated values for averaged pulse.
//* This routine does various calculation for the designate region of the averaged
//* pulse.

//* The realtime clock of the RedPitaya, unfortunately it is a fake RTC, so unless
//* connected to network the time is incorrect.
//* The size of the output buffer we are interested in.
//* The last position in the buffer used for calculations or raw data output.
//* Used to limit amount of data transferred from ADC and accumulated to speed up
//* program.
//* Boolean flag to indicate that process timing should be produced.
//* (Used to improve software performance)
```

```
int main ( int argc, char **argv )
  {
    int      NumSamples   = 10 ;                  //* if N=x is not specified on the command line, the default is 10.
    int      SubGroups    = 1 ;                   //* if S=x is not specified on the command line, the default is 1.
    int      AveragePeaks = 128 ;                 //* if A=x is not specified on the command line, the default is 128.
    int      ZeroBetween  = true ;                //* This flag is used to indicate if the averaging buffers should
                                                  //* cleared between samples, the default is Yes, change with command line Z=N.
    int      OutputRaw    = true ;                //* A boolean flag to indicate that the raw data is required,
                                                  //* the default is yes, change with command line O=N.
    int      WaitForSignal = false ;              //* A boolean flag to indicate an external start signal is being used,
                                                  //* the default is No, change with command line W=Y or W=S.
    int      WaitEveryPulse = true ;              //* A boolean flag to indicate to wait between every sample.
    int      DualChannel  = true ;                //* If true read both channels, otherwise only read channel 1.
    int      FastRate     = false ;               //* If true read input channels at 125MHz, otherwise read at 15.625MHz.
    int      Format       = 3 ;                   //* A bit map for the output information and format required.
                                                  //* Bit 0, (1) [R=A] if set include simple average of calculation zones.
                                                  //* Bit 1, (2) [R=L] if set include linear regression of calculation zones.
                                                  //* Bit 2, (4) not used.
                                                  //* Bit 3, (8) not used.
                                                  //* Bit 4, (16) [R=C] if set include sample count in output.
                                                  //* Bit 5, (32) [R=E] if set include pump on / off elapsed time from program start.
                                                  //* Bit 6, (64) [R=E] if set include pump on / off real time.
                                                  //*     ( Only correct when connected to network )
                                                  //* Bit 7, (128) [R=+] set means produced verbose output instead of CSV.

    uint32_t buff_size = 16384 ;
    int      BuffStop ;                           //* The next buffer stop when creating the pulse form.
    int      Steps ;
    double   Volts ;
    double   NewVolts ;
    double   DeltaVolts ;
    int      Calculations ;                       //* The number of calculation zones being used, usually 2
                                                  //*     ( base line before peak and peak top).
    int      StartList[ 10 ] ;                    //* The list of calculation zones (start and finish).
    int      FinishList[ 10 ] ;
    int      Start ;                              //* Used when interpreting calculation zones.
    int      Finish ;
    char     SampleTitle[ 64 ] ;                  //* Used to store the determined sample title for output and calculations.
    int      PumpTime ;                           //* The time in milli seconds to turn pump on between samples (command line P:c,v)
    float    PumpVoltage ;                        //* The voltage level supplied to turn on the pump, determine how fast the pump runs.
    int      Readings ;                           //* The number of samples in the reading.  Should be AveragePeaks * SubGroups
                                                  //* when complete.
    int      SubReadings ;                        //* The number of samples in the sub reading.  Should be AveragePeaks when complete.
    int      ReadingNum ;                         //* The number of the current reading.
    int      SubLoop ;
    int      Loop ;
```

```
int      Loop2 ;
int      Pos ;

if ( rp_Init() != RP_OK )
  {                                                    //* Print error, if rp_Init() function failed.
    fprintf( stderr, "Rp api init failed!\n" ) ;
  }

float *out1 = (float *)malloc( buff_size * sizeof( float )) ;     //* Output buffer that will be transferred to the FPGA, LED voltage.
float *zero = (float *)malloc( buff_size * sizeof( float )) ;     //* Buffer to be transferred to FPGA to zero the output.
float *in1  = (float *)malloc( buff_size * sizeof( float )) ;     //* Input buffer transferred from the FPGA for the detector.
float *in2  = (float *)malloc( buff_size * sizeof( float )) ;     //* Input buffer transferred from the FPGA for the LED current.

Pos = 0 ;                                              //* Initialize the required variables.
Volts = 0.0 ;
Calculations = 0 ;
OutputSize = 500 ;
MaxCalculation = 0 ;
DoCodeTiming = false ;

for ( Loop = 1; Loop < argc; Loop++ )                  //* Interpret the command line parameters.
  { if (( argv[ Loop ][ 1 ] == '=' ) || ( argv[ Loop ][ 1 ] == ':' ))
      { if ( argv[ Loop ][ 0 ] == 'N' )                //* Number of readings to collect.
          { sscanf ( &argv[ Loop ][ 2 ], "%d", &NumSamples ) ;
            if ( NumSamples < 1 )
              { NumSamples = 1 ; }
            fprintf ( stderr, "Setting number of samples to %d\n", NumSamples ) ;
          }
        if ( argv[ Loop ][ 0 ] == 'S' )                //* Number of sub groups in a reading.
          { sscanf ( &argv[ Loop ][ 2 ], "%d", &SubGroups ) ;
            if ( SubGroups < 1 )
              { SubGroups = 1 ; }
            fprintf ( stderr, "Setting number of sub groups to %d\n", SubGroups ) ;
          }
        if ( argv[ Loop ][ 0 ] == 'A' )                //* Number of samples in a sub group reading.
          { sscanf ( &argv[ Loop ][ 2 ], "%d", &AveragePeaks ) ;
            if ( AveragePeaks < 8 )
              { if ( AveragePeaks != 1 )
                  { AveragePeaks = 8 ; }
              }
            fprintf ( stderr, "Setting number peaks per samples to %d\n", AveragePeaks ) ;
          }
        if ( argv[ Loop ][ 0 ] == 'C' )                //* Determine each calculation zone.
          { sscanf ( &argv[ Loop ][ 2 ], "%d,%d", &Start, &Finish ) ;
            if ( Start < 0 )
              { Start = 0 ; }
```

```
    if ( Start > 9999 )
      { Start = 9999 ; }
    if ( Start > Finish )
      { Finish = Start ; }
    if ( Finish > 9999 )
      { Finish = 9999 ; }
    fprintf ( stderr, "Calculation maths for %d to %d inclusive\n", Start, Finish ) ;
    StartList[ Calculations ] = Start ;
    FinishList [ Calculations ] = Finish ;
    if (( Finish + 2 ) > MaxCalculation )
      { MaxCalculation = Finish + 2 ; }
    Calculations++ ;
  }
if ( argv[ Loop ][ 0 ] == 'Z' )                          //* Do not Zero data between readings.
  { if ( argv[ Loop ][ 2 ] == 'N' )
      { ZeroBetween = false ; }
  }
if ( argv[ Loop ][ 0 ] == 'D' )                          //* Analyse both channels.
  { if ( argv[ Loop ][ 2 ] == 'N' )
      { DualChannel = false ; }
  }
if ( argv[ Loop ][ 0 ] == 'F' )                          //* Use fast speed 125MHz instead of slow 15.625MHz.
  { if ( argv[ Loop ][ 2 ] == 'Y' )
      { FastRate = true ; }
  }
if ( argv[ Loop ][ 0 ] == 'W' )                          //* Wait for collection signal.
  { if ( argv[ Loop ][ 2 ] == 'Y' )
      { WaitForSignal = true ; }
    if ( argv[ Loop ][ 2 ] == 'S' )                      //* Only before first reading.
      { WaitForSignal = true ;
        WaitEveryPulse = false ;
      }
  }
if ( argv[ Loop ][ 0 ] == 'O' )                          //* Turn off raw output.
  { if ( argv[ Loop ][ 2 ] == 'N' )
      { OutputRaw = false ;
        OutputSize = 10 ;
      }
    else
      { sscanf( &argv[ Loop ][ 2 ], "%d", &OutputSize ) ; //* or specify how much output to produce.
        if ( OutputSize < 10 )
          { OutputSize = 10 ; }
        if ( OutputSize > 15000 )
          { OutputSize = 15000 ; }
      }
  }
```

```
    if ( argv[ Loop ][ 0 ] == 'T' )                          //* Turn on procedure timing.
      { if ( argv[ Loop ][ 2 ] == 'Y' )
          { DoCodeTiming = true ; }
      }
    if ( argv[ Loop ][ 0 ] == 'R' )                          //* Determine what output data and format is required.
      { Format = 0 ;
        for ( Loop2 = 2; argv[ Loop ][ Loop2 ] != '\0'; Loop2++ )
          { if ( argv[ Loop ][ Loop2 ] == 'A' )              //* Simple average of calculation zones.
              { Format = Format | 1 ; }
            if ( argv[ Loop ][ Loop2 ] == 'L' )              //* Linear regression of calculation zones.
              { Format = Format | 2 ; }
            if ( argv[ Loop ][ Loop2 ] == 'C' )              //* Output sample and sub group numbers.
              { Format = Format | 16 ; }
            if ( argv[ Loop ][ Loop2 ] == 'E' )              //* Output elapsed time at pump on and off.
              { Format = Format | 32 ; }
            if ( argv[ Loop ][ Loop2 ] == 'T' )              //* Output real time at pump on and off.
              { Format = Format | 64 ; }
            if ( argv[ Loop ][ Loop2 ] == '+' )              //* Produce verbose output instead of CSV.
              { Format = Format | 128 ; }
          }
        if ( Format == 0 )                                   //* If command R is used with no valid output, include everything.
          { Format = 255 ; }
      }
    if ( argv[ Loop ][ 0 ] == 'P' )                          //* Indicate that pump is required between samples.
      { sscanf ( &argv[ Loop ][ 2 ], "%f,%d", &PumpVoltage, &PumpTime ) ;
        if ( PumpTime < 500 )                                //* Minimum is half a seconds.
          { PumpTime = 500 ; }
        if ( PumpVoltage < 0.5 )
          { fprintf ( stderr, "Pump voltage too low to turn on pump\n" ) ; }
        if ( PumpVoltage < 0 )
          { PumpVoltage = 0 ; }
        if ( PumpVoltage > 1.8 )
          { PumpVoltage = 1.8 ; }
        PumpTime = PumpTime * 1000 ;                         //* Convert milli seconds to micro seconds.
      }
  }
else
  { sscanf( argv[ Loop ], "%d,%lf", &Steps, &NewVolts ) ;    //* Build the array that defines the pulse shape.
    DeltaVolts = ( NewVolts - Volts ) / Steps ;              //* It is defined as a series of lines taking X steps to new current.
    BuffStop = buff_size ;
    if (( Pos + Steps ) < BuffStop )
      { BuffStop = Pos + Steps ; }
    while ( Pos < BuffStop )
      { out1[ Pos ] = out1[ Pos - 1 ] + DeltaVolts ;
        Pos++ ;
      }
```

```
        fprintf ( stderr, "  ArgV : %d = %s  %4d [ %4d nsec to %lf volts ]\n", Loop, argv[ Loop ], Pos, Steps * 10, NewVolts ) ;
        printf ("  ArgV : %d = %s  %4d [ %4d nsec to %lf volts ]\n", Loop, argv[ Loop ], Pos, Steps * 10, NewVolts ) ;
        out1[ Pos - 1 ] = NewVolts ;
        Volts = NewVolts ;
      }
  }

if ( OutputSize > MaxCalculation )
  { MaxCalculation = OutputSize ; }
fprintf ( stderr, "MaxCalculation = %d\n", MaxCalculation ) ;
for ( Loop = 0; Loop < buff_size; Loop++ )
  { zero[ Loop ] = 0.0 ; }
                                                        //* Allocate all the on the fly accumulation buffers.
                                                        //* Are used by the Accumulation, Calculation and OutputRaw routines.
float  *in1x    = (float *)malloc( MaxCalculation * sizeof( float )) ;
double *in1x2   = (double *)malloc( MaxCalculation * sizeof( double )) ;
float  *in1min  = (float *)malloc( MaxCalculation * sizeof( float )) ;
float  *in1max  = (float *)malloc( MaxCalculation * sizeof( float )) ;
float  *in1sx   = (float *)malloc( MaxCalculation * sizeof( float )) ;
double *in1sx2  = (double *)malloc( MaxCalculation * sizeof( double )) ;
float  *in1smin = (float *)malloc( MaxCalculation * sizeof( float )) ;
float  *in1smax = (float *)malloc( MaxCalculation * sizeof( float )) ;
float  *in2x    = (float *)malloc( MaxCalculation * sizeof( float )) ;
double *in2x2   = (double *)malloc( MaxCalculation * sizeof( double )) ;
float  *in2min  = (float *)malloc( MaxCalculation * sizeof( float )) ;
float  *in2max  = (float *)malloc( MaxCalculation * sizeof( float )) ;
float  *in2sx   = (float *)malloc( MaxCalculation * sizeof( float )) ;
double *in2sx2  = (double *)malloc( MaxCalculation * sizeof( double )) ;
float  *in2smin = (float *)malloc( MaxCalculation * sizeof( float )) ;
float  *in2smax = (float *)malloc( MaxCalculation * sizeof( float )) ;

if ( rp_DpinReset( ) != RP_OK )                         //* Setup the RedPitaya digital IO pins.
  { fprintf ( stderr, "rp_DpinReset failed\n" ) ; }
if ( rp_DpinSetDirection( RP_DIO0_P, RP_IN ) != RP_OK )         //* Pin 0 is also the external trigger to the FPGA ADC and DAC.
  { fprintf ( stderr, "rp_DpinSetDirection failed\n" ) ; }
if ( rp_DpinSetDirection( RP_DIO1_P, RP_OUT ) != RP_OK )        //* Pin 1 is connected to pin 0 to create self triggered ADC and DAC.
  { fprintf ( stderr, "rp_DpinSetDirection failed\n" ) ; }
if ( rp_DpinSetDirection( RP_DIO4_P, RP_OUT ) != RP_OK )        //* Pin 4 drives a simple red LED to indicate that the instrument
                                                        //* is ready and waiting for start signal.
  { fprintf ( stderr, "rp_DpinSetDirection failed\n" ) ; }
if ( rp_DpinSetDirection( RP_DIO5_P, RP_IN ) != RP_OK )         //* Pin 5 is connected to the start button.
  { fprintf ( stderr, "rp_DpinSetDirection failed\n" ) ; }

rp_DpinSetState( RP_DIO1_P, RP_LOW ) ;                  //* Set initial trigger signal low.
rp_DpinSetState( RP_DIO4_P, RP_LOW ) ;                  //* Initially have the ready LED off.
rp_AcqReset( ) ;                                        //* Reset the FPGA acquisition (ADC) state.
```

```
rp_GenReset( ) ;                                                    //* Reset the FPGA generation (DAC) state.

Readings = 0 ;
SetupGeneration( out1 ) ;                                           //* Program the FPGA generation with the desired pulse.
gettimeofday( &RunStart, NULL ) ;
for ( ReadingNum = 0; ReadingNum < NumSamples; ReadingNum++ )
  { if ( WaitForSignal )                                            //* Before each sample wait for the ready go signal if required.
      { WaitUntilSignal ( ) ;
        if ( ! WaitEveryPulse )
          { WaitForSignal = false ; }
      }
    if (( Format & 16 ) == 16 )                                     //* Output the sample number if required.
      { if (( Format & 128 ) == 128 )
          { printf( "Recording peak %d\n", ReadingNum ) ; }
        else
          { printf( "Peak %d,", ReadingNum ) ; }
      }
    fprintf( stderr, "Recording peak %d\n", ReadingNum ) ;
    OutputTime ( Format, "Pump start", RunStart ) ;
    TurnPumpOn ( PumpVoltage, PumpTime ) ;                          //* Turn the pump on if required.
    OutputTime ( Format, "Pump finish", RunStart ) ;
    if ( ZeroBetween )
      { Readings = 0 ; }
    for ( SubLoop = 0; SubLoop < SubGroups; SubLoop++ )
      { if ( ZeroBetween )
          { SubReadings = 0 ; }
        for ( Loop = 0; Loop < AveragePeaks; Loop++ )
          { if ( GenerateAcquire ( DualChannel, FastRate, in1, in2 ))
                                                                    //* Generate a pulse and acquire resulting the data.
              { Accumulate ( Readings, in1, in1x, in1x2, in1min, in1max ) ;
                                                                    //* Accumulate the detected sample into the reading.
                Accumulate ( SubReadings, in1, in1sx, in1sx2, in1smin, in1smax ) ;
                                                                    //* Accumulate the detected sample into the sub group reading.
                if ( DualChannel )
                  { Accumulate ( Readings, in2, in2x, in2x2, in2min, in2max ) ;
                                                                    //* Accumulate the produced current into the reading.
                    Accumulate ( SubReadings, in2, in2sx, in2sx2, in2smin, in2smax ) ;
                                                                    //* Accumulate the produced current into the sub group reading.
                  }
                Readings++ ;
                SubReadings++ ;
              }
          }
        if ( SubGroups > 1 )                                         //* If we have more than one sub group per reading,
                                                                     //* produce data for each sub group.
          { sprintf ( SampleTitle, "Sub total, Group %d", SubLoop ) ;
```

```
            for ( Loop = 0; Loop < Calculations; Loop++ )
              { Calculation ( SampleTitle, StartList[ Loop ], FinishList[ Loop ], DualChannel, SubReadings, in1sx, in2sx, Format ) ; }
            printf( "\n" ) ;
            if ( OutputRaw )
              { OutputRawData ( SampleTitle, AveragePeaks, DualChannel, SubReadings, out1,
                                in1sx, in1sx2, in1smin, in1smax, in2sx, in2sx2, in2smin, in2smax ) ;
              }
          }
      }
    sprintf( SampleTitle, "Total, Sample %d", ReadingNum ) ;       //* Produce the required output for each reading.
    for ( Loop = 0; Loop < Calculations; Loop++ )
      { Calculation ( SampleTitle, StartList[ Loop ], FinishList[ Loop ], DualChannel, Readings, in1x, in2x, Format ) ; }
    printf( "\n" ) ;
    if ( OutputRaw )
      { OutputRawData ( SampleTitle, AveragePeaks, DualChannel, Readings, out1,
                        in1x, in1x2, in1min, in1max, in2x, in2x2, in2min, in2max ) ;
      }
  }

  free( out1 ) ;                                                   //* Release all collection and accumulation buffers.
  free( zero ) ;
  free( in1 ) ;
  free( in2 ) ;
  free( in1x ) ;
  free( in1x2 ) ;
  free( in1min ) ;
  free( in1max ) ;
  free( in1sx ) ;
  free( in1sx2 ) ;
  free( in1smin ) ;
  free( in1smax ) ;
  free( in2x ) ;
  free( in2x2 ) ;
  free( in2min ) ;
  free( in2max ) ;
  free( in2sx ) ;
  free( in2sx2 ) ;
  free( in2smin ) ;
  free( in2smax ) ;
  rp_Release();
  return ( 0 ) ;
}
```

```
/************************************************************************************************************************ WaitUntilSignal */

void WaitUntilSignal ( )
  {                                                         //* This routine turns on the ready LED and waits for the start button to be pressed.
    rp_pinState_t State ;

    rp_DpinSetState( RP_DIO4_P, RP_HIGH ) ;                 //* Turn the status red LED on.
    if ( rp_DpinGetState ( RP_DIO5_P, &State ) != RP_OK )
      { State = RP_LOW ; }
    while ( State != RP_HIGH )                              //* Wait for the button to be pressed.
      { if ( rp_DpinGetState ( RP_DIO5_P, &State ) != RP_OK )
          { State = RP_LOW ; }
      }
    rp_DpinSetState( RP_DIO4_P, RP_LOW ) ;                  //* Turn the status LED off.
  }
```

```
/************************************************************************************************************************** OutputTime */

void OutputTime ( int Format,
                  char *When,
                  struct timeval RunStart )
  {                                                         //* Output the current or elapsed time when required.
    struct timeval Current ;
    long      ElapsedTime ;
    int       Seconds ;
    int       Minutes ;
    time_t    Now ;
    struct tm *TimeInfo ;

    if (( Format & 32 ) == 32 )                             //* Output elapsed time.
      { gettimeofday( &Current, NULL ) ;
        ElapsedTime = ( Current.tv_sec - RunStart.tv_sec ) * 1000 + ( Current.tv_usec - RunStart.tv_usec ) / 1000 ;
        Seconds = ElapsedTime / 1000 ;
        ElapsedTime = ElapsedTime - Seconds * 1000 ;
        Minutes = Seconds / 60 ;
        Seconds = Seconds - Minutes * 60 ;
        if (( Format & 128 ) == 128 )
          { printf ( "%s %d:%.2d.%.3ld\n", When, Minutes, Seconds, ElapsedTime ) ; }
        else
          { printf ( "%2d:%.2d.%.3ld,", Minutes, Seconds, ElapsedTime ) ; }
      }
    if (( Format & 64 ) == 64 )                             //* Output current time.
      { time( &Now ) ;
        TimeInfo = localtime ( &Now ) ;
        if (( Format & 128 ) == 128 )
          { printf ( "%s %s", When, asctime( TimeInfo )) ; }
        else
          { printf ( "%.2d:%.2d:%.2d,", TimeInfo->tm_hour, TimeInfo->tm_min, TimeInfo->tm_sec ) ; }
      }
  }
```

```
/************************************************************************************************************************** TurnPumpOn */

void TurnPumpOn ( float PumpVoltage,
                  int   PumpTime )
  {                                                         //* This routine turns on the pump by supplying the provided voltage
                                                            //* (parameter 1) for the specified time (parameter 2, in micro seconds)
    float SmoothVoltage ;
    long  ClockStart ;
    long  ClockFinish ;

    if ( PumpVoltage >= 0.5 )                               //* If required turn the pump on to get new sample.
      { fprintf( stderr, "Turning on pump for %6.4f seconds\n", (float)PumpTime / 1000000 ) ;
        if ( DoCodeTiming )
          { ClockStart = clock ( ) ; }
        SmoothVoltage = 0.5 ;                               //* Ramp the voltage to the pump up to limit turn on current load.
        while ( SmoothVoltage < PumpVoltage )
          { if ( rp_AOpinSetValue ( 0, SmoothVoltage ) != RP_OK )
              { fprintf( stderr, "Failed to set output voltage to %4.2f\n", SmoothVoltage ) ; }
            usleep ( 10000 ) ;
            SmoothVoltage = SmoothVoltage + 0.1 ;
            if ( SmoothVoltage > PumpVoltage )
              { SmoothVoltage = PumpVoltage ; }
          }
        if ( rp_AOpinSetValue ( 0, PumpVoltage ) != RP_OK )
          { fprintf( stderr, "Failed to set output voltage to %4.2f\n", SmoothVoltage ) ; }
        usleep ( PumpTime ) ;                               //* Leave the pump on at desires voltage for the required time.
        while ( SmoothVoltage > 0.5 )
          { if ( rp_AOpinSetValue ( 0, SmoothVoltage ) != RP_OK )
              { fprintf( stderr, "Failed to set output voltage to %4.2f\n", SmoothVoltage ) ; }
            usleep ( 10000 ) ;
            SmoothVoltage = SmoothVoltage - 0.1 ;
          }
        if ( rp_AOpinSetValue ( 0, 0 ) != RP_OK )           //* Turn the pump off before analysing the sample.
          { fprintf( stderr, "Failed to set output voltage to 0\n" ) ; }
        if ( DoCodeTiming )
          { ClockFinish = clock ( ) ;
            fprintf( stderr, "Pump on time is %8.3lf milli seconds\n",
                        (float)( ClockFinish - ClockStart ) * 1000 / CLOCKS_PER_SEC ) ;
          }
      }
  }
```

```
/************************************************************************************************************************** SetupGenerate */

void SetupGeneration( float out1[] )
  {                                                                  //* This routine load the output wave into the FPGA.
    int      RP_Err ;
    uint32_t buff_size = 16384 ;
    float    freq ;

    rp_GenWaveform( RP_CH_1, RP_WAVEFORM_ARBITRARY ) ;
    rp_GenArbWaveform( RP_CH_1, out1, buff_size ) ;
    rp_GenAmp( RP_CH_1, 1.0 ) ;
    if (( RP_Err = rp_GenGetFreq( RP_CH_1, &freq )) != RP_OK )
      { fprintf( stderr, "Rp_GenGetFreq failed %d\n", RP_Err ) ; }
    fprintf( stderr, "Current frequency = %f\n", freq ) ;
    if (( RP_Err = rp_GenFreq( RP_CH_1, 6103.0 )) != RP_OK )
      { fprintf( stderr, "Rp_GenFreq failed %d\n", RP_Err ) ; }
    if (( RP_Err = rp_GenGetFreq( RP_CH_1, &freq )) != RP_OK )
      { fprintf( stderr, "Rp_GenGetFreq failed %d\n", RP_Err ) ; }
  }
```

```
/************************************************************************************************************************ GenerateAcquire */

int GenerateAcquire ( int   DualChannel,
                      int   FastRate,
                      float in1[],
                      float in2[] )
  {                                                                   //* This routine generates the output wave and acquires the responses.
    uint32_t buff_size = MaxCalculation ;
    int      TriggerWait ;
    long     ClockStart ;
    long     ClockFinish ;

    if ( DoCodeTiming )
      { ClockStart = clock ( ) ; }
    if ( FastRate )
      { rp_AcqSetDecimation( RP_DEC_1 ) ; }                           //* Fast rate at 125MHz.
    else
      { rp_AcqSetDecimation( RP_DEC_8 ) ; }                           //* Slower rate at 15.625MHz.

    rp_AcqSetTriggerLevel( 0 ) ;                                      //* Setup acquisition and trigger on external signal.
    rp_AcqSetTriggerDelay( 8192 ) ;
    rp_AcqStart( ) ;
    rp_AcqSetTriggerSrc( RP_TRIG_SRC_EXT_PE ) ;
    if ( DoCodeTiming )
      { ClockFinish = clock ( ) ;
        fprintf( stderr, "Acquire (setup Acquire) time is %8.3lf milli seconds\n",
                    (float)( ClockFinish - ClockStart ) * 1000 / CLOCKS_PER_SEC ) ;
      }

    rp_GenOutEnable( RP_CH_1 ) ;                                      //* Enable channel 1 and trigger on external signal.
    rp_GenTriggerSource( RP_CH_1, RP_GEN_TRIG_SRC_EXT_PE ) ;
    if ( DoCodeTiming )
      { ClockFinish = clock ( ) ;
        fprintf( stderr, "Acquire (load output) time is %8.3lf milli seconds\n",
                    (float)( ClockFinish - ClockStart ) * 1000 / CLOCKS_PER_SEC ) ;
      }

    rp_acq_trig_state_t state = RP_TRIG_STATE_WAITING ;               //* Wait for the trigger event to occur.
    TriggerWait = 0 ;
    while (( state != RP_TRIG_STATE_TRIGGERED ) && ( TriggerWait < 20 ))
      { rp_AcqGetTriggerState( &state ) ;
        usleep ( 5 ) ;
        rp_DpinSetState( RP_DIO1_P, RP_HIGH ) ;                       //* Produce the external trigger. (Pin 0 and 1 are connected)
        usleep ( 5 ) ;
        rp_DpinSetState( RP_DIO1_P, RP_LOW ) ;
        TriggerWait++ ;
```

```
    }
  if ( DoCodeTiming )
    { ClockFinish = clock ( ) ;
      fprintf( stderr, "Acquire (waiting tigger) time is %8.3lf milli seconds\n",
                  (float)( ClockFinish - ClockStart ) * 1000 / CLOCKS_PER_SEC ) ;
    }

  if ( state != RP_TRIG_STATE_TRIGGERED )
    { fprintf( stderr, "******** Trigger failed : state is %d\n", state ) ;
      return( false ) ;
     }
  else
    { usleep( 1000 ) ;
      if ( DoCodeTiming )
        { ClockFinish = clock ( ) ;
          fprintf( stderr, "Acquire (waiting for data) time is %8.3lf milli seconds\n",
                      (float)( ClockFinish - ClockStart ) * 1000 / CLOCKS_PER_SEC ) ;
        }
      rp_AcqGetOldestDataV( RP_CH_1, &buff_size, in1 ) ;            //* Get the acquired data from the photo diode.
      if ( DoCodeTiming )
        { ClockFinish = clock ( ) ;
          fprintf( stderr, "Acquire (transferred channel 1) time is %8.3lf milli seconds\n",
                      (float)( ClockFinish - ClockStart ) * 1000 / CLOCKS_PER_SEC ) ;
        }
      if ( DualChannel )
        { rp_AcqGetOldestDataV( RP_CH_2, &buff_size, in2 ) ;        //* Get the acquired current from the voltage to current circuit.
          if ( DoCodeTiming )
            { ClockFinish = clock ( ) ;
              fprintf( stderr, "Acquire (transferred channel 2) time is %8.3lf milli seconds\n",
                          (float)( ClockFinish - ClockStart ) * 1000 / CLOCKS_PER_SEC ) ;
            }
        }
      rp_GenOutDisable( RP_CH_1 ) ;                                 //* Turn off the pulse generation.
      if ( DoCodeTiming )
        { ClockFinish = clock ( ) ;
          fprintf( stderr, "Acquire time is %8.3lf milli seconds\n",
                      (float)( ClockFinish - ClockStart ) * 1000 / CLOCKS_PER_SEC ) ;
        }
      return( true ) ;
    }
}
```

```
/************************************************************************************************************************** Accumulate */

void Accumulate ( int   Readings,
                  float in[],
                  float inx[],
                  double inx2[],
                  float inmin[],
                  float inmax[] )
  {                                                          //* This routine takes the acquired data and accumulates it into
                                                             //* accumulation buffers.
    long ClockStart ;
    long ClockFinish ;
    int  j ;

    if ( DoCodeTiming )
      { ClockStart = clock ( ) ; }
    if ( Readings != 0 )
      { for ( j = 0; j < MaxCalculation; j++ )               //* If this is not the first sample, accumulate X and X squared.
          { inx[ j ]  = inx[ j ] + in[ j ] ;
            inx2[ j ] = inx2[ j ] + in[ j ] * in[ j ] ;
            if ( in[ j ] < inmin[ j ] )
              { inmin[ j ] = in[ j ] ; }
            if ( in[ j ] > inmax[ j ] )
              { inmax[ j ] = in[ j ] ; }
          }
      }
    else
      { for ( j = 0; j < MaxCalculation; j++ )               //* If this is the first sample, set inital values.
          { inx[ j ]   = in[ j ] ;
            inx2[ j ]  = in[ j ] * in[ j ] ;
            inmin[ j ] = in[ j ] ;
            inmax[ j ] = in[ j ] ;
          }
      }
    if ( DoCodeTiming )
      { ClockFinish = clock ( ) ;
        fprintf( stderr, "Accumulate time is %8.3lf milli seconds\n",
                    (float)( ClockFinish - ClockStart ) * 1000 / CLOCKS_PER_SEC ) ;
      }
  }
```

```
/************************************************************************************************************************************************ OutputRawData */

void OutputRawData ( char   *Name,
                     int    AveragePeaks,
                     int    DualChannel,
                     int    Readings,
                     float  out1[],
                     float  in1x[],
                     double in1x2[],
                     float  in1min[],
                     float  in1max[],
                     float  in2x[],
                     double in2x2[],
                     float  in2min[],
                     float  in2max[] )
  {                                                                  //* This routine output to a text file comma separated values for averaged pulse.
    double Average1 ;
    double StdDev1 ;
    double Average2 ;
    double StdDev2 ;
    long   ClockStart ;
    long   ClockFinish ;
    int    j ;

    if ( DoCodeTiming )
      { ClockStart = clock ( ) ; }
    for ( j = 0; j < OutputSize; j++ )
      { Average1 = in1x[ j ] / Readings ;
        if ( DualChannel )
          { Average2 = in2x[ j ] / Readings ; }
        if ( AveragePeaks > 3 )                                      //* Work out point average and stdev if we have more than 3 samples.
          { StdDev1  = ( in1x2[ j ] - ( in1x[ j ] / Readings ) * in1x[ j ] ) / ( Readings - 1 ) ;
            if ( StdDev1 <= 0 )
              { fprintf ( stderr, "j=%d, in1x2=%20.12lf, in1x=%f, Readings=%d\n", j, in1x2[j], in1x[j], Readings ) ; }
            StdDev1 = sqrt (( in1x2[ j ] - ( in1x[ j ] / Readings ) * in1x[ j ] ) / ( Readings - 1 )) ;
            if ( DualChannel )                                       //* Output data for both photo diode and current
              { StdDev2  = sqrt (( Readings * in2x2[ j ] - in2x[ j ] * in2x[ j ] ) / ( Readings * ( Readings - 1 ))) ;
                printf( "%5d,%8.5lf,%8.5lf,%12.8lf,%8.5lf,%8.5lf,%8.5lf,%8.5lf,%8.5lf,%8.5lf\n",
                        j, out1[ j ],
                        Average1, StdDev1, in1min[ j ], in1max[ j ],
                        Average2, StdDev2, in2min[ j ], in2max[ j ] ) ;
              }
            else                                                     //* Output data for just the photo diode.
              { printf( "%5d,%8.5lf,%8.5lf,%8.5lf,%8.5lf,%8.5lf\n",
                        j, out1[ j ],
                        Average1, StdDev1, in1min[ j ], in1max[ j ] ) ;
```

```
            }
        }
      else
        { if ( DualChannel )
            { printf( "%5d,%8.5lf,%8.5lf,%8.5lf,%8.5lf,%8.5lf,%8.5lf,%8.5lf\n",
                          j, out1[ j ],
                          Average1, in1min[ j ], in1max[ j ],
                          Average2, in2min[ j ], in2max[ j ] ) ;
            }
          else
            { printf( "%5d,%8.5lf,%8.5lf,%8.5lf,%8.5lf\n", j, out1[ j ],
                          Average1, in1min[ j ], in1max[ j ] ) ;
            }
        }
    }
  printf( "\n\n" ) ;
  if ( DoCodeTiming )
    { ClockFinish = clock ( ) ;
      fprintf( stderr, "Data output time is %8.3lf milli seconds\n",
                  (float)( ClockFinish - ClockStart ) * 1000 / CLOCKS_PER_SEC ) ;
    }
}
```

```
/************************************************************************************************************************** Calculation */

void Calculation ( char  *Name,
                   int   Start,
                   int   Finish,
                   int   DualChannel,
                   int   Readings,
                   float in1[],
                   float in2[],
                   int   Format )
  {                                                          //* This routine does various calculation for the designate region of the averaged
                                                             //* reading and outputs the result.

    double inValue1 ;
    double inValue2 ;
    double Xvalue ;
    double Yvalue ;
    double SumValue1 ;
    double SumSqValue1 ;
    double SumValue2 ;
    double SumSqValue2 ;
    double SumValueX ;
    double SumSqValueX ;
    double Sum1xX ;
    double Sum2xX ;
    double Average1 ;
    double StdDev1 ;
    double Average2 ;
    double StdDev2 ;
    double Intercept1;
    double Slope1 ;
    double Intercept2;
    double Slope2 ;
    double R2ch1 ;
    double R2ch2 ;
    int    Count ;
    long   ClockStart ;
    long   ClockFinish ;
    int    Loop ;

    if ( DoCodeTiming )
      { ClockStart = clock ( ) ; }
    Count = Finish - Start + 1 ;
    SumValue1 = 0.0 ;
    SumSqValue1 = 0.0 ;
    SumValue2 = 0.0 ;
    SumSqValue2 = 0.0 ;
```

```
SumValueX = 0.0 ;
SumSqValueX = 0.0 ;
Sum1xX = 0.0 ;
Sum2xX = 0.0 ;
for ( Loop = Start; Loop <= Finish; Loop++ )
  { inValue1 = in1[ Loop ] / Readings ;
    Xvalue   = Loop * 8 ;
    Xvalue   = Xvalue / 125000 ;
    Xvalue   = Loop - Start ;
    SumValue1 = SumValue1 + inValue1 ;                          //* Do raw calculations of the photo diode.
    SumValueX = SumValueX + Xvalue ;
    SumSqValue1 = SumSqValue1 + inValue1 * inValue1 ;
    SumSqValueX = SumSqValueX + Xvalue * Xvalue ;
    Sum1xX    = Sum1xX + inValue1 * Xvalue ;
    if ( DualChannel )                                          //* Do raw calculations on the current from the V-I circuit.
      { inValue2 = in2[ Loop ] / Readings ;
        SumValue2 = SumValue2 + inValue2 ;
        SumSqValue2 = SumSqValue2 + inValue2 * inValue2 ;
        Sum2xX    = Sum2xX + inValue2 * Xvalue ;
      }
  }

if (( Format & 1 ) == 1 )                                       //* Calculate and output simple average, if required.
  { Average1 = SumValue1 / Count ;
    StdDev1  = sqrt (( Count * SumSqValue1 - SumValue1 * SumValue1 ) / ( Count * ( Count - 1 ))) ;
    if ( DualChannel )
      { Average2 = SumValue2 / Count ;
        StdDev2  = sqrt (( Count * SumSqValue2 - SumValue2 * SumValue2 ) / ( Count * ( Count - 1 ))) ;
        if (( Format & 128 ) == 128 )
          { printf( "Average %s,%d:%d,%8.5lf,%8.5lf,%8.5lf,%8.5lf\n", Name, Start, Finish, Average1, StdDev1, Average2, StdDev2 ) ; }
        else
          { printf( "%8.5lf,%8.5lf,%8.5lf,%8.5lf,", Average1, StdDev1, Average2, StdDev2 ) ; }
      }
    else
      { if (( Format & 128 ) == 128 )
          { printf( "Average %s,%d:%d,%8.5lf,%8.5lf\n", Name, Start, Finish, Average1, StdDev1 ) ; }
        else
          { printf( "%8.5lf,%8.5lf,", Average1, StdDev1 ) ; }
      }
  }

if (( Format & 2 ) == 2 )                                       //* Calculate and output linear regression, if required.
  { Intercept1 = ( SumValue1 * SumSqValueX - SumValueX * Sum1xX ) / ( Count * SumSqValueX - SumValueX * SumValueX ) ;
    Slope1 = ( Count * Sum1xX - SumValueX * SumValue1 ) / ( Count * SumSqValueX - SumValueX * SumValueX ) ;
    R2ch1 = 0.0 ;
    if ( DualChannel )
```

```
      { Intercept2 = ( SumValue2 * SumSqValueX - SumValueX * Sum2xX ) / ( Count * SumSqValueX - SumValueX * SumValueX ) ;
        Slope2 = ( Count * Sum2xX - SumValueX * SumValue2 ) / ( Count * SumSqValueX - SumValueX * SumValueX ) ;
        R2ch2 = 0.0 ;
      }
    for ( Loop = Start; Loop <= Finish; Loop++ )
      { inValue1 = in1[ Loop ] / Readings ;
        inValue2 = in2[ Loop ] / Readings ;
        Xvalue   = Loop * 8 ;
        Xvalue   = Xvalue / 125000 ;
        Xvalue   = Loop - Start ;
        Yvalue   = Intercept1 + Slope1 * Xvalue - inValue1 ;
        R2ch1    = R2ch1 + Yvalue * Yvalue ;
        Yvalue   = Intercept2 + Slope2 * Xvalue - inValue2 ;
        R2ch2    = R2ch2 + Yvalue * Yvalue ;
      }
    R2ch1 = R2ch1 / ( Finish - Start + 1 ) ;
//*    R2ch1 = sqrt ( 1 - R2ch1 ) ;
    if ( DualChannel )
      { R2ch2 = R2ch2 / ( Finish - Start + 1 ) ;
//*        R2ch2 = sqrt ( 1 - R2ch2 ) ;
        if (( Format & 128 ) == 128 )
          { printf( "Linear %s,%d:%d,%8.5lf,%8.5f,%8.5f,%8.5lf,%8.5lf,%8.5lf\n",
                       Name, Start, Finish, Slope1, Intercept1, R2ch1, Slope2, Intercept2, R2ch2 ) ;
          }
        else
          { printf( "%8.5lf,%8.5f,%8.5f,%8.5lf,%8.5lf,%8.5lf,", Slope1, Intercept1, R2ch1, Slope2, Intercept2, R2ch2 ) ; }
      }
    else
      { if (( Format & 128 ) == 128 )
          { printf( "Linear %s,%d:%d,%8.5lf,%8.5f,%8.5f\n", Name, Start, Finish, Slope1, Intercept1, R2ch1 ) ; }
        else
          { printf( "%8.5lf,%8.5f,%8.5f,", Slope1, Intercept1, R2ch1 ) ; }
      }
  }

if ( DoCodeTiming )
  { ClockFinish = clock ( ) ;
    fprintf( stderr, "Calculation time is %8.3lf milli seconds\n",
                (float)( ClockFinish - ClockStart ) * 1000 / CLOCKS_PER_SEC ) ;
  }
}
```